A Path Integral Approach to the Coupled-Mode Equations with Specific Reference to Optical Waveguides

by

Francesca Helen Mountfort

Thesis presented in partial fulfillment of the requirements
for the degree of

Master of Science

at the University of Stellenbosch

Supervisor:
Dr C.M. Steenkamp

Co-Supervisor:
Prof F.G. Scholtz

March 2009

Declaration

By submitting this thesis electronically, I declare that the entirety of the work contained therein is my own, original work, that I am the owner of the copyright thereof (unless explicitly otherwise stated) and that I have not previously in its entirety or in part submitted it for obtaining any qualification.

02-03-2009
Date

Copyright ©2009 Stellenbosch University

All rights reserved

Abstract

The propagation of electromagnetic radiation in homogeneous or periodically modulated media can be described by the coupled mode equations. The aim of this study was to derive analytical expressions modeling the solutions of the coupled-mode equations, as alternative to the generally used numerical and transfer-matrix methods. The path integral formalism was applied to the coupled-mode equations. This approach involved deriving a path integral from which a generating functional was obtained. From the generating functional a Green's function, or propagator, describing the nature of mode propagation was extracted. Initially a Green's function was derived for the propagation of modes having position independent coupling coefficients. This corresponds to modes propagating in a homogeneous medium or in a uniform grating formed by a periodic variation of the index of refraction along the direction of propagation. This was followed by the derivation of a Green's function for the propagation of modes having position dependent coupling coefficients with the aid of perturbation theory. This models propagation through a nonuniform inhomogeneous medium, specifically a modulated grating.

The propagator method was initially tested for the case of propagation in an arbitrary homogeneous medium. In doing so three separate cases were considered namely the copropagation of two modes in the forward and backward directions followed by the counter propagation of the two modes. These more trivial cases were used as examples to develop a rigorous mathematical formalism for this approach. The results were favourable in that the propagator's results compared well with analytical and numerical solutions.

The propagator method was then tested for mode propagation in a periodically perturbed waveguide. This corresponds to the relevant application of mode propagation in uniform gratings in optical fibres. Here two case were investigated. The first scenario was that of the copropagation of two modes in a long period transmission grating. The results achieved compared well with numerical results and analytical solutions. The second scenario was the counter propagation of two modes in a short period reflection grating, specifically a Bragg grating. The results compared well with numerical results and analytical solutions. In both cases it was shown that the propagator accurately predicts many of the spectral properties of these uniform gratings.

Finally the propagator method was applied to a nonuniform grating, that is a grating for which the uniform periodicity is modulated - in this case by a raised-cosine function. The result of this modulation is position dependent coupling coefficients necessitating the use of the Green's function derived using perturbation theory. The results, although physically sensible and qualitatively correct, did not compare well to the numerical solution or the well established transfer-matrix method on a quantitative level at wavelengths approaching the design wavelength of the grating. This can be explained by the breakdown of the assumptions of first order perturbation theory under these conditions.

Opsomming

Die voortplanting van elektromagnetiese golwe as optiese modes in homogene of periodies gemoduleerde media kan beskryf word deur die gekoppelde-mode vergelykings. Die doel van hierdie studie is om analitiese uitdrukkings af te lei wat die oplossings van die gekoppelde-mode vergelykings simuleer as 'n alternatief tot die algemeen gebruikte numeriese en oordragmatriks metodes. Die padintegrasie formalisme is op die gekoppelde-mode vergelykings toegepas. In hierdie benadering word 'n padintegral afgelei waaruit 'n voortbringende funksie verkry word. Die voortbringende funksie lewer 'n Green se funksie, of voortplantingsfunksie, wat die gedrag van die modevoortplanting volledig beskryf. Aanvanklik is 'n Green se funksie van die voortplanting vir modes met posisie onafhanklike koppelingskoeffisiente afgelei. Dit stem ooreen met die voortplanting van modes in 'n homogene medium of in 'n eenvormige rooster wat deur die periodiese verandering van die brekingsindeks langs die voortplantingsrigting gevorm word. daarna is die Green se funksie vir die voortplanting van modes met posisie afhanklike koppelingskoeffisiente afgelei met behulp van steuringsteorie. Dit simuleer voortplanting in 'n nie-eenvormige nie-homogene medium, spesifiek 'n gemoduleerde rooster.

Die voortplantingsfunksie metode is aanvanklik vir die geval van voortplanting deur 'n willekeurige homogene medium getoets. Drie verskillende gevalle is beskou, naamlik twee modes wat saam in die voorwaartse rigting voortplant, twee modes wat saam in die terugwaartse rigting voortplant en derdens twee modes wat in teenoorgestelde rigtings voortplant. Hierdie eenvoudige gevalle is as voorbeelde gebruik om 'n streng wiskundige formalisme te ontwikkel. Die voortplantingsfunksie se resultate het goed vergelyk met die van analitiese en numeriese oplossings.

Die voortplantingsfunksie metode is toe getoets vir die voortplanting van modes deur 'n periodiese versteurde golfleier. Hierdie geval stem ooreen met die relevante toepassing van modevoortplanting in eenvormige roosters in optiese vesels. Twee gevalle is ondersoek geword. Die eerste geval was die voortplanting van twee modes in die selfde rigting deur 'n lang periode transmissie rooster. Die resultate het goed vergelyk met die van die analitiese en numeriese metodes. Die tweede geval was die voortplanting van twee modes in teenoorgestelde rigtings deur 'n kort periode refleksie rooster, spesifiek 'n Bragg rooster. Weereens het die voortplantingsfunksie se resultate goed vergelyk met die analitiese and numeriese oplossings. In albei gevalle het die voortplantingsfunksie die spektraaleienskappe van die eenvormige roosters noukeurig voorspel.

Laastens is die voortplantingsfunksie metode op 'n nie-eenvormige rooster toegepas. Dit is 'n rooster waarvoor die eenvormige periodisiteit gemoduleer is, in hierdie geval deur 'n verhewe kosinus funksie. Die gevolg van die modulasie is dat die koppelingskoeffisiente posisie afhanklik is, wat dit nodig maak om die Green se funksie te gebruik wat deur steuringsteorie afgelei is. Alhoewel die resultate fisiese sin maak en kwalitatief korrek is, het hul kwantitatief nie goed vergelyk met die resultate van die numeriese en oordragmatriks metodes by golflengtes naby die ontwerpgolflengte van die rooster nie. Die verklaring daarvoor is dat die aannames wat in steuringsteorie gemaak word ongeldig raak onder hierdie spesifieke kondisies.

Acknowledgments

I would like to thank the following:

- Dr CM Steenkamp for her supreme dedication.
- Prof FG Scholtz for his invaluable insight.
- Dr J-N Maran (along with whoever invented Skype) for putting in so much time and effort.
- Everyone at the Laser Research Institute, in particular Mr Attie Hendriks & Miss Nicolene Botha for all the good times.
- Miss Annelle Griessel for having my back at every turn and living the dream with me, there has never been a dull moment over the last two years.
- The polymer chemist, Miss Nathalie "Oats" Bailly for her understanding and willingness to listen to me mope - not to mention all the times she had listen to me rehearse my oral presentations.
- My colleagues in the applied mathematics department, Mr Christo Rautenbach & Miss Jeanne-Marie Roux for their moral support and sense of humour.
- Miss Izaan du Toit, Miss Carmen Hannies & Miss Genevieve du Preez et al. for faith, encouragement and eagerness to make themselves available.
- My mother & father for their unrelenting love & unconditional support.
- My God, in all things with Him, through Him, in Him...

My studies were funded by the National Research Foundation (NRF) and DefenceTek (CSIR)

Contents

Introduction **1**

1 Coupled-Mode Theory **3**
1.1 Waveguide theory . . . 3
1.2 Coupled-mode theory . . . 7
1.2.1 The coupled-mode equations . . . 7
1.2.2 Phase-matching and the overlap integral . . . 10
1.3 Application to fibre gratings . . . 10
1.4 Other approaches to the coupled-mode equations . . . 12

2 Derivation of the Path Integral **16**
2.1 Constructing the path integral . . . 16
2.1.1 Condition of Constraint . . . 25
2.1.2 The source terms and the generating functional . . . 26
2.2 Calculating $\hat{\Gamma}^{-1}$ . . . 29

3 The Homogeneous Waveguide & the Unperturbed Propagator **33**
3.1 Transforming the coupled-mode equations . . . 33
3.2 The case of two forward propagating modes in an unperturbed medium . . . 34
3.2.1 The scenic route from $-\infty$ to ∞ . . . 35
3.2.2 Translating the propagator . . . 36
3.2.3 Results for forward propagation . . . 39
3.3 The case of two backward propagating modes in an unperturbed medium . . . 41
3.3.1 The backward propagator . . . 42
3.3.2 Results for backward propagation . . . 43
3.4 The case of two counter propagating modes in an unperturbed medium . . . 45
3.4.1 A propagator for mixed boundary conditions . . . 45
3.4.2 Results for counter propagation . . . 47

4 A periodically perturbed waveguide: The uniform grating **51**
4.1 Long period gratings (LPGs) . . . 52
4.1.1 Transforming the coupled-mode equations for an LPG . . . 52
4.1.2 The LPG propagator . . . 53
4.1.3 Results for the LPG . . . 54
4.2 Bragg gratings . . . 61
4.2.1 Transforming the coupled-mode equations for a Bragg grating . . . 62

4.2.2 The Bragg propagator 62
4.2.3 Results for the Bragg grating 63

5 Nonuniform Gratings: The Quest for the Perturbed Propagator 71
5.1 The Perturbed Propagator 71
5.2 The coupled-mode equations for a grating modulation 72
5.3 Apodization of the LPG: The raised-cosine modulation 73
5.3.1 A perturbed propagator for a raised-cosine modulation 74
5.3.2 Results 76

6 Summary & Conclusion 79

7 Appendix 81
7.1 Calculating $\left(\overline{a}^{\dagger} \otimes \overline{a}\right) \overline{b}$ 81
7.2 Analytical solution for 2×2 copropagation 82
7.3 Analytical solution for 2×2 counter propagation 83
7.4 The perturbed propagator for a raised-cosine modulation 86

Bibliography 88

List of Figures

1.1 The above is the diagram of one such arbitrary dielectric waveguide. 3
1.2 Illustration of the allowed modes of a waveguide, of diameter a, depending on the magnitude of β_μ. 6
1.3 Illustration of the fourth-order Runge-Kutta method. 13

2.1 This diagram illustrates the way in which the medium is sliced. 17
2.2 This diagram illustrates Equation 2.4. Each T-matrix represents a section and 1 is inserted between sections. The number of sections is given by K, while the actual length of the medium is L. The variable k denotes an arbitrary position. 20
2.3 This diagram illustrates the concept of the vector $\overline{a}_k$, a vector of integration variables for each mode i at a position k. The curved lines represent the amplitudes of modes $i-1$, i and $i+1$ at position k as they change with distance z. 21

3.1 This figure is a schematic representation of the fact that one can equate a complex integral over the real axis with a contour integral with a radius of infinity. 36
3.2 A schematic, for the forward propagating case, of the contour over which integration is done and the position of the poles. 37
3.3 (a) Real part of the field for forward propagation for (i) the analytical solution (ii) ODE45 (iii) forward propagator. (b) Imaginary part of the field for forward propagation for (i) the analytical solution (ii) ODE45 (iii) forward propagator. (c) Modulus squared of the complex amplitudes for forward propagation for (i) the analytical solution (ii) ODE45 (iii) forward propagator. 40
3.4 Above is a schematic, for the backward propagating case, of the contours over which we integrate and the position of the poles of each integral. 43
3.5 (a) Real part of the amplitude for backward propagation for (i) the analytical solution (ii) ODE45 (iii) backward propagator. (b) Imaginary part of the amplitude for forward propagation for (i) the analytical solution (ii) ODE45 (iii) backward propagator. (c) Modulus squared of the complex amplitudes for backward propagation for (i) the analytical solution (ii) ODE45 (iii) backward propagator. 44
3.6 A schematic, for the case of mixed boundaries case, of the contours over which one integrates and the position of the poles. 46

3.7 (a) Real part of the amplitude for counter propagation for (i) the analytical solution (ii) forward propagator (iii) backward propagator (iv) mixed propagator. (b) Imaginary part of the amplitude for counter propagation for (i) the analytical solution (ii) forward propagator (iii) backward propagator (iv) mixed propagator. (c) Modulus squared of the complex amplitudes for counter propagation for (i) the analytical solution (ii) forward propagator (iii) backward propagator (iv) mixed propagator. 48

3.8 (a) Real part of the amplitude for counter propagation for (i) mixed propagator 1 (ii) mixed propagator 2. (b) Imaginary part of the amplitude for counter propagation for (i) mixed propagator 1 (ii) mixed propagator 2. (c) Modulus squared of the complex amplitudes for counter propagation for (i) mixed propagator 1 (ii) mixed propagator 2. 50

4.1 The evolution of the powers of the two forward propagating modes with propagation distance as calculated by (i) an analytical solution (ii) ODE45 and (iii) the propagator for two nonphase-matched conditions (a) $\lambda = 0.95\lambda_D$, (c) $\lambda = 0.99\lambda_D$ and phase-matched condition (e) $\lambda = \lambda_D$. (b) (d) and (f) show the sum of the powers of the two modes with propagation distance calculated using the propagator corresponding to (a), (c) and (e) respectively. 55

4.2 (a) The evolution of the power of the modes for an increased propagation distance of 8 cm with all the other parameters the same as for Figure 4.1(e). (b) The evolution of the power of the modes for a stronger cross-coupling coefficient of $\vartheta = 62.8319\,\mathrm{cm}^{-1}$ as opposed to $\vartheta = 31.415\,\mathrm{cm}^{-1}$ of Figure 4.1(e); all other parameters the same as for Figure 4.1(e). . . . 56

4.3 (a) The bar and cross transmission spectra in the weaker grating limit, $\vartheta L = \frac{\pi}{2}$, produced by (i) an analytical solution, (ii) ODE45 and (iii) the propagator. (b) The error in the propagators results as compared to the analytical solution for both the bar and cross transmission of (a). (c) The error in ODE45's results as compared to the analytical solution for both the bar and cross transmission of (a). (d) The bar and cross transmission spectra in the stronger grating limit, $\vartheta L = \frac{5\pi}{2}$, produced by (i) an analytical solution, (ii) ODE45 and (iii) the propagator. (e) The error in the propagators results as compared to the analytical solution for both the bar and cross transmission of (d). (f) The error in ODE45's results as compared to the analytical solution for both the bar and cross transmission of (d). . . 58

4.4 A comparison of the cross transmission spectra shown in Figures 4.3 (a) and (d) to facilitate a comparison with the results of Othonos et al. [12]. 59

4.5 (a) The bar and cross transmission spectra in the weak grating limit, $\vartheta L = 0.39$, produced by (i) an analytical solution, (ii) ODE45 and (iii) the propagator. (b) A close up of the bar transmission spectrum shown in (a) facilitate a comparison with the results of Erdogan [3]. (c) The error in the propagators results as compared to the analytical solution for both the bar and cross transmission of (a). (c) The error in ODE45's results as compared to the analytical solution for both the bar and cross transmission of (a). 59

4.6 Results of the (i) analytical solution (ii) ODE45 and (iii) the propagator compared. (a) The evolution of the powers of the two counter propagating modes under phase-matched conditions, namely when $\lambda = \lambda_D$ with $v\bar{\delta n} = 1 \times 10^{-3}$. (b) The net power of the modes with propagation distance calculated using the propagator. (c) The evolution of the powers of the two counter propagating modes under nonphase-matched conditions, namely when $\lambda = 0.99\lambda_D$ with $v\bar{\delta n} = 1 \times 10^{-3}$. (d) The net power of the modes with propagation distance calculated using the propagator. (e) The evolution of the powers of the two counter propagating modes under phase-matched conditions with $v\bar{\delta n} = 1 \times 10^{-6}$. (f) The net power of the modes with propagation distance calculated using the propagator. 65

4.7 (a) The reflection spectrum in the weaker grating limit, $\delta n = 1 \times 10^{-4}$, produced by an (i) analytical solution (ii) ODE45 (iii) the propagator. (b) The error in the propagator's results as compared to the analytical solution for both the reflection (a). (c) The error in ODE45's results as compared to the analytical solution for the reflection of (a). (d) The reflection spectrum in the stronger grating limit, $\delta n = 4 \times 10^{-4}$, produced by (i) an analytical solution (ii) ODE45 (iii) the propagator. (e) The error in the propagator's results as compared to the analytical solution for the reflection of (d). (f) The error in ODE45's results as compared to the analytical solution for reflection of (d). 67

4.8 (a) The reflection spectrum in the strong grating limit, $\delta n = 8 \times 10^{-4}$, produced by (i) an analytical solution, (ii) ODE45 (iii) the propagator. (b) The error in the propagator's results as compared to the analytical solution for the reflection of (a). (c) The error in ODE45's results as compared to the analytical solution for the reflection of (a). 68

4.9 The reflection spectrum of a Bragg grating in the strong grating limit, $\vartheta \propto v\bar{\delta n} = 1 \times 10^{-3}$ where the maximum wavelength is equivalent to the design wavelength. In this case $\lambda_D = 1550\,\text{nm}$ and $L = 1\,\text{cm}$ just as the gratings corresponding to Figure 4.7. 69

5.1 (a) Cross and bar transmission ($T_\times$ and $T_=$) for two copropagating modes in a grating modulated by a raised-cosine function as calculated using ODE45, transfer-matrix method and the perturbed propagator respectively. The curves produced by ODE45 coincide with those produced by the transfer-matrix (T-matrix) method. (b) The sum of the complementary cross and bar transmission calculated using the propagator. 76

5.2 A comparison of the uniform grating with the apodized grating illustrating the effect of the apodization. The analytical solution was used to model the uniform grating while the transfer-matrix method was used to simulate the apodized grating. 77

List of Tables

3.1 The results given by ODE45 and the forward propagator are compared to the results of the analytical solution for two forward propagating modes. 39
3.2 The results given by ODE45 and the backward propagator are compared to the results of the analytical solution for two backward propagating modes. 45
3.3 The results given by all four propagators are compared to the results of the analytical solution for two counter propagating modes. 49

4.1 Parameters used in the modeling of the gratings corresponding to Figures 4.1(a), (c) and (e) and Figures 4.2(a) and (b). 56
4.2 The error and time consumption for the simulations associated with Figures 4.1(a), (c) and (e). 57
4.3 Parameters given and calculated from literature [3, 12] and used to generate Figures 4.3(a), 4.3(b) and 4.5(a). 57
4.4 The time consumption for the three simulations both numerically and for the propagator. 61
4.5 Parameters used in the modeling of the gratings corresponding to Figures 4.6(a), (c) and (e). 64
4.6 The error and time consumption for the simulations associated with the spectra of Figures 4.6. 64
4.7 These are parameters given and calculated from literature [3, 12] used to generate the spectra of Figures 4.7, 4.8 and 4.9. 66
4.8 The time consumption for the three simulations both numerically and for the propagator. 69

5.1 These are parameters calculated from literature [3] and used to model the LPG with a raised-cosine modulation. 76
5.2 Time consumption for the simulation the grating corresponding to Figure 5.1 and Table 5.1 for 1000 wavelength samples over the chosen wavelength range. 77

Introduction

There are but a few instances where the exact solution for the propagation of electromagnetic radiation in a periodically inhomogeneous medium can be found. For all other instances only approximate solutions to Maxwell's equations may be obtained. Two approaches that are employed generally are the Bloch wave formalism [22] and a coupled-mode analysis. The latter theory treats the variation to the permittivity of the medium as a perturbation that couples the normal modes of the homogeneous structure in question. The coupled-mode equations derived in this treatment lie at the heart of the very successful fibre grating technology.

Consider a waveguide of length L with modes propagating along it. Some propagate in a forward direction, that is from $z = 0$ to $z = L$ while other modes propagate in a backward direction from $z = L$ to $z = 0$. Depending on the exact nature of the waveguide medium, these modes may couple with one another so that an exchange of energy takes place between the modes as they propagate.

For the problem at hand the initial conditions of the modes are known. The amplitudes of the forward propagating modes are known at $z = 0$ but not at $z = L$ and likewise the amplitudes of the backward propagating modes are known at $z = L$ but not at $z = 0$. A model is needed with which the amplitudes of these modes may be calculated at any point along the waveguide given the initial conditions.

The challenge of modeling a large number of coupled modes is to solve an equally large number of coupled differential equations, the coupled-mode equations, simultaneously. The favoured approach with respect to numerical integration is the Runge-Kutta algorithm but even this method becomes time consuming and exhibits numerical instability as the number of differential equations increases [15]. The most utilized approach to solve the coupled-mode equations is the transfer-matrix method [20]. However, this method involves the multiplication of hundreds of matrices. The dimensions of the transfer matrix are given by the number of modes investigated so that for a large number of modes the calculation becomes cumbersome. The ideal would be to have an analytical expression modeling the coupled-mode amplitudes that can be evaluated at any particular position.

The aim of this study is to derive an analytical expression that models the amplitudes of coupled modes in a waveguide. In this study the path integral formalism is used to derive a Green's function corresponding to the coupled-mode equations. The Green's function is also called a propagator as it contains all the information pertaining to the nature of the medium through which the modes propagate as well as the nature of their coupling. Using this propagator the propagation of the modes through a variety of fibre gratings as well as the spectral properties of these gratings are calculated.

This is not the first time the path integral approach has been used in waveguide analysis. A numerical method has been developed for the calculation of the fundamental and first-order propagation properties of single-mode waveguides. The numerical method is based on the path integral treatment of the optical propagation equation for weakly focusing paraxial media [6]. Green's functions have also been obtained using the path integral approach to optical beam propagation. Examples such as soliton propagation

have been investigated and favorable results reported [17]. Path integral methods have also been used to investigate electromagnetic pulse propagation through a turbulent atmosphere and the Green's functions derived are reported to be applicable to a wide range of pulse propagation problems [9].

In deriving this analytical expression certain approximations have to be made. Specifically perturbation theory is used in this study when modeling nonuniform gratings, so that one cannot expect to obtain an exact solution. However, the error associated with an approximation may be understood and managed whereas numerical instability cannot.

In this thesis the coupled-mode theory is presented, followed by a rigorous derivation of the path integral, the corresponding generating functional and finally the Green's function or propagator for both an unperturbed and perturbed media. The propagator is then used in the investigation of mode propagation in a homogeneous medium. It is in this context that a solid mathematical foundation is laid with regards to applying the propagator. Next mode propagation in uniform Bragg and long period gratings is investigated as well as the spectral properties of these gratings. Finally the propagator for mode propagation in a nonuniform long period grating is analyzed.

Chapter 1

Coupled-Mode Theory

In this chapter the basic properties of waveguides are discussed, to place the study in context. The coupled-mode equations are then derived and examined in depth. The second part of the chapter introduces various methods that have thus far been employed to solve these equations. Particular emphasis is placed on the transfer-matrix method for which this work is the analytical equivalent.

1.1 Waveguide theory

The fundamental requirement pertaining to any guide for electromagnetic radiation, is that the flow of energy takes place only along the length of the waveguide and not perpendicular to it. Consider the propagation of light in an arbitrary dielectric waveguide, as illustrated in Figure 1.1. This dielectric structure will serve as a waveguide provided its dielectric constant is large enough. To put it another way, the index of refraction of the guide must be greater than that of its environment, $n_{\mathrm{II}} > n_{\mathrm{I}}$.

The nature of the propagation can be predicted by solving Maxwell's equations. For the purposes of this study, it is assumed that the medium is source-free, dielectric and a linear electric and magnetic

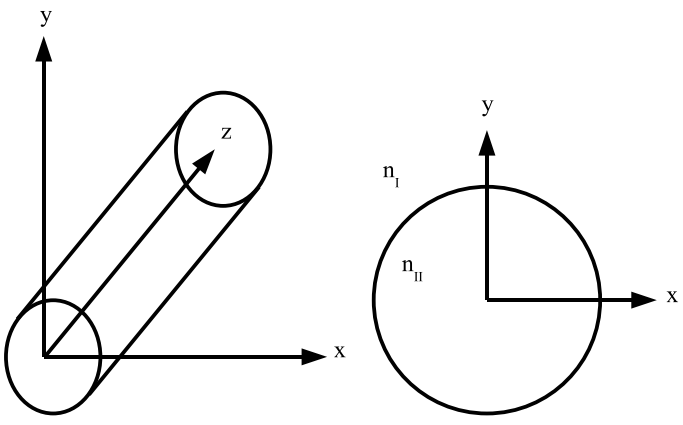

Figure 1.1: The above is the diagram of one such arbitrary dielectric waveguide.

material. Under these conditions Maxwell's equations are reduced to

$$\begin{aligned} \nabla \cdot \bar{D} &= 0 \\ \nabla \cdot \bar{B} &= 0 \\ \nabla \times \bar{E} &= -\frac{\partial \bar{B}}{\partial t} \\ \nabla \times \bar{H} &= \frac{\partial \bar{D}}{\partial t} \end{aligned}$$

The source-free wave equation derived from Maxwell's equations is given by

$$\nabla^2 \bar{E} = \mu_0 \varepsilon_0 \frac{\partial^2 \bar{E}}{\partial t^2} + \mu_0 \frac{\partial^2 \bar{P}}{\partial t^2}. \tag{1.1}$$

In this expression

- $\bar{P}$ is the induced polarization wave associated with electric wave E, having the relation

$$\bar{P} = \varepsilon_0 \chi^{(1)} \bar{E} \tag{1.2}$$

  where $\chi^{(1)}$ is the first order electric susceptibility given by $\chi^{(1)} = (\varepsilon_r - 1)$

- ε_0 is the dielectric permittivity of vacuum.
- ε_r is the relative permittivity, that is the permittivity of a medium relative to free space, $\varepsilon = \varepsilon_0 \varepsilon_r$.
- μ_0 is the magnetic permeability of vacuum.

Using Equation 1.2, Equation 1.1 can be reduced to

$$\nabla^2 \bar{E} = \mu_0 \varepsilon_0 \varepsilon_r \frac{\partial^2 \bar{E}}{\partial t^2}.$$

Using $\varepsilon = \varepsilon_0 \varepsilon_r$ yields

$$\nabla^2 \bar{E} = \mu_0 \varepsilon \frac{\partial^2 \bar{E}}{\partial t^2}. \tag{1.3}$$

The solutions of Equation 1.3 are referred to as optical modes. For light passing through a waveguide, these optical modes describe the confined propagation of electromagnetic radiation.

Assuming the medium of the waveguide is homogeneous in the direction of propagation, the z-direction, the optical modes take on the form

$$\bar{E}_\mu = A_\mu \bar{\xi}_\mu (x, y) \, e^{i(\omega t - \beta_\mu z)}. \tag{1.4}$$

In this expression:

- Subscript μ is the mode number, discrete for bound modes and continuous for unbound modes. The discrete modes correspond to those modes "bound" to the guiding region, the so-called guided modes. Unbound modes correspond to those modes for which the energy is not limited to the guiding region of the waveguide. The unbound modes are often referred to as radiation modes. More on this later...
- A_μ is the amplitude of the mode μ.

- $\bar{\xi}_\mu(x,y)$ is the transverse component of the mode, whose precise form is determined by the geometry of the waveguide. For instance, an optical fibre with a circular cross-section has transverse components that consist of a combination of ordinary and modified Bessel functions.
- ω is the angular frequency of the radiation of wavelength λ and is given by $\omega = 2\pi c/\lambda$.
- β_μ is the propagation constant of mode μ and is given by $\beta_\mu = 2\pi n_\mu/\lambda = \omega\frac{n_\mu}{c} = \frac{\omega}{v_\mu}$.
- n_μ is the effective refractive index of the medium that is seen by the propagating mode μ and v_μ is the speed with which it propagates.

The temporal variation of the mode is governed by $\exp(i\omega t)$ while the spatial behavior is determined by $\exp(-i\beta_\mu z)$.

As solutions to the wave equation (Equation 1.3), these modes must satisfy the following eigenvalue equation

$$\left(\nabla_T^2 + \mu_0\varepsilon(x,y)\,\omega^2 - \beta_\mu^2\right)\bar{\xi}_\mu(x,y) = 0 \tag{1.5}$$

where ∇^2 has been separated into a transverse and a longitudinal part respectively: $\nabla^2 = \nabla_T^2 + \frac{\partial^2}{\partial z^2}$. In the derivation of the eigenvalue equation (Equation 1.5), the expression for the modes in Equation 1.4 is substituted into Equation 1.3. Further $\nabla \cdot E$ is taken as 0 by virtue of the fact that the medium is assumed source-free.

In essence the eigenvalue problem presented governs the transverse behavior of the field. Given a certain permittivity, $\varepsilon(x,y)$, there are in principal infinitely many eigenvalues, β_μ^2 all corresponding to as many ignites $\bar{\xi}_\mu(x,y)$. However, there are boundary and continuity conditions that need to be satisfied, so that only a finite number of these modes are confined and allowed to propagate along the waveguide.

To determine the transverse behavior one is required to solve Equation 1.5 subject to the continuity conditions of the tangential fields at the interfaces and the boundary conditions at infinity. Equation 1.5 must hold in each transversely homogeneous region, that is in region I and region II of Figure 1.2. This brings about a continuity condition which requires the fields to be matched at each point along each interface. An important boundary condition for guided modes is that the field amplitudes are zero at infinity. To satisfy these conditions, the propagation constant β_μ must be the same throughout the waveguide at all points on each interface between media with differing refractive indices. In addition the fundamental property that there is no transverse flow of energy, requires that the fields decay exponentially outside the guide.

From the magnitude of β_μ one can draw many conclusions about the basic physical nature of these modes prior to specifying any particulars of the actual waveguide. Equation 1.5 can be rewritten as

$$\left(\nabla_T^2 + k^2n^2 - \beta_\mu^2\right)\bar{\xi}_\mu(x,y) = 0 \tag{1.6}$$

by making use of the fact that $v = \sqrt{\mu_0\varepsilon}$, $v = \frac{c}{n}$, where v is the propagation speed of mode μ and $\omega = kc$, where k is the wave vector magnitude. Referring to Figure 1.2, Equation 1.6 becomes, for example only considering the coordinate y and neglecting x,

$$\left(\frac{\partial^2}{\partial y^2} + k^2n_{\mathrm{I}}^2 - \beta_\mu^2\right)\bar{\xi}_\mu(x,y) = 0 \tag{1.7}$$

$$\left(\frac{\partial^2}{\partial y^2} + k^2n_{\mathrm{II}}^2 - \beta_\mu^2\right)\bar{\xi}_\mu(x,y) = 0 \tag{1.8}$$

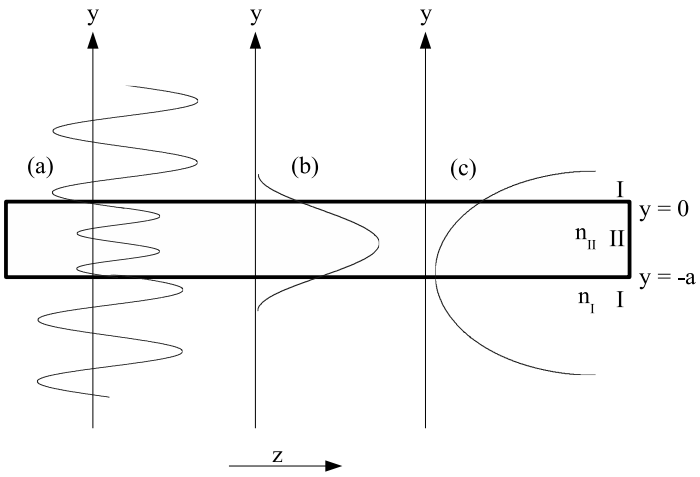

Figure 1.2: Illustration of the allowed modes of a waveguide, of diameter a, depending on the magnitude of β_μ.

in the regions I and II respectively. For $0 < \beta_\mu < kn_{\mathrm{I}}$ (corresponding to Figure 1.2(a)), solving Equations 1.7 and 1.8 yields a sinusoidal $\bar{\xi}_\mu(x,y)$ in both regions. For $kn_{\mathrm{I}} < \beta_\mu < kn_{\mathrm{II}}$ (corresponding to Figure 1.2(b)), $\bar{\xi}_\mu(x,y)$ decays exponentially to zero in region I and is sinusoidal in region II . In this way all the energy of the modes are supported in region II, hence it is the guiding region and these are the guided modes. For $\beta_\mu > kn_{\mathrm{II}}$, $\bar{\xi}_\mu(x,y)$ exhibits exponential behavior in both regions (corresponding to Figure 1.2(c)). For cases (a) and (c), β_μ is continuous while in case (b) β_μ is discrete.

The number of guided modes in case (b) depends on the diameter of the waveguide and on the difference in the indices of refraction. The greater the diameter, the greater the number of modes supported by the waveguide. The greater the difference in the refractive indices the larger the number of allowable eigenmodes. This is analogous to typical potential well problems in quantum mechanics. The wider the potential well and/or the deeper the potential well the greater the number of allowable eigenstates.

These modes also have a useful and important orthogonality property. By making use of the Lorentz Reciprocity Theorem [22] given by

$$\nabla \cdot \left(\bar{E}_\mu \times \bar{H}_\nu - \bar{E}_\nu \times \bar{H}_\mu\right) \quad = \quad 0$$

and using the two-dimensional form of the divergence theorem it can be shown [22] that the orthonormalization of the modes is given by

$$\int dx \int dy \left(\bar{E}_\mu \times \bar{H}_\nu^*\right)_z \quad = \quad \delta_{\mu\nu}. \tag{1.9}$$

This can be reduced further to

$$\frac{1}{2}\frac{\beta_\mu}{\omega\mu_0}\int dx \int dy \bar{\xi}_\mu^*(x,y)\,\bar{\xi}_\nu(x,y) \quad = \quad \delta_{\mu\nu} \tag{1.10}$$

Here the modes have been normalized to carry a power of 1 W.

If an arbitrary electromagnetic field of frequency ω is excited at $z = 0$, then the propagation of this

field can always be expressed in terms of a unique linear combination of the optical modes

$$\bar{E} \quad = \quad \sum_{\mu} A_{\mu} \bar{\xi}_{\mu} (x, y) \, e^{i(\omega t - \beta_{\mu} z)}. \tag{1.11}$$

Such an expansion is possible because these optical modes form a complete set. If a single mode, $\bar{\xi}_{\mu} (x, y) \, e^{i(\omega t - \beta_{\mu} z)}$ is excited at $z = 0$ in a homogeneous waveguide, then the electromagnetic wave will remain in this mode throughout propagation.

1.2 Coupled-mode theory

In this section, the work of Yariv et al. [21, 22] is closely followed especially regarding notation and sign convention but it is amalgamated with the work of Kashyap [8]. Consider the propagation of such an optical mode, $\bar{\xi}_{\mu} (x, y) \, e^{i(\omega t - \beta_{\mu} z)}$ in a waveguide for which the medium has been perturbed. In the case where there is a dielectric perturbation, $\Delta\varepsilon (x, y, z)$, due to waveguide imperfections, surface corrugations, bending etc., the optical modes couple with one another, facilitating a transfer of energy or power between the modes with propagation. The exchange of energy between optical modes, due to a perturbation in the dielectric constant, is analogous to a transition between the eigenstates of an atom experiencing a time-dependent perturbation. Hence, the same mathematical formalism is used, the method of variation of constants. For this procedure we still express the electromagnetic field in terms of a series expansion of the optical modes as in Equation 1.11, however, now the expansion coefficients or amplitudes A_{μ}, are z-dependent since for $\Delta\varepsilon (x, y, z) \neq 0$ the expressions $\bar{\xi}_{\mu} (x, y) \, e^{i(\omega t - \beta_{\mu} z)}$ are no longer the eigenmodes of the waveguide.

The perturbation can be seen in the spatial distribution of the permittivity,

$$\varepsilon (x, y, z) \quad = \quad \varepsilon (x, y) + \Delta\varepsilon (x, y, z) \tag{1.12}$$

where $\varepsilon (x, y)$ represents the unperturbed part and $\Delta\varepsilon (x, y, z)$ is the suitably small perturbation. However, the presence of the dielectric perturbation induces a perturbation in the resulting polarization wave. Now it is this polarization wave, acting as a distributed source, which feeds energy from one mode to another. It is said that the dielectric perturbation couples the modes. Here follows the derivation of the coupled-mode equations. For notational convenience $\xi_{\mu} (x, y) = \xi_{\mu, t}$, where t denotes transverse.

1.2.1 The coupled-mode equations

It is assumed that the optical modes are those corresponding to the propagation in the unperturbed medium with permittivity $\varepsilon (x, y)$ and can be described by Expression 1.4, satisfying Equation 1.5. The polarization response, seen in Equation 1.1 can be separated in two parts, namely a perturbed part associated with $\Delta\varepsilon (x, y, z)$ and an unperturbed part associated with $\varepsilon (x, y)$. Substituting Equation 1.12 into Equation 1.3 yields

$$\left[\nabla^2 - \left(\mu_0 \varepsilon (x, y) + \mu_0 \Delta\varepsilon (x, y, z) \right) \frac{\partial^2}{\partial t^2} \right] \bar{E} \quad = \quad 0 \tag{1.13}$$

For the purposes of deriving a general expression, the exact nature of $\Delta\varepsilon(x,y,z)$ will be included later. The electric field can be expressed as a linear combination of the optical modes

$$\bar{E} = \sum_{\mu} A_{\mu}(z)\,\bar{\xi}_{\mu t} e^{i(\omega t-\beta_{\mu} z)}. \tag{1.14}$$

Substituting Equation 1.14 into Equation 1.13 one obtains

$$\sum_{\mu}\left[\nabla^2-\left(\mu_0\varepsilon(x,y)+\mu_0\Delta\varepsilon(x,y,z)\right)\frac{\partial^2}{\partial t^2}\right]\left(A_{\mu}(z)\,\bar{\xi}_{\mu t} e^{i(\omega t-\beta_{\mu} z)}\right) = 0. \tag{1.15}$$

Equation 1.15 is an eigenvalue equation equivalent to Equation 1.5 corresponding to the perturbed medium. Using the fact that $\nabla^2=\nabla_T^2+\partial^2/\partial z^2$ and carrying out the necessary algebra yields

$$\begin{aligned}
\sum_{\mu}\left[\nabla_T^2+\frac{\partial^2}{\partial z^2}+\mu_0\varepsilon(x,y)\,\omega^2+\mu_0\Delta\varepsilon(x,y,z)\,\omega^2\right]A_{\mu}(z)\,\bar{\xi}_{\mu t}e^{i(\omega t-\beta_{\mu} z)} &= 0\\
\sum_{\mu}\left[\nabla_T^2+\frac{\partial^2}{\partial z^2}+\mu_0\varepsilon(x,y)\,\omega^2\right]A_{\mu}(z)\,\bar{\xi}_{\mu t}e^{i(\omega t-\beta_{\mu} z)} &= -\sum_{\nu}\mu_0\Delta\varepsilon(x,y,z)\,\omega^2 A_{\nu}(z)\,\bar{\xi}_{\nu t}e^{i(\omega t-\beta_{\nu} z)}\\
\sum_{\mu}\left[\nabla_T^2+\mu_0\varepsilon(x,y)\,\omega^2\right]A_{\mu}(z)\,\bar{\xi}_{\mu t}e^{i(\omega t-\beta_{\mu} z)} + \sum_{\mu}\left[\frac{\partial^2 A_{\mu}}{\partial z^2}-2i\beta_{\mu}\frac{\partial A_{\mu}}{\partial z}-A_{\mu}\beta_{\mu}^2\right]\bar{\xi}_{\mu t}e^{i(\omega t-\beta_{\mu} z)} &= -\sum_{\nu}\mu_0\Delta\varepsilon(x,y,z)\,\omega^2 A_{\nu}(z)\,\bar{\xi}_{\mu t}e^{i(\omega t-\beta_{\mu} z)}
\end{aligned} \tag{1.16}$$

Making use of eigenvalue Equation 1.5, Equation 1.16 is simplified yielding

$$\sum_{\mu}\left[\frac{\partial^2 A_{\mu}}{\partial z^2}-2i\beta_{\mu}\frac{\partial A_{\mu}}{\partial z}\right]\bar{\xi}_{\mu t}e^{i(\omega t-\beta_{\mu} z)} = -\sum_{\nu}\mu_0\Delta\varepsilon(x,y,z)\,\omega^2 A_{\nu}(z)\,\bar{\xi}_{\nu t}e^{i(\omega t-\beta_{\nu} z)} \tag{1.17}$$

One assumes a coupling regime weak enough so that the slowly varying envelope approximation (SVEA) can be used. Mathematically, the SVEA amounts to invoking the following condition

$$\frac{\partial^2 A_{\mu}}{\partial z^2} \ll \beta_{\mu}\frac{\partial A_{\mu}}{\partial z}.$$

In other words it is required that the amplitude of a mode changes slowly over a distance of the wavelength of the light. The time dependent factor $\exp(i\omega t)$ can be canceled. The result is that Equation 1.17 is reduced to

$$-\sum_{\mu} i2\beta_{\mu}\frac{\partial A_{\mu}}{\partial z}\bar{\xi}_{\mu t}e^{-i\beta_{\mu} z} = -\sum_{\nu}\mu_0\Delta\varepsilon(x,y,z)\,\omega^2 A_{\nu}(z)\,\bar{\xi}_{\nu t}e^{-i\beta_{\nu} z} \tag{1.18}$$

Taking the scalar product of Equation 1.18 with $\bar{\xi}_{\mu,t}^{*}$ and integrating over the waveguide cross-section,

that is over all x and y, one obtains

$$\begin{aligned}
\sum_{\mu}\int_{-\infty}^{\infty}\int_{-\infty}^{\infty}dxdy\left[i2\beta_{\mu}\frac{\partial A_{\mu}}{\partial z}\bar{\xi}_{\mu t}^{*}\bar{\xi}_{\mu t}e^{-i\beta_{\mu}z}\right] &= \sum_{\nu}\int_{-\infty}^{\infty}\int_{-\infty}^{\infty}\mu_{0}\Delta\varepsilon\left(x,y,z\right)\omega^{2}A_{\nu}\left(z\right)\bar{\xi}_{\mu t}^{*}\bar{\xi}_{\nu t}e^{-i\beta_{\nu}z} \\
\sum_{\mu}i2\beta_{\mu}\frac{\partial A_{\mu}}{\partial z}\left\langle \bar{\xi}_{\mu t}\left|\bar{\xi}_{\mu t}\right.\right\rangle e^{-i\beta_{\mu}z} &= \sum_{\nu}\mu_{0}\omega^{2}\left\langle \bar{\xi}_{\mu t}\left|\Delta\varepsilon\left(x,y,z\right)\right|\bar{\xi}_{\nu t}\right\rangle A_{\nu}\left(z\right)e^{-i\beta_{\nu}z} \\
\left\langle \bar{\xi}_{\mu t}\left|\bar{\xi}_{\mu t}\right.\right\rangle \frac{\partial A_{\mu}}{\partial z} &= \frac{\mu_{0}\omega^{2}}{i2\beta_{\mu}}\sum_{\nu}\left\langle \bar{\xi}_{\mu t}\left|\Delta\varepsilon\left(x,y,z\right)\right|\bar{\xi}_{\nu t}\right\rangle A_{\nu}\left(z\right)\exp\left(-i\left(\beta_{\nu}-\beta_{\mu}\right)z\right)
\end{aligned} \tag{1.19}$$

Here

$$\begin{aligned}
\left\langle \bar{\xi}_{\mu t}\left|\bar{\xi}_{\mu t}\right.\right\rangle &= \int_{-\infty}^{\infty}\int_{-\infty}^{\infty}dxdy\bar{\xi}_{\mu}^{*}\left(x,y\right)\bar{\xi}_{\mu}\left(x,y\right) \\
&= 2\frac{\omega\mu_{0}}{\beta_{\mu}}
\end{aligned}$$

$$\left\langle \bar{\xi}_{\mu t}\left|\Delta\varepsilon\left(x,y,z\right)\right|\bar{\xi}_{\nu t}\right\rangle = \int_{-\infty}^{\infty}\int_{-\infty}^{\infty}dxdy\bar{\xi}_{\mu}^{*}\left(x,y\right)\Delta\varepsilon\left(x,y,z\right)\bar{\xi}_{\nu}\left(x,y\right).$$

Defining the coupling coefficient, indicative of the coupling strength between the modes μ and ν as

$$C_{\mu\nu}\left(z\right) = \frac{\omega}{4}\int_{-\infty}^{\infty}\int_{-\infty}^{\infty}dxdy\bar{\xi}_{\mu}^{*}\left(x,y\right)\Delta\varepsilon\left(x,y,z\right)\bar{\xi}_{\nu}\left(x,y\right) \tag{1.20}$$

the coupled-mode equations (Equation 1.19) can be reduced to

$$\frac{\partial A_{\mu}}{\partial z} = -i\sum_{\nu}C_{\mu\nu}A_{\nu}\left(z\right)\exp\left(-i\left(\beta_{\nu}-\beta_{\mu}\right)z\right). \tag{1.21}$$

Assuming that the media is lossless, it would be useful to note here that regarding the coupling coefficients

$$\begin{aligned}
C_{\mu\nu}^{*}\left(z\right) &= \frac{\omega}{4}\int_{-\infty}^{\infty}\int_{-\infty}^{\infty}dxdy\left(\bar{\xi}_{\mu}^{*}\left(x,y\right)\right)^{*}\Delta\varepsilon\left(x,y,z\right)\bar{\xi}_{\nu}^{*}\left(x,y\right) \\
&= \frac{\omega}{4}\int_{-\infty}^{\infty}\int_{-\infty}^{\infty}dxdy\bar{\xi}_{\nu}^{*}\left(x,y\right)\Delta\varepsilon\left(x,y,z\right)\bar{\xi}_{\mu}\left(x,y\right) \\
&= C_{\nu\mu}\left(z\right).
\end{aligned}$$

This is a Hermitian property. For the purposes of this study however, the coupling coefficients obtained are real, given the choice of polarization of the modes. The polarization of the modes may also be chosen such that they are complex and hence yield complex coupling coefficients.

1.2.2 Phase-matching and the overlap integral

Equation 1.21 is the generalized set of coupled-mode equations. They are generalized in that an explicit form of the dielectric perturbation has not been specified. They are a set of first order ordinary coupled differential equations. At this stage there are in theory infinitely many modal amplitudes involved. In practice, however, only a few modes are ever strongly coupled. In the presence of a periodic perturbation, this occurs for modes that are resonant or near resonant with one another in the presence of a perturbation with a particular period, Λ. Hence the number of equations represented by Equation 1.21 is reduced. First considering just two modes, the condition for resonant coupling is given by

$$\beta_\mu = \beta_\nu + m\frac{2\pi}{\Lambda} \tag{1.22}$$

for some integer m. This is the fundamental condition for longitudinal phase matching. The propagation constant of the driving electric field is β_ν and that of the resultant induced polarization field is β_μ. The phase factor of the perturbation is $m\frac{2\pi}{\Lambda}$.

The induced polarization field is the bound wave generated by the polarization response of the medium which act as distributed sources. These sources come about as the result of the perturbation to the dielectric constant. For any significant coupling between the driving field and the generated field, the two fields must remain in phase over a significant distance. That is, for a continuous transfer of energy Equation 1.22 must be satisfied. A phase mismatch factor is defined as

$$\delta\beta = \beta_\nu - \beta_\mu + m\frac{2\pi}{\Lambda} \tag{1.23}$$

which is of course zero under phase matching conditions. For copropagating modes β_ν and β_μ have the same sign. If they have opposite signs then the interaction is counter propagating in nature.

The second condition for coupling between two modes is a nonzero coefficient as given by Equation 1.20. The orthogonality relationship given by Equation 1.9 states that only modes with the same order will have a nonzero coupling coefficient in a medium with a transversely homogeneous permittivity. However in the presence of a transversely nonsymmetric refractive index modulation, which results in a transversely inhomogeneous permittivity, allows orthogonal modes of differing orders to have nonzero coupling coefficients.

To summarize Sections 1.1 and 1.2, the propagation of electromagnetic radiation in a perturbed dielectric medium can be modeled using the method of the variation of constants. These constants or expansion coefficients are the mode amplitudes and are governed by the coupled-mode equations. For significant coupling to take place between modes μ and ν, two conditions must be satisfied, namely the phase matching condition (kinematical condition) and the condition that the coupling coefficients do not vanish (dynamical condition).

1.3 Application to fibre gratings

In the preceding sections things have been kept as general as possible, making use of an arbitrary waveguide with unspecified geometry and hence unspecified modes. Equation 1.21 can apply to any guide with a variation in the index of refraction. However, the purpose of this study is to model the optical properties of fibre gratings. Basic fibre grating theory is presented in this section.

Fibre gratings are fabricated by exposing an optical fibre to a spatially varying pattern of ultra violet (UV) light. The end result is a periodic variation in the refractive index which is treated as

a perturbation to the effective refractive index "seen" by the propagating mode. This perturbation is periodic and commonly [3, 12] expressed as a raised-cosine function:

$$\delta n(z) = \bar{\delta n}(z)\left\{1 + v\cos\left[\frac{2\pi}{\Lambda}z + \phi(z)\right]\right\} \tag{1.24}$$

Here

- $\bar{\delta n}(z)$ is the dc index change - the envelope of the periodic variation,
- v is the fringe visibility of the index change,
- Λ is the period of the grating,
- $\phi(z)$ is the grating chirp.

The coupling coefficient of Equation 1.20 is expressed in terms of the dielectric constant, but this can easily be expressed in terms of the refractive index of the medium in the following way

$$\begin{aligned} n^2 &= \varepsilon \\ (n + \delta n(x,y,z))^2 &= \varepsilon + \Delta\varepsilon(x,y,z) \\ n^2 + \delta n^2(x,y,z) + 2n\delta n(x,y,z) &= \varepsilon + \Delta\varepsilon(x,y,z) \end{aligned}$$

For a very small modulation δn, i.e. $\delta n \ll n$ it holds that

$$n^2 + 2n\delta n(x,y,z) \approx \varepsilon + \Delta\varepsilon(x,y,z)$$

such that

$$2n\delta n(x,y,z) \approx \Delta\varepsilon(x,y,z). \tag{1.25}$$

In this way the coupling coefficients of Equation 1.20 can be expressed as

$$C_{\mu\nu}(z) = \frac{\omega}{2}n\int_{-\infty}^{\infty}\int_{-\infty}^{\infty} dxdy\bar{\xi}_{\mu}^{*}(x,y)\,\delta n(x,y,z)\,\bar{\xi}_{\nu}(x,y) \tag{1.26}$$

The easiest approach to take, when attempting to model gratings, is that of diffraction theory [3, 12]. A fibre grating is nothing more than an optical diffraction grating hence its effect upon an incident electric field can be described by the grating equation

$$n\sin\theta_2 = n\sin\theta_1 + m\frac{\lambda}{\Lambda} \tag{1.27}$$

where θ_1 is the angle of the incident field with respect to the grating normal, θ_2 the angle of the diffracted field for which constructive interference occurs and m the integer that corresponds to the diffraction order.

There exist two categories of fibre gratings, namely transmission gratings (also called long period gratings (LPGs)) and reflection gratings (also called short period gratings (SPGs)). LPGs facilitate coupling between copropagating modes while SPGs do this for counter propagating modes. The most familiar SPGs is the Bragg grating which couples a single mode into its counter propagating counterpart.

The grating equation, Equation 1.27, can easily be modified to an equation in terms of the respective propagation constants of the modes in question. The effective index of refraction that mode 1 experiences is given by $n_1 = n\sin\theta_1$ and likewise the index of refraction seen by mode 2 is $n_2 = n\sin\theta_2$. Using the fact that the modes' propagation constant can be expressed in terms of their effective refractive index, $\beta = \frac{2\pi}{\lambda}n$, Equation 1.27 can be rewritten as

$$\beta_2 = \beta_1 + m\frac{2\pi}{\Lambda}. \tag{1.28}$$

This however, is exactly the phase-matching condition described by Equation 1.22. In an optical fibre first order diffraction dominates so that $m = -1$. For a reflection grating the resonant wavelength (or design wavelength) for the coupling of a mode with effective index n_1 into a mode with effective index n_2 as derived from Equation 1.28, is

$$\lambda_D = (n_1 + n_2)\,\Lambda.$$

For a Bragg grating where the two modes are identical one obtains

$$\lambda_D = 2n\Lambda.$$

For a transmission grating the resonant wavelength is given by

$$\lambda_D = (n_1 - n_2)\,\Lambda. \tag{1.29}$$

Both LPGs and SPGs can be uniform in nature or nonuniform. A uniform grating is one in which the dc refractive index change, $\bar{\delta n}(z)$, is z-independent. That is, the envelope of the periodic perturbation, in this case given by the raised-cosine function, is uniform. By modulating the perturbation, one creates a nonuniform grating. Typical examples include a Gaussian modulation or even an additional raised-cosine modulation. In this case $\bar{\delta n}(z)$ is given by a Gaussian or raised-cosine function respectively. Obviously the latter would have a period much larger than that of the original grating.

There are other examples of nonuniform gratings which do not involve modulating the envelope of the uniform grating. Chirped gratings are such an example. Here the period of the grating becomes z-dependent. As another example, one may also incorporate a discrete phase shift in the periodicity of the grating. One also finds grating superstructures where the uniform grating section occurs periodically in the waveguide.

1.4 Other approaches to the coupled-mode equations

Analytical solutions are only available for Equation 1.21 when the coupling coefficients given by Equation 1.20 are constant. There have been efforts to solve the coupled-mode equations for z-dependent coupling coefficients by using analytical or semi analytical techniques. Such approaches include using the phase-integral or WKB approach [16], making use of a Hamiltonian formulation [7] and a variational technique [14].

There are two standard numerical approaches to solving the coupled-mode equations for the optical properties of these gratings. The first approach is direct numerical integration. However, this is probably the most time consuming approach to take. Generally, adaptive-stepsize Runge-Kutta techniques are preferred [3]. The Runge-Kutta methods are a family of implicit and explicit iterative techniques for

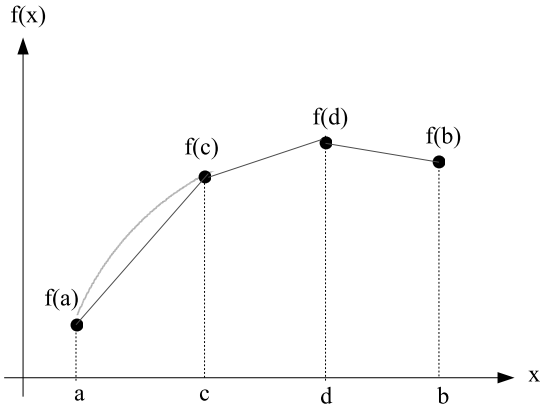

Figure 1.3: Illustration of the fourth-order Runge-Kutta method.

approximating the solutions to differential equations. In short, the Runge-Kutta method takes into account not only the slope of a function but also the curvature, to extrapolate a function. Whereas the Euler method will extrapolate from point a to point b only taking into consideration the first derivative at a, the Runge-Kutta method involves using the Euler method to approximate function values between points a and b to better approximate the function value at b. The order of the Runge-Kutta method corresponds to the number of derivatives calculated in determining the function values at b. Referring to Figure 1.3, the fourth order Runge-Kutta method involves calculating the derivative at a, at two intermediate points c and d and then finally at point b, to calculate the function value at b. The methods do become more sophisticated in that there are adaptive step size algorithms and hybrid methods. For a more in depth look at such techniques, *"Numerical Recipes in C: The Art of Scientific Computing"* by William H. Press et al. [15] is a very good place to start.

The second approach is to employ matrix methods, the most popular of which is the transfer-matrix method [20]. There are also several other matrix techniques, the effective index method [12, 19], Rouard's method [8, 16], an extension of this method by Weller-Brophy and Hall [12, 18] and a discrete-time approach based on digital signal processing by Frolik and Yagle [12, 5]. The transfer-matrix method will be discussed in depth as the aim of this study is to provide an analytical alternative to this method.

The transfer-matrix method is also often referred to as the piecewise-uniform method. This model is based on slicing up the nonuniform grating and then treating each grating slice as a uniform grating. For each slice an $N \times N$ matrix is identified, where N is the number of modes. Each matrix contains the solution for the transformation of the field within that particular slice. All the matrices are then multiplied together yielding one $N \times N$ transfer-matrix containing all the information of the field transformations through each section of the grating. The explanation that follows pertains to the simple case of two interacting modes, but can be generalized to N modes and closely follows the conventions of Erdogan et al. [3, 2].

For a grating of length L, from $z = -L/2$ to $z = L/2$, the grating is divided into M uniform slices. Let F_k and B_k be the forward and backward propagating field amplitudes respectively after traversing

grating slice k where $k = 1, 2, \cdots, K+1$. For a Bragg grating the convention is to use initial conditions

$$\begin{aligned} F_0 &= F(L/2) \\ &= 1 \end{aligned} \tag{1.30}$$

and

$$\begin{aligned} B_0 &= B(L/2) \\ &= 0 \end{aligned} \tag{1.31}$$

while for copropagation the initial conditions are given by

$$\begin{aligned} F_{1,0} &= F_1(-L/2) \\ &= 1 \end{aligned} \tag{1.32}$$

and

$$\begin{aligned} F_{2,0} &= F_2(-L/2) \\ &= 0. \end{aligned} \tag{1.33}$$

F and B are the forward and backward propagating amplitudes respectively, they are respectively the forward and backward equivalent of A_μ in Equation 1.21. So for Bragg gratings, increasing k runs backwards from $L/2$ to $-L/2$, so that the field amplitudes are calculated backwards. For copropagation increasing k runs from $-L/2$ to $L/2$. However, either way the field amplitudes are calculated by

$$\begin{bmatrix} F_k \\ B_k \end{bmatrix} = T_k \begin{bmatrix} F_{k-1} \\ B_{k-1} \end{bmatrix}.$$

Here T_k is the transformation matrix describing how the field amplitudes evolve in slice k. For the entire length of the grating

$$\begin{bmatrix} F_{K+1} \\ B_{K+1} \end{bmatrix} = T \begin{bmatrix} F_1 \\ B_1 \end{bmatrix}$$

for $T = T_K \times \cdots \times T_2 \times T_1$.

For a Bragg grating the transformation matrix for a single grating slice is given by [3]

$$T_k^{Bragg} = \begin{bmatrix} \cosh(\gamma_B \Delta z) - i\frac{\hat{\varrho}}{\gamma_B}\sinh(\gamma_B \Delta z) & -i\frac{\vartheta}{\gamma_B}\sinh(\gamma_B \Delta z) \\ i\frac{\vartheta}{\gamma_B}\sinh(\gamma_B \Delta z) & \cosh(\gamma_B \Delta z) + i\frac{\hat{\sigma}}{\gamma_B}\sinh(\gamma_B \Delta z) \end{bmatrix}$$

and for the case of two copropagating modes

$$T_k^{co} = \begin{bmatrix} \cos(\gamma_{co} \Delta z) + i\frac{\hat{\varrho}}{\gamma_{co}}\sin(\gamma_{co} \Delta z) & i\frac{\vartheta}{\gamma_{co}}\sin(\gamma_{co} \Delta z) \\ i\frac{\vartheta}{\gamma_{co}}\sin(\gamma_{co} \Delta z) & \cos(\gamma_{co} \Delta z) - i\frac{\hat{\varrho}}{\gamma_{co}}\sin(\gamma_{co} \Delta z) \end{bmatrix}.$$

Here $\hat{\varrho}$ and ϑ are self-coupling and cross-coupling coefficients respectively and γ_B and γ_{co} are terms relating to these coupling coefficients between the respective modes for the cases for the Bragg and copropagation respectively. Both these particular matrices consist of terms relating to the analytical solution for the

uniform grating for their respective types of propagation. The matter of coupling coefficients will be dealt with in greater depth in the relevant chapters that follow.

The number of sections required for the transfer-matrix method is determined by the accuracy required.

Chapter 2

Derivation of the Path Integral

2.1 Constructing the path integral

The system of differential equations, given by Equation 1.21, describing the evolution of forward and backward propagating coupled modes can be expressed in matrix notation by the following expression:

$$\frac{d\overline{U}}{dz} = M(z)\overline{U}(z). \tag{2.1}$$

$M(z) \in \mathbb{C}^{N\times N}$ is the coupling matrix containing all the coupling coefficients which themselves are Hermitian in nature, as expressed in Equation 1.26, where N is the number of modes - both forward and backward propagating modes.

$$\overline{U}(z) = \begin{bmatrix} U^{(1)}(z) \\ U^{(2)}(z) \\ \vdots \\ U^{(i)}(z) \\ \vdots \\ U^{(N)}(z) \end{bmatrix}$$

is a vector with each element $U^{(i)}(z)$ the field amplitude of an individual mode $\forall i = \{1, \cdots, N\}$. $U^{(i)}(z)$ is equivalent to the $A_\mu(z)$ of Equation 1.21. In the case of a forward propagating mode $U^{(i)}(z) = F_i(z)$ or $U^{(i)}(z) = B_i(z)$ in the case of a backward propagating mode. Working on the premise that for every forward propagating amplitude there exists a corresponding backward propagating amplitude, N will always be an even number.

By definition, the derivative is given by

$$\frac{d\overline{U}}{dz} = \lim_{\Delta z\to 0}\frac{\overline{U}(z+\Delta z) - \overline{U}(z)}{\Delta z}.$$

A finite difference approximation is made by assuming Δz to be small so that it is reasonable to approximate the derivative by

$$\frac{d\overline{U}}{dz} = \frac{\overline{U}(z+\Delta z) - \overline{U}(z)}{\Delta z}.$$

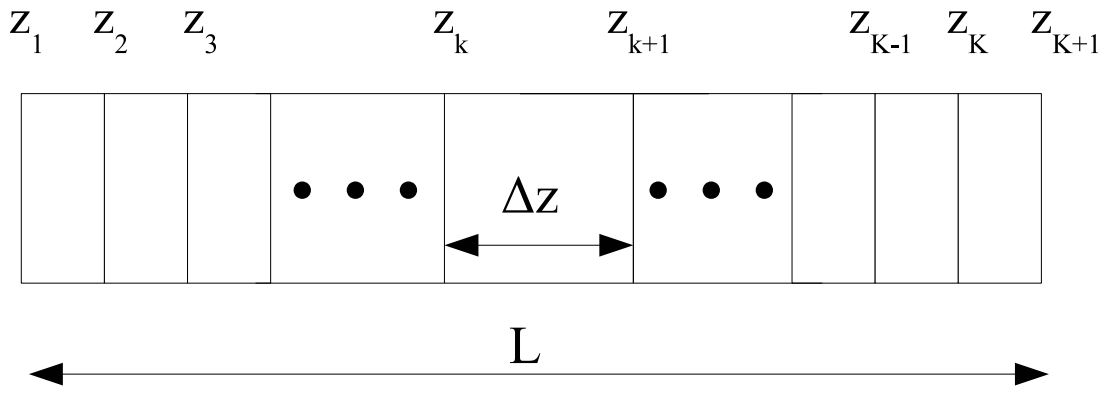

Figure 2.1: This diagram illustrates the way in which the medium is sliced.

Hence

$$\begin{aligned}
\frac{\overline{U}(z+\Delta z)-\overline{U}(z)}{\Delta z} &= M(z)\overline{U}(z) \\
\overline{U}(z+\Delta z)-\overline{U}(z) &= \Delta z M(z)\overline{U}(z) \\
\overline{U}(z+\Delta z) &= \overline{U}(z)+\Delta z M(z)\overline{U}(z) \\
\overline{U}(z+\Delta z) &= (1+\Delta z M(z))\overline{U}(z)
\end{aligned}$$

In the limit where $\Delta z \to 0$, it follows that[1]

$$\overline{U}(z+\Delta z) = e^{\Delta z M(z)}\overline{U}(z)+O\left(\Delta z^2\right) \tag{2.2}$$

where the higher order terms will be neglected.

In the case of an application to an optical medium with finite length L, where K is the number of sections into which the medium is sliced,

$$\Delta z = \frac{L}{K}.$$

The (z) positions of section boundaries are denoted by z_i, with

$$\begin{aligned}
z_1 &= 0 \\
z_{K+1} &= L \\
z_{k+1} &= z_k+\Delta z
\end{aligned}$$

as illustrated in Figure 2.1. With these definitions, Equation 2.2, with the higher order terms neglected, yields

$$\begin{aligned}
\overline{U}(z_{k+1}) &= \overline{U}(z_k+\Delta z) \\
&= e^{\Delta z M(z_k)}\overline{U}(z_k).
\end{aligned}$$

[1]This is done by noting that for a Taylor series expansion and to a first order approximation $e^{\Delta z M(z)} = 1+\Delta z M(z)+O\left(\Delta z^2\right)$ where $O\left(\Delta z^2\right)$ represents the higher order terms.

However, in turn

$$\overline{U}(z_k) = e^{\Delta z M(z_{k-1})}\overline{U}(z_{k-1})$$

so that

$$\overline{U}(z_{k+1}) = e^{\Delta z M(z_k)}e^{\Delta z M(z_{k-1})}\overline{U}(z_{k-1})$$

This procedure can repeated until the amplitude at position z_{k+1} is expressed in terms of the initial amplitude at z_1. Hence

$$\overline{U}(z_{k+1}) = e^{\Delta z M(z_k)}e^{\Delta z M(z_{k-1})}\cdots e^{\Delta z M(z_1)}\overline{U}(z_1)$$

The following simplifying notation is introduced: for the modes

$$\overline{U}_k = \overline{U}(z_k)$$

and for the z-dependent matrix

$$M_k = M(z_k)$$

so that

$$\begin{aligned}\overline{U}_{k+1} &= e^{\Delta z M_k}e^{\Delta z M_{k-1}}\cdots e^{\Delta z M_1}\overline{U}_1 \\ \overline{U}_{k+1} &= \prod_{k=1}^{k} e^{\Delta z M_k}\overline{U}_1.\end{aligned}$$

At the end of the medium at position $k = K + 1$ it follows that

$$\overline{U}_{K+1} = \prod_{k=1}^{K} e^{\Delta z M_k}\overline{U}_1.$$

Defining

$$T_k = e^{\Delta z M_k}$$

the amplitude at the end of the medium can be expressed as

$$\begin{aligned}\overline{U}_{K+1} &= \prod_{k=1}^{K} T_k\overline{U}_1 \\ &= T\overline{U}_1\end{aligned}$$

where

$$T = \prod_{k=1}^{K}\exp(\Delta z M_k). \tag{2.3}$$

This result yields a vector of which the elements are the field amplitudes of the particular modes at

the end of the medium,

$$\overline{U}_{K+1} = \begin{bmatrix} U_{K+1}^{(1)} \\ U_{K+1}^{(2)} \\ \vdots \\ U_{K+1}^{(i)}, \\ \vdots \\ U_{K+1}^{(N)} \end{bmatrix}$$

$\forall i = \{1, \cdots, N\}$. Introducing a basis vector, $\overline{v}_i$, defined as

$$\overline{v}_i = \begin{bmatrix} 0 \\ 0 \\ \vdots \\ 1 \\ \vdots \\ 0 \\ 0 \end{bmatrix}$$

one is able to select the amplitude of the i-th mode. Essentially $\overline{v}_i$ is the basis vector for mode i. Now the amplitude of an explicit mode, i, can be expressed at the end of the medium in terms of its basis in the following way

$$U_{K+1}^{(i)} = \overline{v}_i^{\dagger} T \overline{U}_1.$$

This solution, now a mere number, is calculated by the product of many exponential matrices, as seen in expression 2.3. This resembles the transfer-matrix method. However, the exponential matrix can be reduced to an ordinary number by the following procedures. These entail expanding T into its constituent exponential matrices, T_k and multiplying each with the number 1 which does not alter the mathematical expression.

$$\overline{v}_i^{\dagger} T \overline{U}_1 = \overline{v}_i^{\dagger} \times 1_{K+1} \times T_K \times 1_K \times \cdots \times T_2 \times 1_2 \times T_1 \times \overline{U}_1 \tag{2.4}$$

where the subscripts denote the position with which the 1 in question is associated. An illustration is given in Figure 2.2 .

The 1s are represented by Gaussian integrals. To do so, a set of vectors, $\{\overline{a}_k\}$, needs to be introduced. In keeping with the chosen line of notation, we define $\overline{a}\,(z_k) = \overline{a}_k$ where

$$\overline{a}_k = \begin{bmatrix} a_k^{(1)} \\ a_k^{(2)} \\ \vdots \\ a_k^{(i)} \\ \vdots \\ a_k^{(N)} \end{bmatrix}$$

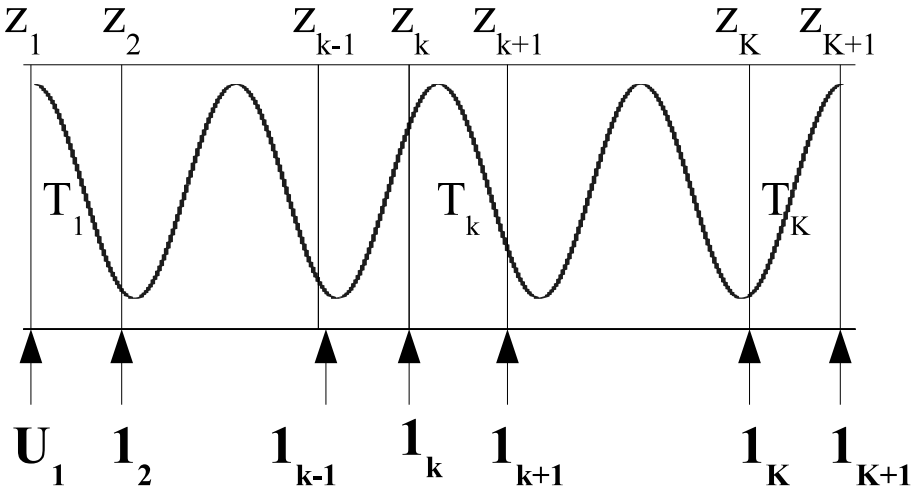

Figure 2.2: This diagram illustrates Equation 2.4. Each T-matrix represents a section and 1 is inserted between sections. The number of sections is given by K, while the actual length of the medium is L. The variable k denotes an arbitrary position.

$\forall i = \{1, \cdots, N\}$ and $\forall k = \{1, \cdots, K+1\}$. This means that for every position, k, there exists a defined vector $\overline{a}_k$, consisting of elements $a_k^{(i)} \in \mathbb{C}$, one for each mode, i. Vector $\overline{a}_k$ is a vector of integration variables, and each of its elements, $a_k^{(i)}$, is the integration variable associated with mode i at position k. This concept is illustrated in Figure 2.3 . With these vectors, the Gaussian integral at a position k, 1_k, takes on the form

$$\begin{aligned} \int \left[\prod_{i=1}^{N} da_k^{(i)*} da_k^{(i)}\right] \exp\left\{-\sum_{i=1}^{N}\left|a_k^{(i)}\right|^2\right\}\left(\overline{a}_k^\dagger \otimes \overline{a}_k\right) &\propto 1 \\ \sharp \int \left[\prod_{i=1}^{N} da_k^{(i)*} da_k^{(i)}\right] \exp\left\{-\left|\overline{a}_k^\dagger \overline{a}_k\right|\right\}\left(\overline{a}_k^\dagger \otimes \overline{a}_k\right) &= 1 \end{aligned}$$

for some constant of proportionality, $\sharp$. In this way a term $T_k 1_k T_{k-1}$ is expressed as

$$\begin{aligned} T_k 1_k T_{k-1} &= T_k\left[\sharp \int \left[\prod_{i=1}^{N} da_k^{(i)*} da_k^{(i)}\right] \exp\left\{-\left|\overline{a}_k^\dagger \overline{a}_k\right|\right\}\left(\overline{a}_k^\dagger \otimes \overline{a}_k\right)\right] T_{k-1} \\ &= \sharp \int \left[\prod_{i=1}^{N} da_k^{(i)*} da_k^{(i)}\right] \exp\left\{-\left|\overline{a}_k^\dagger \overline{a}_k\right|\right\} T_k\left(\overline{a}_k^\dagger \otimes \overline{a}_k\right) T_{k-1} \end{aligned}$$

Hence for all positions k along the medium

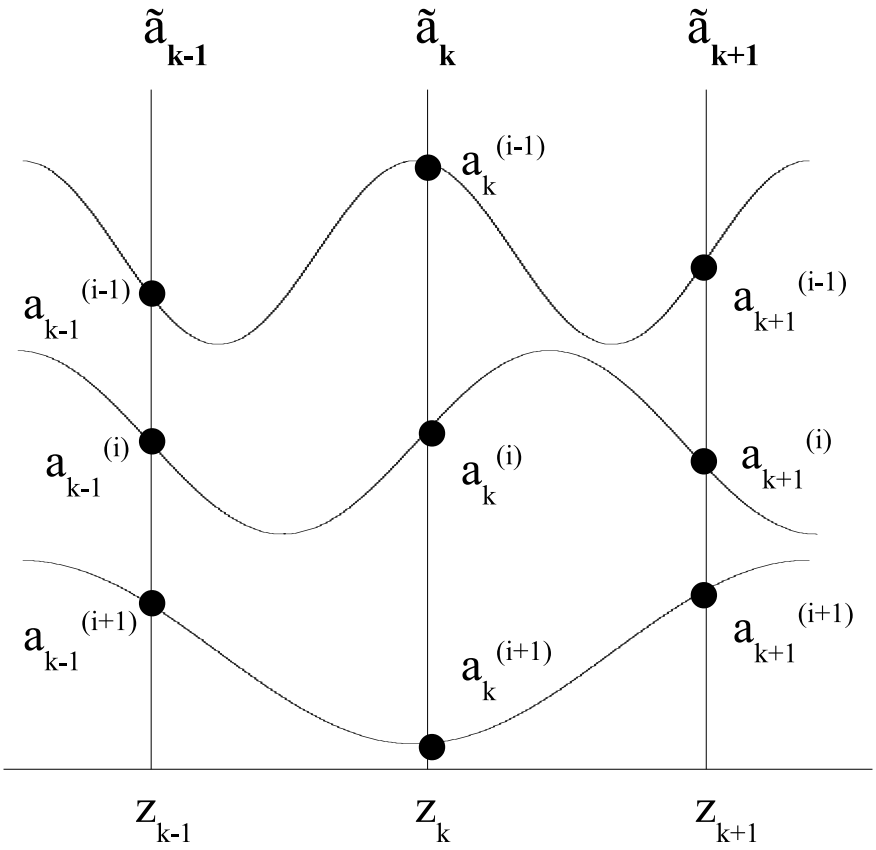

Figure 2.3: This diagram illustrates the concept of the vector $\overline{a}_k$, a vector of integration variables for each mode i at a position k. The curved lines represent the amplitudes of modes $i-1$, i and $i+1$ at position k as they change with distance z.

$$\begin{aligned}
U_{K+1}^{(i)} &= \overline{v}_i^\dagger T \overline{U}_1 \\
&= \overline{v}_i^\dagger \times 1_{K+1} \times T_K \times 1_K \times \cdots \times T_2 \times 1_2 \times T_1 \times \overline{U}_1 \\
&= \sharp \int \left[\prod_{k=2}^{K+1} \prod_{i=1}^{N} da_k^{(i)*} da_k^{(i)} \right] \exp\left\{ - \sum_{k=2}^{K+1} \left| \overline{a}_k^\dagger \overline{a}_k \right| \right\} \\
&\quad \times \overline{v}_i^\dagger \left(\overline{a}_{K+1}^\dagger \otimes \overline{a}_{K+1} \right) T_K \left(\overline{a}_K^\dagger \otimes \overline{a}_K \right) \cdots T_2 \left(\overline{a}_2^\dagger \otimes \overline{a}_2 \right) T_1 \overline{U}_1 \\
&= \sharp \int \left[Da_k^{(i)} \right] \exp\left\{ - \sum_{k=2}^{K+1} \left| \overline{a}_k^\dagger \overline{a}_k \right| \right\} \overline{v}_i^\dagger \left(\overline{a}_{K+1}^\dagger \otimes \overline{a}_{K+1} \right) T_K \left(\overline{a}_K^\dagger \otimes \overline{a}_K \right) \cdots T_2 \left(\overline{a}_2^\dagger \otimes \overline{a}_2 \right) T_1 \overline{U}_1
\end{aligned} \tag{2.5}$$

Here the i and the k are still left in the factor $\left[Da_k^{(i)} \right] = \prod_{k=2}^{K+1} \prod_{i=1}^{N} da_k^{(i)*} da_k^{(i)}$ as a reminder that it represents the product of all modes at all positions, this is merely a notational matter.

Now for both the forward and backward propagating modes, the initial conditions can be derived. It is shown in Appendix that for two arbitrary vectors $\overline{b}_1$ and $\overline{b}_2$

$$\left(\overline{b}_1^\dagger \otimes \overline{b}_1 \right) \overline{b}_2 = \left(\overline{b}_1^\dagger \overline{b}_2 \right) \overline{b}_1 \tag{2.6}$$

So, using Equation 2.6, the initial term $\left(\overline{a}_2^\dagger \otimes \overline{a}_2 \right) T_1 \overline{U}_1$ can be determined as follows:

$$\begin{aligned}
\left(\overline{a}_2^\dagger \otimes \overline{a}_2 \right) T_1 \overline{U}_1 &= \left(\overline{a}_2^\dagger \otimes \overline{a}_2 \right) e^{\Delta z M_1} \overline{U}_1 \\
&= \left(\overline{a}_2^\dagger \otimes \overline{a}_2 \right) (1 + \Delta z M_1) \overline{U}_1 \\
&= \left(\overline{a}_2^\dagger \otimes \overline{a}_2 \right) \overline{U}_1 + \Delta z \left(\overline{a}_2^\dagger \otimes \overline{a}_2 \right) M_1 \overline{U}_1 \\
&= \left(\overline{a}_2^\dagger \overline{U}_1 \right) \overline{a}_2 + \Delta z \left(\overline{a}_2^\dagger M_1 \overline{U}_1 \right) \overline{a}_2 \\
&= \left[1 + \Delta z \frac{\overline{a}_2^\dagger M_1 \overline{U}_1}{\overline{a}_2^\dagger \overline{U}_1} \right] \left(\overline{a}_2^\dagger \overline{U}_1 \right) \overline{a}_2 \\
&= exp\left\{ \Delta z \frac{\overline{a}_2^\dagger M_1 \overline{U}_1}{\overline{a}_2^\dagger \overline{U}_1} \right\} \left(\overline{a}_2^\dagger \overline{U}_1 \right) \overline{a}_2 \\
&= e^{X_1} \left(\overline{a}_2^\dagger \overline{U}_1 \right) \overline{a}_2
\end{aligned}$$

for $X_1 = \Delta z \frac{\overline{a}_2^\dagger M_1 \overline{U}_1}{\overline{a}_2^\dagger \overline{U}_1}$, which is now merely a number[2]. Hence we no longer have the complication of multiplying together a large number of exponential matrices. This initial term, which is only a vector now (the product of two ordinary numbers and a vector), is applied, from the right, to the term $\left(\overline{a}_3^\dagger \otimes \overline{a}_3 \right) T_2$

[2]In the second last step the Taylor series expansion for an exponential was used and higher order terms neglected.

in a similar fashion as follows

$$\begin{aligned}
\left(\overline{a}_3^\dagger \otimes \overline{a}_3\right) T_2 \left(\overline{a}_2^\dagger \otimes \overline{a}_2\right) T_1 \overline{U}_1 &= \left(\overline{a}_3^\dagger \otimes \overline{a}_3\right) T_2 e^{X_1} \left(\overline{a}_2^\dagger \overline{U}_1\right) \overline{a}_2 \\
&= e^{X_1} \left(\overline{a}_2^\dagger \overline{U}_1\right) \left(\overline{a}_3^\dagger \otimes \overline{a}_3\right) T_2 \overline{a}_2 \\
&= e^{X_1} \left(\overline{a}_2^\dagger \overline{U}_1\right) \left(\overline{a}_3^\dagger \otimes \overline{a}_3\right) e^{\Delta z M_2} \overline{a}_2 \\
&= e^{X_1} \left(\overline{a}_2^\dagger \overline{U}_1\right) \left(\overline{a}_3^\dagger \otimes \overline{a}_3\right) \left(1 + \Delta z M_2\right) \overline{a}_2 \\
&= e^{X_1} \left(\overline{a}_2^\dagger \overline{U}_1\right) \left[\left(\overline{a}_3^\dagger \otimes \overline{a}_3\right) \overline{a}_2 + \Delta z \left(\overline{a}_3^\dagger \otimes \overline{a}_3\right) M_2 \overline{a}_2\right] \\
&= e^{X_1} \left(\overline{a}_2^\dagger \overline{U}_1\right) \left[1 + \Delta z \frac{\overline{a}_3^\dagger M_2 \overline{a}_2}{\overline{a}_3^\dagger \overline{a}_2}\right] \left(\overline{a}_3^\dagger \overline{a}_2\right) \overline{a}_3 \\
&= e^{X_1} \left(\overline{a}_2^\dagger \overline{U}_1\right) exp\left\{\Delta z \frac{\overline{a}_3^\dagger M_2 \overline{a}_2}{\overline{a}_3^\dagger \overline{a}_2}\right\} \left(\overline{a}_3^\dagger \overline{a}_2\right) \overline{a}_3 \\
&= e^{X_1} e^{X_2} \left(\overline{a}_2^\dagger \overline{U}_1\right) \left(\overline{a}_3^\dagger \overline{a}_2\right) \overline{a}_3 \\
&= e^{X_1 + X_2} \left(\overline{a}_2^\dagger \overline{U}_1\right) \left(\overline{a}_3^\dagger \overline{a}_2\right) \overline{a}_3
\end{aligned}$$

where $X_2 = \Delta z \frac{\overline{a}_3^\dagger M_2 \overline{a}_2}{\overline{a}_3^\dagger \overline{a}_2}$. For a position, k, this result can be generalized as

$$\begin{aligned}
\left(\overline{a}_{k+1}^\dagger \otimes \overline{a}_{k+1}\right) T_k \overline{a}_k &= \exp\left\{\Delta z \frac{\overline{a}_{k+1}^\dagger M_k \overline{a}_k}{\overline{a}_{k+1}^\dagger \overline{a}_k}\right\} \left(\overline{a}_{k+1}^\dagger \overline{a}_k\right) \overline{a}_{k+1} \\
&= e^{X_{k+1}} \left(\overline{a}_{k+1}^\dagger \overline{a}_k\right) \overline{a}_{k+1}
\end{aligned}$$

where $X_{k+1} = \Delta z \frac{\overline{a}_{k+2}^\dagger M_{k+1} \overline{a}_{k+1}}{\overline{a}_{k+2}^\dagger \overline{a}_{k+1}}$. The output at position $k = K+1$, which consists of the product of all the T_k matrices with the tensor products $\overline{a}_k^\dagger \otimes \overline{a}_k$, contains the term

$$\left(\overline{a}_{K+1}^\dagger \otimes \overline{a}_{K+1}\right) T_K \left(\overline{a}_K^\dagger \otimes \overline{a}_K\right) \cdots \left(\overline{a}_2^\dagger \otimes \overline{a}_2\right) T_1 \left(\overline{a}_1^\dagger \otimes \overline{a}_1\right) \overline{U}_1 = \exp\left\{\sum_{k=1}^{K} X_k\right\} \left(\overline{a}_2^\dagger \overline{U}_1\right) \prod_{k=2}^{K} \left(\overline{a}_{k+1}^\dagger \overline{a}_k\right) \overline{a}_{K+1}$$

where

$$X_k = \Delta z \frac{\overline{a}_{k+1}^\dagger M_k \overline{a}_k}{\overline{a}_{k+1}^\dagger \overline{a}_k}$$

In this generalization $\overline{a}_1 = \overline{U}_1$. Substituting this result back into Equation 2.5 yields

$$U_{K+1}^{(i)} = \sharp \int \left[Da_k^{(i)}\right] \exp\left\{-\sum_{k=2}^{K+1} \left|\overline{a}_k^\dagger \overline{a}_k\right|\right\} \exp\left\{\sum_{k=1}^{K} X_k\right\} \left(\overline{a}_2^\dagger \overline{U}_1\right) \prod_{k=2}^{K} \left(\overline{a}_{k+1}^\dagger \overline{a}_k\right) \overline{v}_i^\dagger \overline{a}_{K+1}.$$

Using the fact that $\prod_n x_n = \exp\left\{\sum_n \ln(x_n)\right\}$, the above discrete integral can be reduced to

$$\begin{aligned} U_{K+1}^{(i)} &= \sharp\int \left[Da_k^{(i)}\right]\left(\overline{a}_2^\dagger \overline{U}_1\right)\left(\overline{v}_i^\dagger \overline{a}_{K+1}\right)\times \\ &\quad \exp\left\{\sum_{k=1}^{K} X_k\right\}\exp\left\{-\sum_{k=2}^{K+1}\left|\overline{a}_k^\dagger \overline{a}_k\right|\right\}\exp\left\{\sum_{k=2}^{K}\ln\left(\overline{a}_{k+1}^\dagger \overline{a}_k\right)\right\} \end{aligned} \tag{2.7}$$

From the definition $\overline{a}_k \equiv \overline{a}(z_k)$, it naturally follows that, in the limit where $\Delta z \to 0$

$$\begin{aligned} \left.\frac{d\overline{a}}{dz}\right|_{z=z_k} &= \frac{\overline{a}(z_{k+1}) - \overline{a}(z_k)}{\Delta z} \\ \dot{\overline{a}}_k &= \frac{\overline{a}_{k+1} - \overline{a}_k}{\Delta z} \\ \overline{a}_{k+1} &= \overline{a}_k + \Delta z \dot{\overline{a}}_k. \end{aligned}$$

Hence in Equation 2.7 it follows that

$$\begin{aligned} \exp\left\{\sum_{k=2}^{K}\ln\left(\overline{a}_{k+1}^\dagger \overline{a}_k\right)\right\} &= \exp\left\{\sum_{k=2}^{K}\ln\left[\left(\overline{a}_k + \Delta z\dot{\overline{a}}_k\right)^\dagger \overline{a}_k\right]\right\} \\ &= \exp\left\{\sum_{k=2}^{K}\ln\left[\overline{a}_k^\dagger \overline{a}_k + \Delta z\dot{\overline{a}}_k{}^\dagger \overline{a}_k\right]\right\} \\ &= \exp\left\{\sum_{k=2}^{K}\ln\left[\overline{a}_k^\dagger \overline{a}_k\left(1 + \Delta z\frac{\dot{\overline{a}}_k{}^\dagger \overline{a}_k}{\overline{a}_k^\dagger \overline{a}_k}\right)\right]\right\} \\ &= \exp\left\{\sum_{k=2}^{K}\left[\ln\left(\overline{a}_k^\dagger \overline{a}_k\right) + \ln\left(1 + \Delta z\frac{\dot{\overline{a}}_k{}^\dagger \overline{a}_k}{\overline{a}_k^\dagger \overline{a}_k}\right)\right]\right\}. \end{aligned}$$

In the limit where $\Delta z \to 0$ the approximation can be made[3],

$$\ln\left(1 + \Delta z\frac{\dot{\overline{a}}_k{}^\dagger \overline{a}_k}{\overline{a}_k^\dagger \overline{a}_k}\right) \approx \Delta z\frac{\dot{\overline{a}}_k{}^\dagger \overline{a}_k}{\overline{a}_k^\dagger \overline{a}_k}$$

so that

$$\begin{aligned} \exp\left\{\sum_{k=2}^{K}\ln\left(\overline{a}_{k+1}^\dagger \overline{a}_k\right)\right\} &= \exp\left\{\sum_{k=2}^{K}\left[\ln\left(\overline{a}_k^\dagger \overline{a}_k\right) + \Delta z\frac{\dot{\overline{a}}_k{}^\dagger \overline{a}_k}{\overline{a}_k^\dagger \overline{a}_k}\right]\right\} \\ &= \exp\left\{\sum_{k=2}^{K}\ln\left(\overline{a}_k^\dagger \overline{a}_k\right)\right\}\exp\left\{\sum_{k=2}^{K}\Delta z\frac{\dot{\overline{a}}_k{}^\dagger \overline{a}_k}{\overline{a}_k^\dagger \overline{a}_k}\right\}. \end{aligned}$$

Hence the discrete integral of Equation 2.7 further evolves in form to

$$\begin{aligned} U_{K+1}^{(i)} &= \sharp\int \left[Da_k^{(i)}\right]\left(\overline{a}_2^\dagger \overline{U}_1\right)\left(\overline{v}_i^\dagger \overline{a}_{K+1}\right)\times \\ &\quad \exp\left\{\sum_{k=1}^{K} X_k\right\}\exp\left\{-\sum_{k=2}^{K+1}\left|\overline{a}_k^\dagger \overline{a}_k\right|\right\}\exp\left\{\sum_{k=2}^{K}\ln\left(\overline{a}_k^\dagger \overline{a}_k\right)\right\}\exp\left\{\sum_{k=2}^{K}\Delta z\frac{\dot{\overline{a}}_k{}^\dagger \overline{a}_k}{\overline{a}_k^\dagger \overline{a}_k}\right\}. \end{aligned} \tag{2.8}$$

[3]The Taylor series expansion, $\ln(1+x) = x + O(x^2)$ for $x \ll 1$, is used.

2.1.1 Condition of Constraint

The discrete path integral of Equation 2.8 consists of factors dependent on Δz (including X_k) and others that are independent of Δz. After some rearranging, those factors dependent on Δz are grouped together in the first exponential factor:

$$\begin{aligned} U_{K+1}^{(i)} &= \sharp \int \left[Da_k^{(i)}\right] \left(\overline{a}_2^\dagger \overline{U}_1\right) \left(\overline{v}_i^\dagger \overline{a}_{K+1}\right) \times \\ &\quad \exp\left\{\sum_{k=1}^{K} X_k + \sum_{k=2}^{K} \Delta z \frac{\dot{\overline{a}}_k{}^\dagger \overline{a}_k}{\overline{a}_k^\dagger \overline{a}_k}\right\} \exp\left\{-\sum_{k=2}^{K+1} \left|\overline{a}_k^\dagger \overline{a}_k\right| + \sum_{k=2}^{K} \ln\left(\overline{a}_k^\dagger \overline{a}_k\right)\right\}. \end{aligned} \tag{2.9}$$

In the path integral formalism, one obtains the path integral from the discrete integral by taking the number of spatial slices of the discrete path integral to infinity, such that the replacement $\sum_{k=1}^{K} \Delta z \to \int_0^L dz$ can be made. However, to achieve this the exponential factor that is independent of Δz needs to be modified in the following way

$$\begin{aligned} \exp\left\{-\sum_{k=2}^{K+1} \left|\overline{a}_k^\dagger \overline{a}_k\right| + \sum_{k=2}^{K} \ln\left(\overline{a}_k^\dagger \overline{a}_k\right)\right\} &= \exp\left\{-\frac{1}{\Delta z}\sum_{k=2}^{K+1} \Delta z \left|\overline{a}_k^\dagger \overline{a}_k\right| + \frac{1}{\Delta z}\sum_{k=2}^{K} \Delta z \ln\left(\overline{a}_k^\dagger \overline{a}_k\right)\right\} \\ &= \exp\left\{-\frac{K}{L}\int dz \left(\left|\overline{a}^\dagger(z)\,\overline{a}(z)\right| - \ln\left(\overline{a}^\dagger(z)\,\overline{a}(z)\right)\right)\right\}. \end{aligned}$$

As $K \to \infty$ this integral can be treated exactly in the saddle-point approximation.

Let $F\left[\overline{a}^\dagger \overline{a}\right]$ be the functional where

$$F\left[\overline{a}^\dagger \overline{a}\right] = \int dz \left[\left|\overline{a}^\dagger(z)\,\overline{a}(z)\right| - \ln\left(\overline{a}^\dagger(z)\,\overline{a}(z)\right)\right].$$

To find F's stationary point one takes the functional derivative

$$\begin{aligned} \frac{\delta}{\delta\left(\overline{a}^\dagger(z')\,\overline{a}(z')\right)} F\left[\overline{a}^\dagger \overline{a}\right] &= 0 \\ \frac{\delta}{\delta\left(\overline{a}^\dagger(z')\,\overline{a}(z')\right)} \int dz \left[\left|\overline{a}^\dagger(z)\,\overline{a}(z)\right| - \ln\left(\overline{a}^\dagger(z)\,\overline{a}(z)\right)\right] &= 0 \\ 1 - \frac{1}{\overline{a}^\dagger(z')\,\overline{a}(z')} &= 0 \\ \overline{a}^\dagger(z')\,\overline{a}(z') &= 1. \end{aligned}$$

The path integral is thus constrained to a set of normalized vectors, $\overline{a}^\dagger(z)\,\overline{a}(z) = 1$.

Substitution into the functional F yields the constant

$$\begin{aligned} \exp\left\{-\frac{K}{L}\int_0^L dz \left[\left|\overline{a}^\dagger(z)\,\overline{a}(z)\right| - \ln\left(\overline{a}^\dagger(z)\,\overline{a}(z)\right)\right]\right\} &= \exp\left\{-\frac{K}{L}\int_0^L dz\right\} \\ &= e^{-K} \end{aligned}$$

where the fluctuations are completely suppressed due to the $K \to \infty$ limit. Of course in the limit $K \to \infty$, $e^{-K} \to 0$. However, upon normalizing the generating functional later, the constant is canceled and thus it is carried along for the moment

The Δz-dependent terms in the discrete integral (Equation 2.9) are reduced under the condition of

the constraint as follows

$$\begin{aligned}
\exp\left\{\sum_{k=1}^{K} X_k + \sum_{k=2}^{K} \Delta z \frac{\dot{\overline{a}_k}^{\dagger}\overline{a}_k}{\overline{a}_k^{\dagger}\overline{a}_k}\right\} &= \exp\left\{\sum_{k=1}^{K} \Delta z \frac{\overline{a}_{k+1}^{\dagger} M_k \overline{a}_k}{\overline{a}_{k+1}^{\dagger}\overline{a}_k} + \sum_{k=2}^{K} \Delta z \frac{\dot{\overline{a}_k}^{\dagger}\overline{a}_k}{\overline{a}_k^{\dagger}\overline{a}_k}\right\} \\
&= \exp\left\{\sum_{k=1}^{K} \Delta z \frac{\left(\overline{a}_k + \Delta z \dot{\overline{a}_k}\right)^{\dagger} M_k \overline{a}_k}{\left(\overline{a}_k + \Delta z \dot{\overline{a}_k}\right)^{\dagger}\overline{a}_k} + \sum_{k=2}^{K} \Delta z \dot{\overline{a}_k}^{\dagger}\overline{a}_k\right\} \\
&= \exp\left\{\sum_{k=1}^{K} \Delta z \frac{\overline{a}_k^{\dagger} M_k \overline{a}_k}{\overline{a}_k^{\dagger}\overline{a}_k + \Delta z \dot{\overline{a}_k}^{\dagger}\overline{a}_k} + (\Delta z)^2 \frac{\dot{\overline{a}_k}^{\dagger} M_k \overline{a}_k}{\overline{a}_k^{\dagger}\overline{a}_k + \Delta z \dot{\overline{a}_k}^{\dagger}\overline{a}_k} + \sum_{k=2}^{K} \Delta z \dot{\overline{a}_k}^{\dagger}\overline{a}_k\right\}
\end{aligned}$$

However, $\overline{a}_k^{\dagger}\overline{a}_k = 1$ and $\Delta z \ll 1$, such that

$$\exp\left\{\sum_{k=1}^{K} X_k + \sum_{k=2}^{K} \Delta z \frac{\dot{\overline{a}_k}^{\dagger}\overline{a}_k}{\overline{a}_k^{\dagger}\overline{a}_k}\right\} = \exp\left\{\sum_{k=1}^{K} \Delta z \overline{a}_k^{\dagger} M_k \overline{a}_k + \sum_{k=2}^{K} \Delta z \dot{\overline{a}_k}^{\dagger}\overline{a}_k\right\}.$$

After these simplifications the discrete path integral is significantly reduced to

$$\begin{aligned}
U_{K+1}^{(i)} &= \sharp \int \left[Da_k^{(i)}\right] \left(\overline{a}_2^{\dagger}\overline{U}_1\right) \left(\overline{v}_i^{\dagger}\overline{a}_{K+1}\right) \times \\
&\quad e^{-K} \exp\left\{\sum_{k=1}^{K} \Delta z \overline{a}_k^{\dagger} M_k \overline{a}_k\right\} \exp\left\{\sum_{k=2}^{K} \Delta z \dot{\overline{a}_k}^{\dagger}\overline{a}_k\right\}
\end{aligned}$$

To obtain the path integral, the continuous limit is taken. This yields:

$$\begin{aligned}
U^{(i)}(L) &= \# \int \left[Da^{(i)}(z)\right] \left(\overline{a}^{\dagger}(0)\overline{U}_1\right) \left(\overline{v}_i^{\dagger}\overline{a}(L)\right) \times \\
&\quad e^{-K} \exp\left\{\int dz \overline{a}^{\dagger}(z) M(z) \overline{a}(z)\right\} \exp\left\{\int dz \dot{\overline{a}}^{\dagger}(z) \overline{a}(z)\right\}. \qquad (2.10)
\end{aligned}$$

2.1.2 The source terms and the generating functional

The next step is to formulate a generating functional from the path integral of Equation 2.10. A generating functional is a generalized path integral. However, it is a very powerful tool because depending on how one differentiates the generating functional with respect to certain source terms, any information regarding the manner in which the amplitudes propagate can be obtained.

The boundary conditions for the system lie in the two factors $\left(\overline{a}^{\dagger}(0)\overline{U}_1\right)$ and $\left(\overline{v}_i^{\dagger}\overline{a}(L)\right)$. The first of these is the projection of the initial condition $\overline{U}_1$ onto the first vector integration variable. The second factor is the projection of the amplitude at the end of the medium with the basis vector of the particular mode of interest. Being an inner product of two vectors both these factors are merely numbers. We can handle these numbers by introducing a source term for each into the path integral, this way constructing

a generating functional. This generating functional is given by

$$\begin{aligned} W\left[\bar{J}^{\dagger}(z),\bar{J}(z)\right] &= \sharp\int\left[Da^{(i)}(z)\right]e^{-K}\exp\left\{\int dz\overline{a}^{\dagger}(z)M(z)\overline{a}(z)\right\}\times \\ &\quad \exp\left\{\int dz\dot{\overline{a}}^{\dagger}(z)\overline{a}(z)\right\}\exp\left\{\int dz\bar{J}^{\dagger}(z)\overline{a}(z)\right\}\exp\left\{\int dz\overline{a}^{\dagger}(z)\bar{J}(z)\right\} \\ &= \sharp\int\left[Da^{(i)}(z)\right]e^{-K}\times \\ &\quad \exp\left\{\int dz\left(\overline{a}^{\dagger}(z)M(z)\overline{a}(z)-\overline{a}^{\dagger}(z)\frac{d\overline{a}}{dz}+\bar{J}^{\dagger}(z)\overline{a}(z)+\overline{a}^{\dagger}(z)\bar{J}(z)\right)\right\} \\ W\left[\bar{J}^{\dagger}(z),\bar{J}(z)\right] &= \sharp e^{-K}\int\left[Da^{(i)}(z)\right]\times \\ &\quad \exp\left\{\int dz\left(\overline{a}^{\dagger}(z)\hat{\Gamma}\overline{a}(z)+\bar{J}^{\dagger}(z)\overline{a}(z)+\overline{a}^{\dagger}(z)\bar{J}(z)\right)\right\} \end{aligned} \tag{2.11}$$

where

$$\hat{\Gamma} = M(z)-\frac{d}{dz} \tag{2.12}$$

is an operator.

The original path integral can be obtained from the generating functional by functional differentiation of Equation 2.11 with respect to the source terms. The following calculation demonstrates this.

$$\begin{aligned} \frac{\delta}{\delta J_i^*(0)\,\delta J_j(L)}W\left[\bar{J}^{\dagger}(z),\bar{J}(z)\right] &= \frac{\delta}{\delta J_i^*(0)\,\delta J_j(L)}\left(\sharp e^{-K}\int\left[Da^{(i)}(z)\right]\times\right. \\ &\quad \left.\exp\left\{\int dz\left(\overline{a}^{\dagger}(z)\hat{\Gamma}\overline{a}(z)+\bar{J}^{\dagger}(z)\overline{a}(z)+\overline{a}^{\dagger}(z)\bar{J}(z)\right)\right\}\right) \\ &= \frac{\delta}{\delta J_i^*(0)}\left(\sharp e^{-K}\int\left[Da^{(i)}(z)\right]\times\right. \\ &\quad \left.a_j^{\dagger}(L)\exp\left\{\int dz\left(\overline{a}^{\dagger}(z)\hat{\Gamma}\overline{a}(z)+\bar{J}^{\dagger}(z)\overline{a}(z)+\overline{a}^{\dagger}(z)\bar{J}(z)\right)\right\}\right) \\ &= \sharp e^{-K}\int\left[Da^{(i)}(z)\right]\times \\ &\quad a_i(0)\,a_j^{\dagger}(L)\exp\left\{\int dz\left(\overline{a}^{\dagger}(z)\hat{\Gamma}\overline{a}(z)+\bar{J}^{\dagger}(z)\overline{a}(z)+\overline{a}^{\dagger}(z)\bar{J}(z)\right)\right\} \end{aligned}$$

The source terms are set to zero and the path integral of Equation 2.10 results

$$\begin{aligned} \frac{\delta}{\delta J_i^*(0)\,\delta J_j(L)}W\left[\bar{J}^{\dagger}(z),\bar{J}(z)\right]\Big|_{J=J^{\dagger}=0} &= \sharp e^{-K}\int\left[Da^{(i)}(z)\right]\times \\ &\quad a_i(0)\,a_j^{\dagger}(L)\exp\left\{\int dz\left(\overline{a}^{\dagger}(z)\hat{\Gamma}\overline{a}(z)\right)\right\} \\ &= U^{(i)}(L) \end{aligned}$$

A solution for the generating functional must be obtained next.

In the generating functional 2.11 one must complete the square to obtain a quadratic action, as the

argument for the exponential, for which the solution is easily obtained. Completing the square,

$$\begin{aligned}\overline{a}^{\dagger}(z)\hat{\Gamma}\overline{a}(z)+\bar{J}^{\dagger}(z)\overline{a}(z)+\overline{a}^{\dagger}(z)\bar{J}(z) &= \left(\overline{a}^{\dagger}(z)+\bar{J}^{\dagger}(z)\hat{\Gamma}^{-1}\right)\hat{\Gamma}\left(\overline{a}(z)+\hat{\Gamma}^{-1}\bar{J}(z)\right)\\ &\quad -\bar{J}^{\dagger}(z)\hat{\Gamma}^{-1}\bar{J}(z)\end{aligned}$$

so that the generating functional, with $\left[Da^{(i)}(z)\right]=\prod_{i=1}^{N}da^{\dagger(i)}(z)\,da^{(i)}(z)$, becomes

$$\begin{aligned}W\left[\bar{J}^{\dagger}(z),\bar{J}(z)\right] &= \sharp e^{-K}\int\left[Da^{(i)}(z)\right]\times\\ &\quad \exp\left\{\int dz\left(\overline{a}^{\dagger}(z)+\bar{J}^{\dagger}(z)\hat{\Gamma}^{-1}\right)\hat{\Gamma}\left(\overline{a}(z)+\hat{\Gamma}^{-1}\bar{J}(z)\right)\right\}\times\\ &\quad \exp\left\{-\int dz\left(\bar{J}^{\dagger}(z)\hat{\Gamma}^{-1}\bar{J}(z)\right)\right\}.\end{aligned}$$

Making the following transformation

$$\overline{y}(z) = \overline{a}(z)+\hat{\Gamma}^{-1}\bar{J}(z)$$

it follows that

$$\begin{aligned}\overline{y}^{\dagger}(z) &= \left(\overline{a}(z)+\hat{\Gamma}^{-1}\bar{J}(z)\right)^{\dagger}\\ &= \overline{a}^{\dagger}(z)+\left(\hat{\Gamma}^{-1}\bar{J}(z)\right)^{\dagger}\\ &= \overline{a}^{\dagger}(z)+\left(\bar{J}(z)\right)^{\dagger}\left(\hat{\Gamma}^{-1}\right)^{\dagger}\\ &= \overline{a}^{\dagger}(z)+\bar{J}^{\dagger}(z)\hat{\Gamma}^{-1}.\end{aligned}$$

In addition $dy^{(i)*}(z)=da^{(i)*}(z)$ and $dy^{(i)}(z)=da^{(i)}(z)$ so that the generating functional is reduced to

$$\begin{aligned}W\left[\bar{J}^{\dagger}(z),\bar{J}(z)\right] &= \sharp\int\left[Dy^{(i)}(z)\right]e^{-K}\exp\left[\int dz\left(\overline{y}^{\dagger}\hat{\Gamma}\overline{y}-\bar{J}^{\dagger}(z)\hat{\Gamma}^{-1}\bar{J}(z)\right)\right]\\ &= \sharp e^{-K}e^{-\int dz\left[\bar{J}^{\dagger}(z)\hat{\Gamma}^{-1}\bar{J}(z)\right]}\int\left[Dy^{(i)}(z)\right]e^{\int dz\left[\overline{y}^{\dagger}\hat{\Gamma}\overline{y}\right]}\end{aligned}$$

This functional integral is well known:

$$\int\left[Dy^{(i)}(z)\right]e^{\int dz\left[\overline{y}^{\dagger}\hat{\Gamma}\overline{y}\right]} = \frac{1}{\sqrt{\det\left(\hat{\Gamma}\right)}}$$

yielding the well known form of the generating functional

$$W\left[\bar{J}^{\dagger}(z),\bar{J}(z)\right] = \frac{\sharp e^{-K}e^{-\int dz\left[\bar{J}^{\dagger}(z)\hat{\Gamma}^{-1}\bar{J}(z)\right]}}{\sqrt{\det\left(\hat{\Gamma}\right)}} \tag{2.13}$$

We can normalize $W\left[\bar{J}^{\dagger}(z),\bar{J}(z)\right]$ in the following way

$$\begin{aligned} Z\left[\bar{J}^{\dagger}(z),\bar{J}(z)\right] &= \frac{W\left[J(z),J^{\dagger}(z)\right]}{W\left[J(z)=0,J^{\dagger}(z)=0\right]} \\ &= \frac{\frac{\sharp e^{-K} e^{-\int dz\left[\bar{J}^{\dagger}(z)\hat{\Gamma}^{-1}\bar{J}(z)\right]}}{\sqrt{\det\left(\hat{\Gamma}\right)}}}{\frac{\sharp e^{-K} e^{-\int dz\left[0\hat{\Gamma}^{-1}0\right]}}{\sqrt{\det\left(\hat{\Gamma}\right)}}} \\ &= \frac{\sharp e^{-K} e^{-\int dz\left[\bar{J}^{\dagger}(z)\hat{\Gamma}^{-1}\bar{J}(z)\right]}}{\sqrt{\det\left(\hat{\Gamma}\right)}} \times \frac{\sqrt{\det\left(\hat{\Gamma}\right)}}{\sharp e^{-K}} \\ Z\left[\bar{J}^{\dagger}(z),\bar{J}(z)\right] &= e^{-\int dz\left[\bar{J}^{\dagger}(z)\hat{\Gamma}^{-1}\bar{J}(z)\right]} \end{aligned} \tag{2.14}$$

Functional differentiation of $Z\left[\bar{J}^{\dagger}(z),\bar{J}(z)\right]$ yields

$$\frac{\delta}{\delta J_i^*(0)\,\delta J_j(L)} Z\left[\bar{J}^{\dagger}(z),\bar{J}(z)\right]\Big|_{J=J^{\dagger}=0} = \hat{\Gamma}^{-1}$$

Here $\hat{\Gamma}^{-1}$ is a Green's function also called a propagator, which describes the evolution of the amplitudes. The specific Green's function corresponds to a specific choice of boundary conditions. Applying a certain set of initial conditions, the propagator describes exactly how the amplitudes propagate. The Green's function has to be calculated explicitly under the conditions relevant to the application.

In summary, a path integral was set up by discretizing the medium. The path integral was generalized to formulate the generating functional. The functional differentiation of the generating functional yields the Green's function.

2.2 Calculating $\hat{\Gamma}^{-1}$

In matrix representation $\hat{\Gamma} = M - \frac{d}{dz}$ can be expressed as

$$\hat{\Gamma} = \begin{bmatrix} M_{11}(z)-\frac{d}{dz} & M_{12}(z) & \cdots & \cdots & M_{1N}(z) \\ M_{21}(z) & M_{22}(z)-\frac{d}{dz} & \cdots & \cdots & M_{2N}(z) \\ \vdots & \vdots & \ddots & \cdots & \vdots \\ \vdots & \vdots & \vdots & \ddots & \vdots \\ M_{N1}(z) & M_{N2}(z) & \cdots & \cdots & M_{NN}(z)-\frac{d}{dz} \end{bmatrix}.$$

It holds that $\hat{\Gamma}\hat{\Gamma}^{-1} = \mathrm{I}$, where $\hat{\Gamma}^{-1}$ is the Green's operator. So, let $\hat{G} = \hat{\Gamma}^{-1}$and note that $G(z,z')$, in function notation is equivalent to the operator $\hat{G}$ then,

$$\begin{aligned}
\hat{\Gamma}G\left(z,z'\right) &= \frac{1}{2\pi}\int_{-\infty}^{\infty} dke^{ik\cdot\left(z-z'\right)} \\
G\left(z,z'\right) &= \frac{1}{2\pi}\int_{-\infty}^{\infty} dk\hat{\Gamma}^{-1}e^{ik\cdot\left(z-z'\right)} \\
G\left(z,z'\right) &= \frac{1}{2\pi}\int_{-\infty}^{\infty} dk\left(M\left(z\right)-\frac{d}{dz}\right)^{-1}e^{ik\cdot\left(z-z'\right)}.
\end{aligned}$$

Here z and z' can be interpreted as the final and initial positions respectively. Making use of a Taylor series expansion we obtain a power series for $\hat{\Gamma}^{-1}$ in the following way

$$\begin{aligned}
\left(M\left(z\right)-\frac{d}{dz}\right)^{-1} &= \left(M\left(z\right)\left(1-M\left(z\right)^{-1}\frac{d}{dz}\right)\right)^{-1} \\
&= \left(1-M\left(z\right)^{-1}\frac{d}{dz}\right)^{-1}M\left(z\right)^{-1} \\
&= \left(1+M\left(z\right)^{-1}\frac{d}{dz}+\left(M\left(z\right)^{-1}\frac{d}{dz}\right)^{2}+\cdots\right)M\left(z\right)^{-1} \\
&= \sum_{n=0}^{\infty}\left(M\left(z\right)^{-1}\frac{d}{dz}\right)^{n}M\left(z\right)^{-1}.
\end{aligned}$$

Now if the coupling matrix $M\left(z\right)$ was independent of z i.e. $M\left(z\right)=M_0$ then

$$\left(M_0-\frac{d}{dz}\right)^{-1} = \sum_{n=0}^{\infty}M_0^{-n-1}\frac{d^n}{dz^n}$$

From this it follows that

$$\begin{aligned}
G\left(z,z'\right) &= \frac{1}{2\pi}\int_{-\infty}^{\infty} dk\sum_{n=0}^{\infty}M_0^{-n-1}\frac{d^n}{dz^n}e^{ik\cdot\left(z-z'\right)} \\
&= \frac{1}{2\pi}\int_{-\infty}^{\infty} dk\sum_{n=0}^{\infty}M_0^{-n-1}\left(ik\right)^n e^{ik\cdot\left(z-z'\right)} \\
&= \frac{1}{2\pi}\int_{-\infty}^{\infty} dkM_0^{-1}\left(1-ikM_0^{-1}\right)^{-1}e^{ik\cdot\left(z-z'\right)} \\
&= \frac{1}{2\pi}\int_{-\infty}^{\infty} dk\left(M_0-ik\right)^{-1}e^{ik\cdot\left(z-z'\right)}. \qquad (2.15)
\end{aligned}$$

This is the propagator used for a homogeneous medium. M_0 is the $N\times N$ coupling matrix coupling (or not coupling in the homogeneous case) N optical modes in the waveguide.

When investigating the case where the coupling matrix is dependent on z, perturbation theory is

employed. As seen above

$$\begin{aligned}\hat{\Gamma}\hat{G} &= \mathrm{I} \\ \hat{G} &= \hat{\Gamma}^{-1}\end{aligned}$$

We can separate $M(z)$ into its unperturbed and perturbing parts, $M(z) = M_0 + \Delta M(z)$. The operator $\hat{\Gamma}$ is modified in the following way

$$\begin{aligned}\hat{\Gamma} &= M_0 - \frac{d}{dz} + \Delta M \\ &= \hat{\Gamma}_0 + \Delta M.\end{aligned}$$

Expanding $\hat{\Gamma}^{-1} = \left(\hat{\Gamma}_0 + \Delta M\right)^{-1}$ in a Taylor series

$$\begin{aligned}\left(\hat{\Gamma}_0 + \Delta M\right)^{-1} &= \left(\hat{\Gamma}_0\left(1 + \hat{\Gamma}_0^{-1}\Delta M\right)\right)^{-1} \\ &= \left(1 + \hat{\Gamma}_0^{-1}\Delta M\right)^{-1}\Gamma_0^{-1} \\ &= \left(1 - \hat{\Gamma}_0^{-1}\Delta M + \left(\hat{\Gamma}_0^{-1}\Delta M\right)^2 - \ldots\right)\Gamma_0^{-1} \\ &= \sum_{n=0}^{\infty}(-1)^n\left(\hat{\Gamma}_0^{-1}\Delta M\right)^n\hat{\Gamma}_0^{-1} \\ &= \sum_{n=0}^{\infty}(-1)^n\hat{\Gamma}_0^{-n}\Delta M^n\hat{\Gamma}_0^{-1}\end{aligned}$$

Again taking the first order approximation

$$\left(\hat{\Gamma}_0 + \Delta M\right)^{-1} = \hat{\Gamma}_0^{-1} - \hat{\Gamma}_0^{-1}\Delta M\hat{\Gamma}_0^{-1}.$$

In this way

$$\begin{aligned}\langle z'|\,\hat{G}\,|z\rangle &= \langle z'|\,\hat{\Gamma}^{-1}\,|z\rangle \\ &= \langle z'|\left(\hat{\Gamma}_0 + \Delta M\right)^{-1}|z\rangle \\ &= \langle z'|\left(\hat{\Gamma}_0^{-1} - \hat{\Gamma}_0^{-1}\Delta M\hat{\Gamma}_0^{-1}\right)|z\rangle \\ &= \langle z'|\,\hat{\Gamma}_0^{-1}\,|z\rangle - \langle z'|\,\hat{\Gamma}_0^{-1}\Delta M\hat{\Gamma}_0^{-1}\,|z\rangle \\ &= \langle z'|\,\hat{G}_0\,|z\rangle - \langle z'|\,\hat{G}_0\Delta M\hat{G}_0\,|z\rangle \\ &= \langle z'|\,\hat{G}_0\,|z\rangle - \langle z'|\,\hat{G}_0 1\Delta M 1\hat{G}_0\,|z\rangle\,.\end{aligned}$$

In the final step the 1s were introduced where $1 = \int dx \left|x\right\rangle \left\langle x\right|$. Hence

$$\begin{aligned} G\left(z,z'\right) &= G_0\left(z,z'\right) - \left\langle z'\right| \hat{G}_0 \int dx \left|x\right\rangle \left\langle x\right| \Delta M \int dy \left|y\right\rangle \left\langle y\right| \hat{G}_0 \left|z\right\rangle \\ &= G_0\left(z,z'\right) - \int dx \int dy \left\langle z'\right| \hat{G}_0 \left|x\right\rangle \left\langle x\right| \Delta M \left|y\right\rangle \left\langle y\right| \hat{G}_0 \left|z\right\rangle \\ &= G_0\left(z,z'\right) - \int dx \int dy G_0\left(x,z'\right) \Delta M\left(y\right) \left\langle x\right| \left. y\right\rangle G_0\left(z,y\right) \\ &= G_0\left(z,z'\right) - \int dx \int dy G_0\left(x,z'\right) \Delta M\left(y\right) \delta\left(x-y\right) G_0\left(z,y\right). \end{aligned}$$

Using the fact that $\int dy \Delta M\left(y\right) \delta\left(x-y\right) G_0\left(z,y\right) = \Delta M\left(x\right) G_0\left(z,x\right)$ it follows that

$$G\left(z,z'\right) = G_0\left(z,z'\right) - \int dx G_0\left(x,z'\right) \Delta M\left(x\right) G_0\left(z,x\right)$$

For the case where M_0 has no z-dependence, $G_0\left(z,z'\right)$ is merely the solution to the problem where the coupling coefficients are z-independent, that is the solution of Equation 2.15. The final solution for the Green's function correct only to a first order in perturbation theory is thus given by

$$\begin{aligned} G\left(z,z'\right) &= \int_{-\infty}^{\infty} \frac{dk}{2\pi} \left(M_0 - ik\right)^{-1} e^{ik\cdot\left(z-z'\right)} \\ &\quad - \int_{-\infty}^{\infty} \frac{dk}{2\pi} \int_{-\infty}^{\infty} \frac{dq}{2\pi} \int dx \left(M_0 - ik\right)^{-1} e^{ik\cdot\left(x-z'\right)} \Delta M\left(x\right) \left(M_0 - iq\right)^{-1} e^{iq\cdot\left(z-x\right)}. \end{aligned} \quad (2.16)$$

Chapter 3

The Homogeneous Waveguide & the Unperturbed Propagator

Having derived a path integral, generating functional and the associated Green's function, it remains to establish whether the propagator does indeed predict the correct behaviour of modes propagating through a medium. In this chapter the propagator's results for the evolution of two modes through a homogeneous waveguide are presented. This application serves as a basic test for the applicability of the propagator to propagation in a waveguide. The application also provides a simple backdrop for developing the mathematical framework for solving these integrals as well as insight into the physical significance of the mathematical foundation.

3.1 Transforming the coupled-mode equations

The coupled-mode equations for forward and backward propagating modes, most often used in literature [12, 3, 2], are of the form

$$\frac{dF_\mu}{dz} = -i\sum_\nu C_{\mu\nu}F_\nu e^{-i(\beta_\nu-\beta_\mu)z} - i\sum_\nu C_{\mu\nu}B_\nu e^{i(\beta_\nu+\beta_\mu)z} \tag{3.1}$$

$$\frac{dB_\mu}{dz} = i\sum_\nu C_{\mu\nu}F_\nu e^{-i(\beta_\nu+\beta_\mu)z} + i\sum_\nu C_{\mu\nu}B_\nu e^{i(\beta_\nu-\beta_\mu)z}. \tag{3.2}$$

These equations account explicitly for both forward, F_μ and backward, B_μ propagating modes, unlike those derived in Section 1.2, given by Equation 1.21. $C_{\nu\mu}$ denotes the coupling coefficient between modes μ and ν and is given by Equation 1.26. Equations 3.1 and 3.2 reveal that for the homogeneous waveguide, where the coupling coefficients are zero, the entire system of equations reduces to the trivial case. This comes about because for a homogeneous medium there is no perturbation to the permittivity, $\Delta\varepsilon = 0$ in Equation 1.20. Hence the coupling coefficients vanish. This however, can be corrected for with the use of a suitable transformation. The following transformations are made:

$$\tilde{F}_\nu = F_\nu e^{-i\beta_\nu z}$$
$$\tilde{B}_\nu = B_\nu e^{i\beta_\nu z}.$$

In these transformations the rapidly varying z-dependence of the optical mode, $\exp(-i\beta_\mu z)$, is incorporated in the amplitude (compare to Equation 1.4). $\tilde{F}_\mu(z)$ and $\tilde{B}_\mu(z)$ describe the complex amplitude of the electric field of mode μ as it varies in the longitudinal (or z) direction for the forward and backward modes respectively. Subsequently $\tilde{F}_\mu(z)$ and $\tilde{B}_\mu(z)$ will be referred to as the amplitudes of the mode μ.

Substituting these transformations into Equations 3.1 and 3.2 the modified coupled-mode equations are given by

$$\frac{d}{dz}\tilde{F}_\mu = -i\sum_\nu^N (C_{\nu\mu}+\beta_\nu\delta_{\nu\mu})\tilde{F}_\nu - i\sum_\nu^N C_{\nu\mu}\tilde{B}_\nu \tag{3.3}$$

$$\frac{d}{dz}\tilde{B}_\mu = i\sum_\nu^N C_{\nu\mu}\tilde{F}_\nu + i\sum_\nu^N (C_{\nu\mu}+\beta_\nu\delta_{\nu\mu})\tilde{B}_\nu. \tag{3.4}$$

Equations 3.3 and 3.4 are simplified further by noting that for the homogeneous waveguide all the coupling coefficients are zero yielding

$$\frac{d}{dz}\tilde{F}_\mu = -i\textstyle\sum_\nu^N \beta_\nu\delta_{\nu\mu}\tilde{F}_\nu = -i\beta_\mu\tilde{F}_\mu \tag{3.5}$$

$$\frac{d}{dz}\tilde{B}_\mu = i\textstyle\sum_\nu^N \beta_\nu\delta_{\nu\mu}\tilde{B}_\nu = i\beta_\mu\tilde{B}_\mu. \tag{3.6}$$

3.2 The case of two forward propagating modes in an unperturbed medium

For the case of two forward propagating modes, the coupled-mode equations of Equation 3.5 are

$$\begin{aligned}\frac{d}{dz}F_1 &= -i\beta_1 F_1\\ \frac{d}{dz}F_2 &= -i\beta_2 F_2.\end{aligned} \tag{3.7}$$

An analytical solution to this system of equations can easily be obtained, since in the absence of the coupling coefficients the coupled-mode equations are reduced to a system of uncoupled ordinary differential equations. The forward propagating amplitude, F_1 can be solved for in the following way.

$$\begin{aligned}\frac{d}{dz}F_1 &= -i\beta_1 F_1\\ \int\frac{dF_1}{F_1} &= -i\beta_1\int dz\\ \ln(F_1) &= -i\beta_1 z + A_1\\ F_1(z) &= A_2 e^{-i\beta_1 z}\end{aligned}$$

For $z=0$,

$$A_2 = F_1(0)$$

so that,

$$F_1(z) = F_1(0)\,e^{-i\beta_1 z}.$$

Similarly,

$$F_2(z) = F_2(0)\, e^{-i\beta_2 z}.$$

Now using the Green's function derived from the path integral formalism, the propagator (Equation 2.15) is given by,

$$G_0(z, z') = \int_{-\infty}^{\infty} \frac{dk}{2\pi} (M_0 - ik)^{-1} e^{ik\cdot(z-z')} \tag{3.8}$$

The path integral formalism yields an expression for the propagator, given by the Green's function, that describes the evolution of the complex amplitudes while traveling through a medium, in terms of a complex integral over the real axis. The problem of solving this integral can be reduced to solving a contour integral with an infinite radius.

3.2.1 The scenic route from $-\infty$ to ∞

In its present form, the propagator is the integral of a complex integrand over the real axis from $-\infty$ to ∞, which has to be solved. Using the notation $z = re^{i\theta}$, one is required to solve an integral of the form $\int_{-\infty}^{\infty} drf(r)$. This is equivalent to solving $\lim_{R\to\infty} \int_{-R}^{R} drf(r)$, since

$$\int_{-\infty}^{\infty} drf(r) = \lim_{R\to\infty} \int_{-R}^{R} drf(r).$$

In terms of z, a contour integral, over some contour γ, can be decomposed into integrals over the respective coordinates as illustrated in Figure 3.1

$$\oint_{\gamma} dzf(z) = \int_{-R}^{R} drf(r) + iR \int_{0}^{\pi} d\theta e^{i\theta} f\left(Re^{i\theta}\right).$$

In this case, the radius, R, must be such that the entire real axis is covered, from $-\infty$ to ∞. Therefore the desired contour integral is given by

$$\oint_{\gamma} dzf(z) = \lim_{R\to\infty} \int_{-R}^{R} drf(r) + \lim_{R\to\infty} iR \int_{0}^{\pi} d\theta e^{i\theta} f\left(Re^{i\theta}\right).$$

However, in order to apply this to the problem at hand, it is required that $\lim_{R\to\infty} iR \int_0^{\pi} d\theta e^{i\theta} f\left(Re^{i\theta}\right)$ goes to zero, so that only the integral over the real axis contributes. Jordan's Lemma [1] stipulates that if $f(z) \sim \frac{1}{z^2}$, which would imply that $f\left(Re^{i\theta}\right) \sim \frac{1}{R^2 e^{2i\theta}}$, then $\lim_{R\to\infty} iR \int_0^{\pi} d\theta e^{i\theta} f\left(Re^{i\theta}\right) \to 0$.

In practice, this means that an integral over the real axis, can be equated to a contour integral whose contour has an infinite radius, as illustrated in Figure 3.1. The advantage of translating the propagator from an integral over the real axis to a contour integral, is that the results of complex analysis are at one's disposal to solve these integrals.

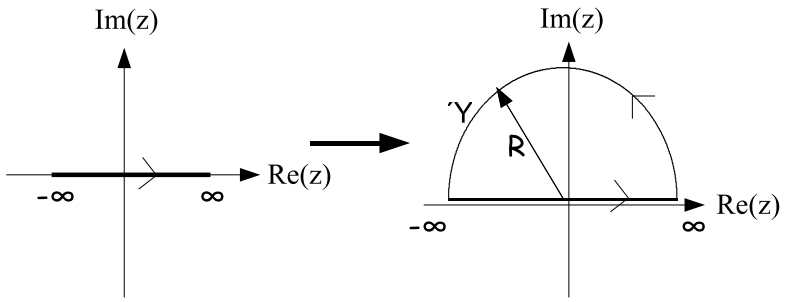

Figure 3.1: This figure is a schematic representation of the fact that one can equate a complex integral over the real axis with a contour integral with a radius of infinity.

3.2.2 Translating the propagator

The propagator to be solved is given by Equation 3.8, reproduced here

$$G_0(z,z') = \int_{-\infty}^{\infty} \frac{dk}{2\pi} (M_0 - ik)^{-1} e^{ik\cdot(z-z')}$$

where the so-called coupling matrix M_0, is expressed as

$$M_0 = \begin{bmatrix} -i\beta_1 & 0 \\ 0 & -i\beta_2 \end{bmatrix}. \tag{3.9}$$

The subscript zero denotes the fact that we are looking at the unperturbed case. The matrix $(M_0 - ik)^{-1}$ is calculated in the following way

$$\begin{aligned} (M_0 - ik)^{-1} &= \begin{bmatrix} -i\beta_1 - ik & 0 \\ 0 & -i\beta_2 - ik \end{bmatrix}^{-1} \\ &= (i)^{-1} \begin{bmatrix} -\beta_1 - k & 0 \\ 0 & -\beta_2 - k \end{bmatrix}^{-1} \\ &= \frac{1}{i(-\beta_1 - k)(-\beta_2 - k)} \begin{bmatrix} -\beta_2 - k & 0 \\ 0 & -\beta_1 - k \end{bmatrix}. \end{aligned} \tag{3.10}$$

Here $(-\beta_1 - k)(-\beta_2 - k)$ is the determinant of matrix

$$\begin{bmatrix} -\beta_1 - k & 0 \\ 0 & -\beta_2 - k \end{bmatrix}.$$

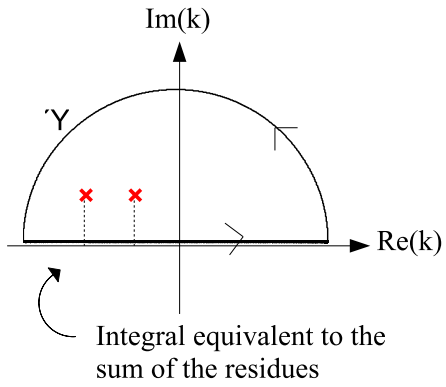

Figure 3.2: A schematic, for the forward propagating case, of the contour over which integration is done and the position of the poles.

The eigenvalues of $\mathrm{Im}(M_0)$ are the roots of its determinant, $k = -\beta_1$ and $k = -\beta_2$. Inserting Equation 3.10 back into the propagator yields

$$G_0(z,z') = \frac{1}{2\pi i}\int_{-\infty}^{\infty} dk \frac{1}{(-\beta_1 - k)(-\beta_2 - k)} \begin{bmatrix} -\beta_2 - k & 0 \\ 0 & -\beta_1 - k \end{bmatrix} e^{ik\cdot(z-z')}.$$

As discussed in Section 3.2.1, this integral over the real axis is equated with a contour integral. The form of the integrand determines the nature of the contour. The integrand contains a dominating exponential term which will determine the form of the contour. The case of forward propagation means that $(z - z') > 0$, with z the final position and z' the initial position. Using the notation $k = k_r + ik_i$ in the exponential term, it follows that

$$\begin{aligned} \exp\{ik(z-z')\} &= \exp\{i(k_r + ik_i)(z-z')\} \\ &= \exp\{ik_r(z-z') - k_i(z-z')\} \\ &= e^{-k_i(z-z')} e^{ik_r(z-z')}. \end{aligned}$$

The imaginary factor, $e^{ik_r(z-z')}$, is a quantity that will only ever oscillate between -1 and 1, so it is of no concern. However, $e^{-k_i(z-z')}$ is a more dominant factor that determines the behavior of the contour. This term will result in the contour closing down in the upper half of the plane where $k_i > 0$. In the lower half of the plane, where $k_i < 0$, the exponential term blows up so that there cannot be a contour for forward propagation in the lower half of the complex plane.

Instead of integrating over the real axis one integrates over this contour, a semi-circle with infinite radius in the upper complex plane as illustrated in Figure 3.2 ,

$$\begin{aligned} G_0(z,z') &= \frac{1}{2\pi i}\int_{-\infty}^{\infty} dk \frac{1}{(-\beta_1 - k)(-\beta_2 - k)} \begin{bmatrix} -\beta_2 - k & 0 \\ 0 & -\beta_1 - k \end{bmatrix} e^{ik\cdot(z-z')} \\ &= \frac{1}{2\pi i}\oint_{\gamma} dk \frac{1}{(-\beta_1 - k)(-\beta_2 - k)} \begin{bmatrix} -\beta_2 - k & 0 \\ 0 & -\beta_1 - k \end{bmatrix} e^{ik\cdot(z-z')}. \end{aligned}$$

The two poles, $-\beta_1$ and $-\beta_2$, are real, occurring on the real axis, which is of no use. To obtain a

nonzero result from this contour integral these poles must occur in the region surrounded by the contour. From Cauchy's Formula [1], this contribution from the contour integral is then equivalent to the sum of the residues. To make use of Cauchy's theory, a small imaginary part is added to the each pole, just to shift it off the axis. The poles become $-\beta_1 + i\varepsilon$ and $-\beta_2 + i\varepsilon$. Then the limit, $\varepsilon \to 0$, of the result is taken. Therefore it would be more appropriate to express the Green's function as

$$G_0(z,z') = \lim_{\varepsilon\to 0}\left\{\frac{1}{2\pi i}\oint_\gamma dk \frac{1}{((-\beta_1+i\varepsilon)-k)((-\beta_2+i\varepsilon)-k)}\begin{bmatrix} -(\beta_2+i\varepsilon)-k & 0 \\ 0 & -(\beta_1+i\varepsilon)-k \end{bmatrix} e^{ik\cdot(z-z')}\right\}$$

Cauchy's Integral Formula is given by

$$\frac{1}{2\pi i}\oint_C dz \frac{f(z)}{z-z_0} = f(z_0)$$

for pole z_0. When there are multiple poles, z_0, $z_1 \ldots z_n$, the result is generalized to

$$\frac{1}{2\pi i}\oint_C dz \frac{f(z)}{(z-z_0)(z-z_1)\cdots(z-z_n)} = \sum_{i=1}^{n} F(z_i)$$

where for pole z_i,

$$F(z_i) = \frac{f(z_i)}{(z_i-z_0)\cdots(z_i-z_{i-1})(z_i-z_{i+1})\cdots(z_i-z_n)}.$$

In this case there are two poles, corresponding to the two propagation constants of the respective modes. After evaluating the integral at poles, $k = -\beta_1$ and $k = -\beta_2$, and taking the limit $\varepsilon \to 0$ the propagator is given by:

$$G_0(z,z') = \left\{\frac{1}{\beta_1-\beta_2}\begin{bmatrix} -\beta_2+\beta_1 & 0 \\ 0 & -\beta_1+\beta_1 \end{bmatrix} e^{-i\beta_1\cdot(z-z')} + \frac{1}{\beta_2-\beta_1}\begin{bmatrix} -\beta_2+\beta_2 & 0 \\ 0 & -\beta_1+\beta_2 \end{bmatrix} e^{-i\beta_2\cdot(z-z')}\right\}. \tag{3.11}$$

The advantage of this analytical function is that given the initial conditions at position z' one merely has to apply them to $G_0(z,z')$ and evaluate it at the position of interest, z. For example $z = L$ and $z' = 0$, with initial conditions $F_1(0)$ and $F_2(0)$ (subscripts denote mode number) only the matrix multiplication

$$\begin{bmatrix} F_1(L) \\ F_2(L) \end{bmatrix} = [G_0(L,0)]\begin{bmatrix} F_1(0) \\ F_2(0) \end{bmatrix}$$

where $G(L,0)$ is a 2×2 matrix has to be carried out. To select either $F_1(L)$ or $F_2(L)$ multiplication by a basis vector $v_1 = \begin{bmatrix} 1 & 0 \end{bmatrix}$ or $v_2 = \begin{bmatrix} 0 & 1 \end{bmatrix}$ respectively, is done in the following way

$$F_1(L) = \begin{bmatrix} 1 & 0 \end{bmatrix}[G_0(L,0)]\begin{bmatrix} F_1(0) \\ F_2(0) \end{bmatrix}$$

$$F_2(L) = \begin{bmatrix} 0 & 1 \end{bmatrix}[G_0(L,0)]\begin{bmatrix} F_1(0) \\ F_2(0) \end{bmatrix}$$

Cumulative error	Forward ODE45	Forward propagator
Real amplitude 1	4.7354e-10	0
Imaginary amplitude 1	4.7920e-10	0
Real amplitude 2	4.5814e-10	0
Imaginary amplitude2	4.6312e-10	0
Modulus squared 1	9.4687e-10	8.8491e-17
Modulus squared 2	9.1613e-10	8.9834e-17
Time consumption [s]	0.7190	0.4540

Table 3.1: The results given by ODE45 and the forward propagator are compared to the results of the analytical solution for two forward propagating modes.

This basis vector is equivalent to the basis vector $\bar{v}_i$ of Chapter 2, while $F_1(0)$ and $F_2(0)$ are the elements of vector $\bar{U}_1$.

3.2.3 Results for forward propagation

To ascertain whether the propagator yields acceptable results, it was tested against the analytical solution of the differential equations and also a numerical solution obtained using Matlab's ODE45 function. The ODE45 function uses a fourth- and fifth-order hybrid Runge-Kutta algorithm to numerically differentiate the given ordinary differential equations. Figure 3.3(a) shows the result for the real part of the calculated amplitude, while Figure 3.3(b) shows the results of the imaginary part of the calculated amplitude. Figures 3.3(a) and 3.3(b) show that the results of all three methods, that is analytical, numerical and the propagator, compare favourably. From Figure 3.3(c), which shows the square of the complex amplitude, it is clear that there is no transfer of energy between the modes. This is exactly what one would expect given that there is no perturbation to facilitate any coupling of the modes.

Table 3.1 provides the results of a quantitative comparison between the results produced by ODE45 and those produced by the forward propagator. The error shown in Table 3.1 is a cumulative error given by

$$\sigma = \frac{\sum \|\varphi_{ana} - \varphi_{calc}\|}{\sum \|\varphi_{ana}\|} \tag{3.12}$$

where φ_{ana} is the analytical solution and φ_{calc} is the solution calculated either using ODE45 or the propagator. Since the propagator produces the exact result, it is no surprise that the error is zero. This error value of zero is indeed zero. Simplifying the expression for the propagator given by Equation 3.11 yields

$$\begin{aligned} G_0(z,z') &= \left\{ \frac{1}{-\beta_2+\beta_1} \begin{bmatrix} -\beta_2+\beta_1 & 0 \\ 0 & -\beta_1+\beta_1 \end{bmatrix} e^{-i\beta_1\cdot(z-z')} + \frac{1}{-\beta_1+\beta_2} \begin{bmatrix} -\beta_2+\beta_2 & 0 \\ 0 & -\beta_1+\beta_2 \end{bmatrix} e^{-i\beta_2\cdot(z-z')} \right\} \\ &= \begin{bmatrix} e^{-i\beta_1\cdot(z-z')} & 0 \\ 0 & e^{-i\beta_2\cdot(z-z')} \end{bmatrix}. \end{aligned}$$

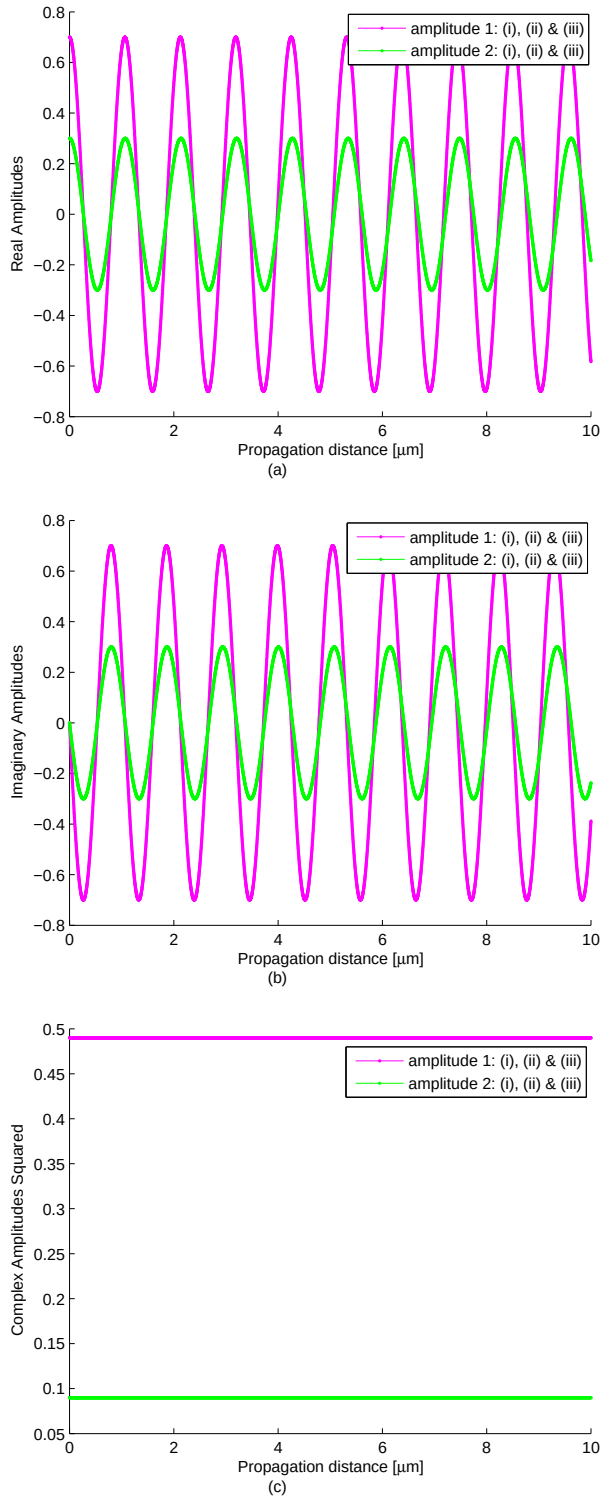

Figure 3.3: (a) Real part of the field for forward propagation for (i) the analytical solution (ii) ODE45 (iii) forward propagator. (b) Imaginary part of the field for forward propagation for (i) the analytical solution (ii) ODE45 (iii) forward propagator. (c) Modulus squared of the complex amplitudes for forward propagation for (i) the analytical solution (ii) ODE45 (iii) forward propagator.

To demonstrate that $G_0(z, z')$ produces the exact result for initial position z' and final position z:

$$\begin{aligned}\begin{bmatrix} F_1(z) \\ F_2(z) \end{bmatrix} &= \begin{bmatrix} e^{-i\beta_1\cdot(z-z')} & 0 \\ 0 & e^{-i\beta_2\cdot(z-z')} \end{bmatrix} \begin{bmatrix} F_1(z') \\ F_2(z') \end{bmatrix} \\ &= \begin{bmatrix} F_1(z')\, e^{-i\beta_1\cdot(z-z')} \\ F_2(z')\, e^{-i\beta_2\cdot(z-z')} \end{bmatrix}.\end{aligned}$$

This is system of equations corresponds exactly with the solutions of Equations 3.7 for an initial position $z' = 0$. The result is that the numerator in Equation 3.12 will be zero as, for this case, $\varphi_{ana} = \varphi_{calc}$. However, the error in the calculation for the square of the amplitude is not zero but of the order 10^{-17}. In calculating this error the square of the calculated solution was subtracted from the square of the analytical solution. An arithmetic operation, such as taking the square of the amplitude, introduces rounding errors of the order 2^{-53} or 10^{-16}, that is Matlab has a precision of 10^{-16}. The consequence of this fact is that when performing operations with values that are of the order of 10^{-16} or smaller, the significance of rounding errors associated with arithmetic operations is greatly increased. Hence the nonzero error corresponding to the square of the amplitude calculated using the propagator, is most probably due to rounding errors (Matlab's precision) that occur when taking the square of the amplitudes and not due to the existence of an actual error between the analytical and calculated amplitudes.

The error in ODE45's result however, cannot be explained using this argument alone since, at an order of 10^{-10} it is simply too large to compare with Matlab's precision. Table 3.1 also shows the time consumption of each method. In determining the time consumption of each method, Matlab's tic.m and toc.m functions were used. As both are under 1 s they compare well and it cannot be said that one method holds an advantage over the other in this regard, although the propagator is marginally faster.

3.3 The case of two backward propagating modes in an unperturbed medium

For two backward propagating modes the coupled-mode Equations 3.6 are reduced to

$$\begin{aligned}\frac{d}{dz}B_1 &= i\beta_1 B_1 \\ \frac{d}{dz}B_2 &= i\beta_2 B_2.\end{aligned} \tag{3.13}$$

The analytical solutions for these equations are given by

$$\begin{aligned}B_1 &= B_1(0)\, e^{i\beta_1 z} \\ B_2 &= B_2(0)\, e^{i\beta_2 z}.\end{aligned}$$

These solutions were obtained in the same manner as those corresponding to Equations 3.7 in Section 3.2

3.3.1 The backward propagator

The associated coupling matrix for these uncoupled differential equations is given by

$$M_0 = \begin{bmatrix} i\beta_1 & 0 \\ 0 & i\beta_2 \end{bmatrix}. \tag{3.14}$$

The term $(M_0 - ik)^{-1}$, appearing in the propagator, is evaluated as in Section 3.2.2,

$$\begin{aligned} (M_0 - ik)^{-1} &= \begin{bmatrix} i\beta_1 - ik & 0 \\ 0 & i\beta_2 - ik \end{bmatrix}^{-1} \\ &= (i)^{-1} \begin{bmatrix} \beta_1 - k & 0 \\ 0 & \beta_2 - k \end{bmatrix}^{-1} \\ &= \frac{1}{i\left(\beta_1 - k\right)\left(\beta_2 - k\right)} \begin{bmatrix} \beta_2 - k & 0 \\ 0 & \beta_1 - k \end{bmatrix}. \end{aligned}$$

Hence the propagator is expressed as

$$G_0\left(z, z'\right) = \frac{1}{2\pi i} \int_{-\infty}^{\infty} dk \frac{1}{\left(\beta_1 - k\right)\left(\beta_2 - k\right)} \begin{bmatrix} \beta_2 - k & 0 \\ 0 & \beta_1 - k \end{bmatrix} e^{ik\cdot\left(z - z'\right)}.$$

$G_0\left(z, z'\right)$ is equated to a contour integral, in a manner similar to the case for forward propagation. However, for backward propagation, $(z - z') < 0$. For the exponential term determining the behaviour of the contour, it follows that

$$\begin{aligned} \exp\left\{ik\left(z - z'\right)\right\} &= \exp\left\{i\left(k_r + ik_i\right)\left(z - z'\right)\right\} \\ &= \exp\left\{ik_r\left(z - z'\right) - k_i\left(z - z'\right)\right\} \\ &= e^{-k_i\left(z - z'\right)} e^{ik_r\left(z - z'\right)}. \end{aligned}$$

The term $e^{-k_i\left(z - z'\right)}$ will result in the contour closing down in the lower half of the plane where $k_i < 0$. In the upper half of the plane, where $k_i > 0$, the exponential term blows up so that there cannot be a contour for backward propagation in the upper half of the complex plane. Instead of integrating over the real axis one integrates over this contour, a semi-circle with infinite radius in the lower complex plane as illustrated in Figure 3.4.

Regarding the poles, which are real, to ensure that they occur in the region surrounded by the contour, a small imaginary part is subtracted, shifting the poles down into the lower half of the complex plane, off the real axis, as illustrated in Figure 3.4. Hence the propagator is given by

$$\begin{aligned} G_0\left(z, z'\right) &= \frac{1}{2\pi i} \int_{-\infty}^{\infty} dk \frac{1}{\left(\beta_1 - k\right)\left(\beta_2 - k\right)} \begin{bmatrix} \beta_2 - k & 0 \\ 0 & \beta_1 - k \end{bmatrix} e^{ik\cdot\left(z - z'\right)} \\ &= \lim_{\varepsilon \to 0} \left\{ \frac{1}{2\pi i} \oint_{\gamma} dk \frac{1}{\left(\left(\beta_1 - i\varepsilon\right) - k\right)\left(\left(\beta_2 - i\varepsilon\right) - k\right)} \begin{bmatrix} \left(\beta_2 - i\varepsilon\right) - k & 0 \\ 0 & \left(\beta_1 - i\varepsilon\right) - k \end{bmatrix} e^{ik\cdot\left(z - z'\right)} \right\}. \end{aligned}$$

Evaluating the integral as previously discussed, with poles at the eigenvalues of $\mathrm{Im}(M_0)$ namely $k = \beta_1$

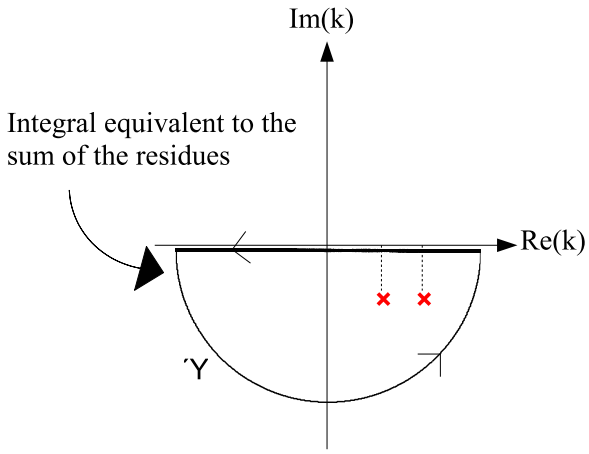

Figure 3.4: Above is a schematic, for the backward propagating case, of the contours over which we integrate and the position of the poles of each integral.

and $k = \beta_2$, yields

$$G_0(z, z') = \left\{ \frac{1}{\beta_2 - \beta_1} \begin{bmatrix} \beta_2 - \beta_1 & 0 \\ 0 & \beta_1 - \beta_1 \end{bmatrix} e^{i\beta_1 \cdot (z - z')} + \frac{1}{\beta_1 - \beta_2} \begin{bmatrix} \beta_2 - \beta_2 & 0 \\ 0 & \beta_1 - \beta_2 \end{bmatrix} e^{i\beta_2 \cdot (z - z')} \right\}.$$

For backward propagation $z' = L$ and $z = 0$ so that one solves the system

$$\begin{bmatrix} B_1(0) \\ B_2(0) \end{bmatrix} = [G_0(0, L)] \begin{bmatrix} B_1(L) \\ B_2(L) \end{bmatrix}$$

where $B_1(0)$ and $B_2(0)$ are the unknowns for which one solves.

3.3.2 Results for backward propagation

Repeating the analysis of the forward propagating case, it was again found that the propagator's calculation agreed with numerical results produced by ODE45 and the analytical solutions to the differential equations. This can be seen in Figures 3.5(a) and 3.5(b), which show the results of all three methods for the real and imaginary parts of the amplitude respectively.

In addition, Figure 3.5(c) shows that the square of the amplitudes remains constant with propagation distance. Again, this is exactly what is expected physically, as there is no perturbation to facilitate any coupling between these modes.

Additionally the forward and backward propagator produced the same results. This is illustrated by comparing Figures 3.3(a) and 3.3(b) with Figures 3.5(a) and 3.5(b) respectively. The values of the respective amplitudes at the end of the waveguide calculated using the forward propagator were used as initial conditions for the backward propagator. The result, using the backward propagator, for the values of the amplitudes at the beginning of the waveguide, were exactly those values of the amplitudes used as initial conditions for the calculation using the forward propagator. So, both the forward and backward propagator produce the same results in the absence of a perturbation, i.e in the absence of any physical z-dependence of the coupling matrix. This is what is expected from the theory of mode propagation as represented by the analytical solution of the coupled-mode equations. This is confirmation that the path integral method is correct for the unperturbed case with copropagating modes.

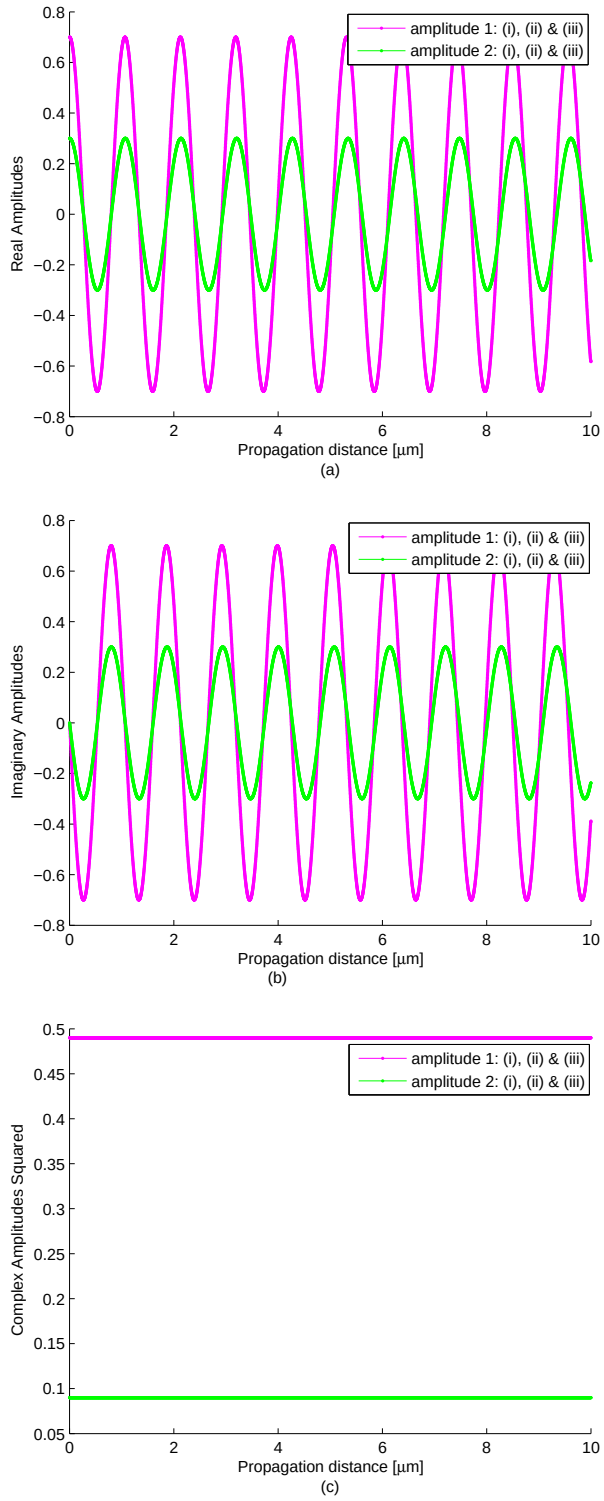

Figure 3.5: (a) Real part of the amplitude for backward propagation for (i) the analytical solution (ii) ODE45 (iii) backward propagator. (b) Imaginary part of the amplitude for forward propagation for (i) the analytical solution (ii) ODE45 (iii) backward propagator. (c) Modulus squared of the complex amplitudes for backward propagation for (i) the analytical solution (ii) ODE45 (iii) backward propagator.

Cumulative error	Backward ODE45	Backward propagator
Real amplitude 1	4.7354e-10	0
Imaginary amplitude 1	4.7920e-10	0
Real amplitude 2	4.5814e-10	0
Imaginary amplitude2	4.6312e-10	0
Modulus squared 1	9.4687e-10	8.8491e-17
Modulus squared 2	9.1613e-10	8.9834e-17
Time consumption [s]	0.5780	0.4840

Table 3.2: The results given by ODE45 and the backward propagator are compared to the results of the analytical solution for two backward propagating modes.

Table 3.2 compares the cumulative error of ODE45 and the propagator. As was the case with the forward propagator, the backward propagator produces an error of zero for the calculated amplitudes which is expected as the propagator is equivalent to the analytical solution. The error for the square of the amplitude is of the order 10^{-17}, which can be explained when taking Matlab's precision into account. ODE45 produces errors of the order 10^{-10}, 7 orders of magnitude greater than those produced by the propagator. Table 3.2 also shows the respective time consumptions of the two methods. The backward propagator is marginally faster than ODE45 in this regard.

3.4 The case of two counter propagating modes in an unperturbed medium

For this particular case the coupled-mode equations, given by Equations 3.1 and 3.2 are reduced to

$$\begin{aligned} \frac{d}{dz}F &= -i\beta_1 F \\ \frac{d}{dz}B &= i\beta_2 B. \end{aligned} \tag{3.15}$$

Analytically, the solutions to these equations are given by

$$\begin{aligned} F &= F(0)\, e^{-i\beta_1 z} \\ B &= B(0)\, e^{i\beta_2 z} \end{aligned}$$

respectively.

3.4.1 A propagator for mixed boundary conditions

The coupling matrix is given by

$$M_0 = \begin{bmatrix} -i\beta_1 & 0 \\ 0 & i\beta_2 \end{bmatrix}. \tag{3.16}$$

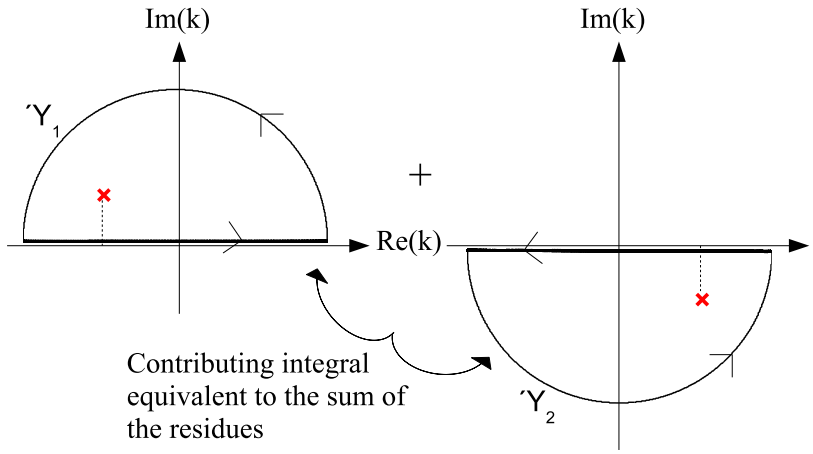

Figure 3.6: A schematic, for the case of mixed boundaries case, of the contours over which one integrates and the position of the poles.

As before

$$\begin{aligned}(M_0 - ik)^{-1} &= \begin{bmatrix} -i\beta_1 - ik & 0 \\ 0 & i\beta_2 - ik \end{bmatrix}^{-1} \\ &= \frac{1}{i\left(-\beta_1 - k\right)\left(\beta_2 - k\right)} \begin{bmatrix} \beta_2 - k & 0 \\ 0 & -\beta_1 - k \end{bmatrix}\end{aligned}$$

and the propagator is expressed as

$$G_0\left(z, z'\right) = \frac{1}{2\pi i}\int_{-\infty}^{\infty} dk \frac{1}{\left(-\beta_1 - k\right)\left(\beta_2 - k\right)} \begin{bmatrix} \beta_2 - k & 0 \\ 0 & -\beta_1 - k \end{bmatrix} e^{ik\cdot\left(z - z'\right)}.$$

Here $G_0\left(z, z'\right)$ can be equated to two contour integrals. One contour occurs in the upper complex plane containing only one pole, $k = -\beta_1$, corresponding to the forward propagating mode. The other contour occurs in the lower complex plane, containing the other pole, $k = \beta_2$, corresponding to the backward propagating mode. Hence,

$$\begin{aligned}G_0\left(z, z'\right) &= \frac{1}{2\pi i}\int_{-\infty}^{\infty} dk \frac{1}{\left(-\beta_1 - k\right)\left(\beta_2 - k\right)} \begin{bmatrix} \beta_2 - k & 0 \\ 0 & -\beta_1 - k \end{bmatrix} e^{ik\cdot\left(z - z'\right)} \left(\theta\left(z - z'\right) + \theta\left(z' - z\right)\right) \\ &= \lim_{\varepsilon \to 0}\left\{ \frac{1}{2\pi i}\oint_{\gamma_1} dk \frac{1}{\left(-\left(\beta_1 + i\varepsilon\right) - k\right)\left(\left(\beta_2 - i\varepsilon\right) - k\right)} \begin{bmatrix} \left(\beta_2 - i\varepsilon\right) - k & 0 \\ 0 & -\left(\beta_1 + i\varepsilon\right) - k \end{bmatrix} e^{ik\cdot\left(z - z'\right)} \theta\left(z - z'\right) \right\} \\ &+ \frac{1}{2\pi i}\oint_{\gamma_2} dk \frac{1}{\left(-\left(\beta_1 + i\varepsilon\right) - k\right)\left(\left(\beta_2 - i\varepsilon\right) - k\right)} \begin{bmatrix} \left(\beta_2 - i\varepsilon\right) - k & 0 \\ 0 & -\left(\beta_1 + i\varepsilon\right) - k \end{bmatrix} e^{ik\cdot\left(z - z'\right)} \theta\left(z' - z\right) \Bigg\}\end{aligned}$$

In evaluating this integral, contributions are made from both contours, γ_1 and γ_2, as each contains a pole. See Figure 3.6 . The result is given by

$$G_0(z,z') = \left\{ \frac{1}{\beta_2+\beta_1} \begin{bmatrix} \beta_2+\beta_1 & 0 \\ 0 & -\beta_1+\beta_1 \end{bmatrix} e^{-i\beta_1\cdot(z-z')} + \frac{1}{-\beta_1-\beta_2} \begin{bmatrix} \beta_2-\beta_2 & 0 \\ 0 & -\beta_1-\beta_2 \end{bmatrix} e^{i\beta_2\cdot(z-z')} \right\}.$$

When solving the system $\bar{U}(L) = G_0\bar{U}(0)$, the case of two counter propagating modes cannot be solved in one calculation as is the case with co-propagating modes, because the initial conditions of both amplitudes at one initial position - whether it be $z' = 0$ or $z' = L$ - need to be known to be applied to the propagator. The propagator is inherently dependent on position and its operation is associated with a specific direction. The propagator cannot model both directions at once. The problem itself in solving these differential equations has moved from being an initial value problem to that of a boundary value problem. However, knowing the initial condition of the forward mode at $z' = 0$ and the initial condition of the backward mode at $z' = L$, one can (analytically) calculate the final state of the backward mode at $z = 0$ in terms of its initial condition at $z' = L$ and the initial condition of the forward mode at $z' = 0$, simply by carrying out matrix multiplication and solving for the unknown. One can then apply the conditions at an initial position and treat the problem as an initial value problem.

The boundary conditions can be handled in the following way. Let $F(0)$ and $B(L)$ be known and $B(0)$ and $F(L)$ unknown.

$$\begin{aligned} \bar{U}(L) &= G_0\bar{U}(0) \\ \begin{bmatrix} F(L) \\ B(L) \end{bmatrix} &= \begin{bmatrix} G_{0,11}(L,0) & G_{0,12}(L,0) \\ G_{0,21}(L,0) & G_{0,22}(L,0) \end{bmatrix} \begin{bmatrix} F(0) \\ B(0) \end{bmatrix} \end{aligned}$$

From this system of linear equations it follows that

$$B(L) = G_{0,21}(L,0)\,F(0) + G_{0,22}(L,0)\,B(0).$$

Therefore

$$B(0) = \frac{B(L) - G_{0,21}(L,0)\,F(0)}{G_{0,22}(L,0)}. \tag{3.17}$$

Having calculated the magnitude of the backward amplitude at $z = 0$ the propagator can be used to calculate the unknown $F(L)$ as it was used for the case of two forward propagating modes.

3.4.2 Results for counter propagation

The results compare favourably with those of the forward and backward propagator for the same initial and final conditions for the amplitudes. This can be seen in Figures 3.7(a) and (b) which compare the real and imaginary parts, respectively, of the analytical solution, forward propagator solution, backward propagator solution and this mixed propagator solution. Figure 3.7 shows that all four solutions exhibit the same result for the square of the amplitudes. Hence it can said this mixed propagator works.

The mixed propagator can be solved in a second way. Instead of calculating the unknown $B(0)$ analytically and then using forward propagation to calculate the unknown $F(L)$, one can solve analytically

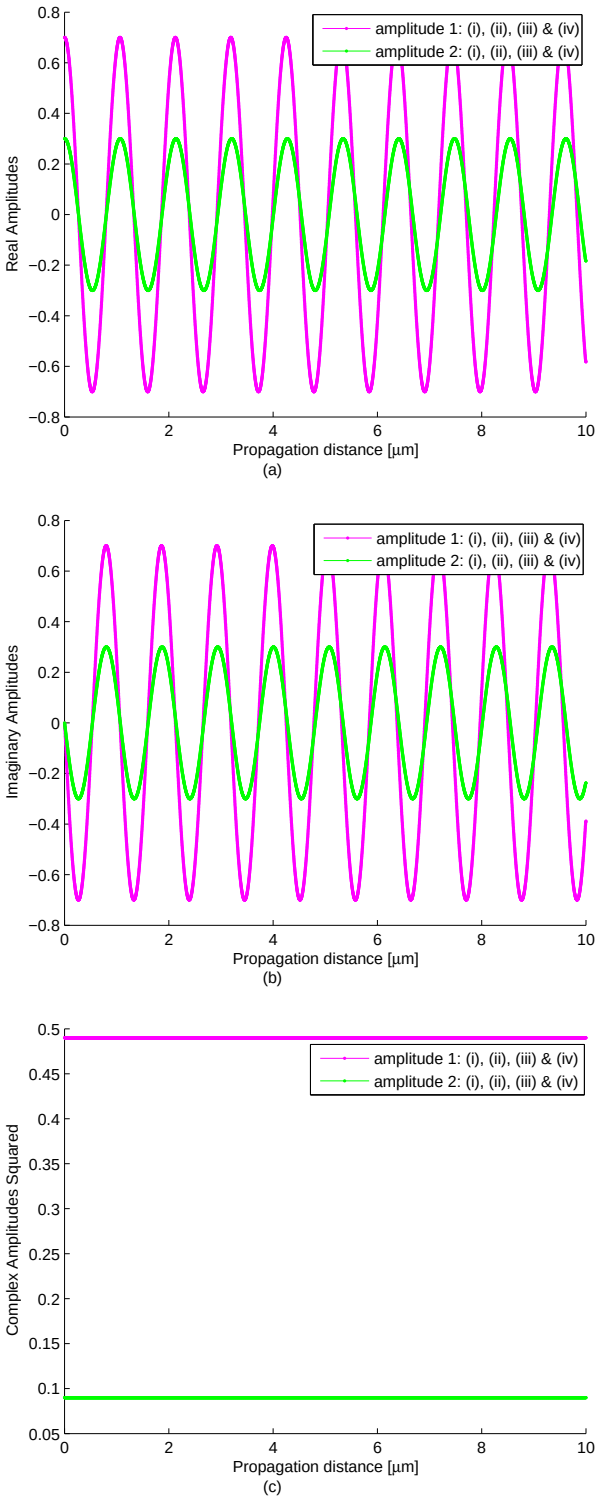

Figure 3.7: (a) Real part of the amplitude for counter propagation for (i) the analytical solution (ii) forward propagator (iii) backward propagator (iv) mixed propagator. (b) Imaginary part of the amplitude for counter propagation for (i) the analytical solution (ii) forward propagator (iii) backward propagator (iv) mixed propagator. (c) Modulus squared of the complex amplitudes for counter propagation for (i) the analytical solution (ii) forward propagator (iii) backward propagator (iv) mixed propagator.

Cumulative error	Forward Propagator	Backward Propagator	Mixed Propagator 1	Mixed propagator 2
Real amplitude 1	0	0	0	6.3229e-15
Imaginary amplitude 1	0	0	0	6.1865-15
Real amplitude 2	0	0	3.9312e-15	0
Imaginary amplitude2	0	0	3.8269e-15	0
Modulus squared 1	8.8491e-17	8.8491e-17	8.8433e-17	8.8433e-16
Modulus squared 2	8.9834e-17	8.9834e-17	1.7613e-16	1.7127e-17
Time consumption [s]	0.4540	0.4840	1.0310	1.0160

Table 3.3: The results given by all four propagators are compared to the results of the analytical solution for two counter propagating modes.

for $F(L)$ and then use backward propagation to calculate $B(0)$. This is seen as follows

$$\begin{aligned} \bar{U}(0) &= G_0 \bar{U}(L) \\ \begin{bmatrix} F(0) \\ B(0) \end{bmatrix} &= \begin{bmatrix} G_{0,11}(0,L) & G_{0,12}(0,L) \\ G_{0,21}(0,L) & G_{0,22}(0,L) \end{bmatrix} \begin{bmatrix} F(L) \\ B(L) \end{bmatrix} \end{aligned}$$

From this system of linear equations it follows that

$$F(0) = G_{0,11}(0,L) F(L) + G_{0,12}(L,0) B(L).$$

Therefore

$$F(L) = \frac{F(0) - G_{0,12}(0,L) B(L)}{G_{0,11}(L,0)}. \tag{3.18}$$

The results of this latter form of the mixed propagator compare well with the results of the former mixed propagator. This is seen in Figures 3.8(a) and (b) which compare the real and imaginary parts of the field produced by both propagators for the same set of physical and initial conditions. Figure 3.8(c) shows that the modulus squared of the complex amplitudes of both propagators are in agreement, showing that physically the latter mixed boundaries propagator produces sensible results too.

Table 3.3 compares the cumulative error of the forward and backward propagators with both mixed propagators. The first mixed propagator, most probably does not produce a zero error for amplitude 2 due to the arithmetic operations required to find its "initial" condition at $z = 0$. These arithmetic operations are given by Equation 3.17. Compounding this explanation is the fact that for amplitude 1, for which no such calculations are required, the error is zero.

The error results for the second mixed propagator mirror those results for the first mixed propagator. The error associated with amplitude 1 is not zero however, the error corresponding to amplitude 2 is zero. This is probably due to the fact that, in this instance, the "initial" conditions for amplitude 1 are calculated using Equation 3.18 and hence an error is introduced.

The time consumption for the respective propagators are also shown in Table 3.3. The mixed propagators are comparable with one another however, they are slower than the forward and backward propagators. This is probably due to the fact that when using the mixed propagator, the initial conditions of the one of the amplitudes must first be calculated.

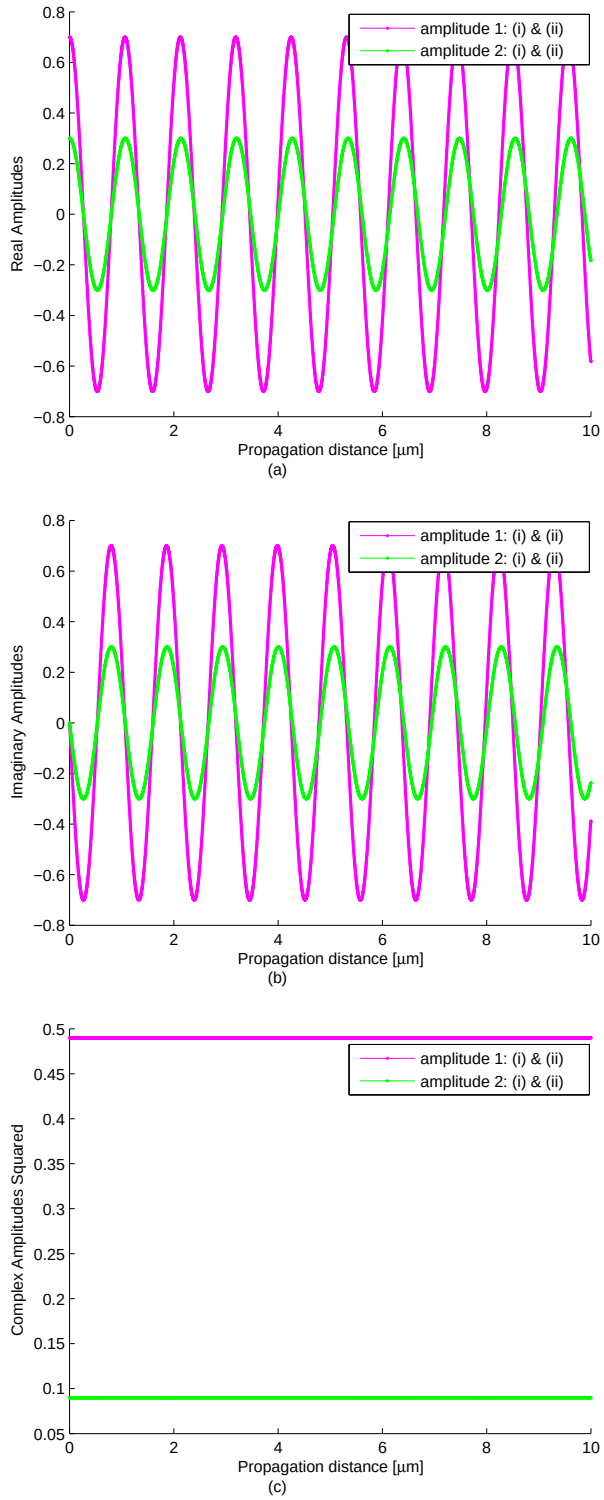

Figure 3.8: (a) Real part of the amplitude for counter propagation for (i) mixed propagator 1 (ii) mixed propagator 2. (b) Imaginary part of the amplitude for counter propagation for (i) mixed propagator 1 (ii) mixed propagator 2. (c) Modulus squared of the complex amplitudes for counter propagation for (i) mixed propagator 1 (ii) mixed propagator 2.

Chapter 4

A periodically perturbed waveguide: The uniform grating

The effect of adding a periodic perturbation to the permittivity of the medium is investigated in this chapter. The relation between the permittivity of a medium and its index of refraction has been discussed in Section 1.3. Using this relation, namely $\varepsilon = n^2$, it was shown that the perturbation to the permittivity, $\Delta\varepsilon$ can be expressed in terms of the resulting perturbation to the index of refraction by $\Delta\varepsilon = 2n\delta n$ (Equation 1.25). In this way one can express the coupling coefficients in terms of the perturbation to the refractive index as given by Equation 1.26. It was chosen to represent this periodicity in the refractive index by a longitudinally varying raised-cosine function (Equation 1.24), namely

$$\delta n\left(z\right) \quad = \quad \bar{\delta n}\left\{1 + v\cos\left(\frac{2\pi}{\Lambda}z\right)\right\}.$$

In the presence of this periodic perturbation the coupling coefficients are no longer zero as was the case in Chapter 3. The coupling coefficients take on the form of the perturbation according to Equation 1.26.

$$\begin{aligned} C_{\mu\nu}\left(z\right) &= \frac{\omega}{4}\int_{-\infty}^{\infty}\int_{-\infty}^{\infty} dxdy\bar{\xi}^{*}_{\mu,t}\delta n\left(z\right)\bar{\xi}_{\nu,t} \\ &= \frac{\omega}{4}2n\delta n\left(z\right)\int_{-\infty}^{\infty}\int_{-\infty}^{\infty} dxdy\bar{\xi}^{*}_{\mu,t}\bar{\xi}_{\nu,t} \\ &= \frac{\omega}{2}n\bar{\delta n}\left\{1 + v\cos\left(\frac{2\pi}{\Lambda}z\right)\right\}\int_{-\infty}^{\infty}\int_{-\infty}^{\infty} dxdy\bar{\xi}^{*}_{\mu,t}\bar{\xi}_{\nu,t} \end{aligned}$$

Following the convention of most literature sources [3, 2, 12], the coupling coefficients can be split into dc and ac coupling coefficients. The dc coefficients are given by

$$\varrho_{\mu\nu} \quad = \quad \frac{\omega}{2}n\bar{\delta n}\int_{-\infty}^{\infty}\int_{-\infty}^{\infty} dxdy\bar{\xi}^{*}_{\mu,t}\bar{\xi}_{\nu,t} \tag{4.1}$$

while the ac coefficients are given by

$$\begin{aligned}\vartheta_{\mu\nu} &= v\frac{\omega}{4}n\bar{\delta n}\int_{-\infty}^{\infty}\int_{-\infty}^{\infty}dxdy\bar{\xi}^{*}_{\mu,t}\bar{\xi}_{\nu,t}\\ &= \frac{v}{2}\varrho_{\mu\nu}\end{aligned} \tag{4.2}$$

so that

$$C_{\mu\nu}(z) = \varrho_{\mu\nu} + 2\vartheta_{\mu\nu}\cos\left(\frac{2\pi}{\Lambda}z\right).$$

In keeping with the fact that only real coupling coefficients are used it follows that $\varrho_{\mu\nu}$ and $\vartheta_{\mu\nu}$.

In what follows, the path integral formalism is applied to examples of both uniform LPGs and Bragg gratings.

4.1 Long period gratings (LPGs)

Long period gratings couple copropagating modes. Typically their periodicity is such that fundamental guided modes are coupled to forward propagating cladding modes. The choice of the periodicity is dictated by the phase-matching condition. The phase-matching condition for an LPG is given by

$$\Delta\beta = \frac{2\pi}{\Lambda}. \tag{4.3}$$

This condition is dependent on the difference between the propagation constants of the interacting modes, $\Delta\beta = \beta_1 - \beta_2$, and since their propagation constants have the same sign, this difference is very small. Equation 4.3 shows that the period of the grating, Λ is inversely proportional to $\Delta\beta$ so that for copropagating modes Λ is larger than for reflection gratings, hence the name long period gratings.

4.1.1 Transforming the coupled-mode equations for an LPG

The complications that accompany calculations with z-dependent coupling coefficients can be avoided by making synchronous transformations after Erdogan et al. [3, 12]. Since an LPG is a transmission grating it couples modes traveling in the same direction. The following transformation is applicable for two such modes:

$$\begin{aligned}\tilde{F}_1(z) &= F_1(z)\exp\left\{-i\left(\frac{\varrho_{11}+\varrho_{22}}{2}-\delta\beta\right)z\right\}\\ \tilde{F}_2(z) &= F_2(z)\exp\left\{-i\left(\frac{\varrho_{11}+\varrho_{22}}{2}+\delta\beta\right)z\right\}.\end{aligned}$$

Here $\delta\beta = \frac{1}{2}(\beta_1-\beta_2) - \frac{\pi}{\Lambda}$ is the detuning parameter. It can be shown [3, 12] that the coupled-mode equations for two forward propagating modes (Equation 3.1), reduce to

$$\begin{aligned}\frac{d\tilde{F}_1}{dz} &= i\varrho^{+}\tilde{F}_1(z) + i\vartheta\tilde{F}_2(z)\\ \frac{d\tilde{F}_2}{dz} &= i\vartheta^{*}\tilde{F}_1(z) - i\varrho^{+}\tilde{F}_2(z).\end{aligned} \tag{4.4}$$

Here $\vartheta = \vartheta_{12} = \vartheta_{21}^*$ is the ac cross-coupling coefficient, which needs to be calculated numerically and ϱ^+ is the general dc self-coupling coefficient given by $\varrho^+ = \frac{(\varrho_{11}-\varrho_{22})}{2} + \delta\beta$. Making these transformations yields a set of coupled ordinary differential equations, for which closed form solutions can be found.

4.1.2 The LPG propagator

The coupled-mode equations corresponding to Equation 4.4, having no z-dependent coefficients, can be solved by making use of the unperturbed propagator (Equation 2.15) as it was used in Chapter 3. In this case however, the off-diagonal components of the coupling matrix that account for the cross coupling of the two modes, are nonzero. The coupling matrix is given by

$$\begin{aligned} M_0 &= \begin{bmatrix} i\varrho^+ & i\vartheta \\ i\vartheta & -i\varrho^+ \end{bmatrix} \\ &= \begin{bmatrix} i\left[\frac{1}{2}(\beta_1-\beta_2) - \frac{\pi}{\Lambda} + \frac{\varrho_{11}-\varrho_{22}}{2}\right] & i\vartheta \\ i\vartheta & -i\left[\frac{1}{2}(\beta_1-\beta_2) - \frac{\pi}{\Lambda} + \frac{\varrho_{11}-\varrho_{22}}{2}\right] \end{bmatrix}. \end{aligned}$$

Simply using co-factor expansion, $(M_0 - ik)^{-1}$ and the poles of the propagator may be calculated easily.

$$\begin{aligned} (M_0 - ik)^{-1} &= \begin{bmatrix} i\varrho^+ - ik & i\vartheta \\ i\vartheta & -i\varrho^+ - ik \end{bmatrix}^{-1} \\ &= \frac{1}{\det[M_0 - ik]} \begin{bmatrix} -i\varrho^+ - ik & -i\vartheta \\ -i\vartheta & i\varrho^+ - ik \end{bmatrix} \\ &= \frac{1}{i(k-e_1)(k-e_2)} \begin{bmatrix} -\varrho^+ - k & -\vartheta \\ -\vartheta & \varrho^+ - k \end{bmatrix}. \end{aligned}$$

Here e_1 and e_2 are the eigenvalues of $\mathrm{Im}(M_0)$ and the poles of the propagator. Substituting this expression for $(M_0 - ik)^{-1}$ into the propagator yields

$$\begin{aligned} G(z,z') &= \int_{-\infty}^{\infty} \frac{dk}{2\pi} (M_0 - ik)^{-1} e^{ik(z-z')} \\ &= \frac{1}{2\pi i} \int_{-\infty}^{\infty} dk \frac{1}{(k-e_1)(k-e_2)} \begin{bmatrix} -\varrho^+ - k & -\vartheta \\ -\vartheta & \varrho^+ - k \end{bmatrix} e^{ik(z-z')}. \end{aligned}$$

The equivalent contour integral is given by,

$$G(z,z') = \frac{1}{2\pi i} \oint_{\gamma} dk \frac{1}{(k-e_1)(k-e_2)} \begin{bmatrix} -\varrho^+ - k & -\vartheta \\ -\vartheta & \varrho^+ - k \end{bmatrix} e^{ik(z-z')}.$$

The solution to the contour integral, given by the sum of the residues, yields

$$\begin{aligned} G(z,z') &= \left\{ \frac{1}{(e_1-e_2)} \begin{bmatrix} -\varrho^+ - e_1 & -\vartheta \\ -\vartheta & \varrho^+ - e_1 \end{bmatrix} \exp\{ie_1(z-z')\} \right. \\ &+ \left. \frac{1}{(e_2-e_1)} \begin{bmatrix} -\varrho^+ - e_2 & -\vartheta \\ -\vartheta & \varrho^+ - e_2 \end{bmatrix} \exp\{ie_2(z-z')\} \right\}. \end{aligned}$$

4.1.3 Results for the LPG

In the application of the propagator to the LPG, the associated power flow of the the modes was investigated along with the transmission spectra of the simulated LPGs. These results were then compared to numerical (ODE45), analytical and published results respectively.

As a first approach the power flow of the modes (the modulus squared of the complex amplitudes) was calculated as a function of propagation distance. The choice of normalization of the modes determines whether the mode power or mode intensity is calculated. In this case, the power carried by the modes was calculated in order to compare it to data in literature. The cumulative errors of both the propagator's results and those of ODE45 were calculated. It also remained to ascertain whether the result is physical. Hence the two methods were applied to both phase-matched and nonphase-matched conditions. In addition the conservation of energy was also tested.

To quantify the accuracy of ODE45 and the propagator, it was necessary to derive analytical solutions for each mode from Equations 4.4. These solutions are

$$\begin{aligned} \tilde{F}_1(z) &= \cos(\alpha z) + i\frac{\varrho^+}{\alpha}\sin(\alpha z) \\ \tilde{F}_2(z) &= i\frac{\vartheta}{\alpha}\sin(\alpha z) \end{aligned}$$

where $\alpha = \sqrt{\varrho^{+2} + \vartheta^2}$. The derivation of these solutions can be found in Section 7.2 of the Appendix. The results of the propagator and ODE45 are compared to the analytical solution to calculate the percentage difference, that is considered the error in ODE45 and the propagator results.

As discussed in Section 1.2.2 and 1.3, phase-matching corresponds to the grating condition for which

$$\lambda = \lambda_D \equiv \Delta n \Lambda$$

where λ is the operating wavelength, λ_D the design wavelength of the grating, Δn the difference in the refractive indices of the two modes and Λ the period of the grating, as given by Equation 1.29. When the operating wavelength corresponds to the grating condition, $\lambda = \lambda_D$ and the fields of the two modes are phase-matched. Only under phase-matched conditions a complete exchange of energy between the two modes takes place.

The parameters used to generate Figures 4.1 and 4.2 are provided Table 4.1. Figures 4.1(a) and (c) show the power flow between the two modes for a λ at 95% and 99% of λ_D respectively. It can be seen that the exchange of power between the two modes increases as λ approaches λ_D. Figure 4.1(e) shows the coupling between the two modes under phase-matched conditions with $\lambda = \lambda_D$. The complete exchange of energy that takes place over the length of the grating is seen; as mode 1 begins with a power of 1 W which depletes to 0 W by the time it traverses the length of the grating, mode 2 begins with a power of 0 W which accumulates with propagation to 1 W at the output of the grating. The results in Figures 4.1 are expected given the phase-matching conditions.

This analysis also provides insight into certain physical criteria that need to be considered when designing such gratings. Specifically, the coupling-length product, ϑL, is of particular importance. In the case of Figure 4.1(e), the length of the grating was suitable for a full exchange of power. All the input power carried by mode 1 at the beginning of the grating is carried by mode 2 at the output of the grating. In many applications it is advantageous to have as much of the available energy as possible concentrated in one particular mode. Given a cross-coupling coefficient, the length of the grating must be such that at the output of the grating, the power associated with mode 2 is at at maximum and that

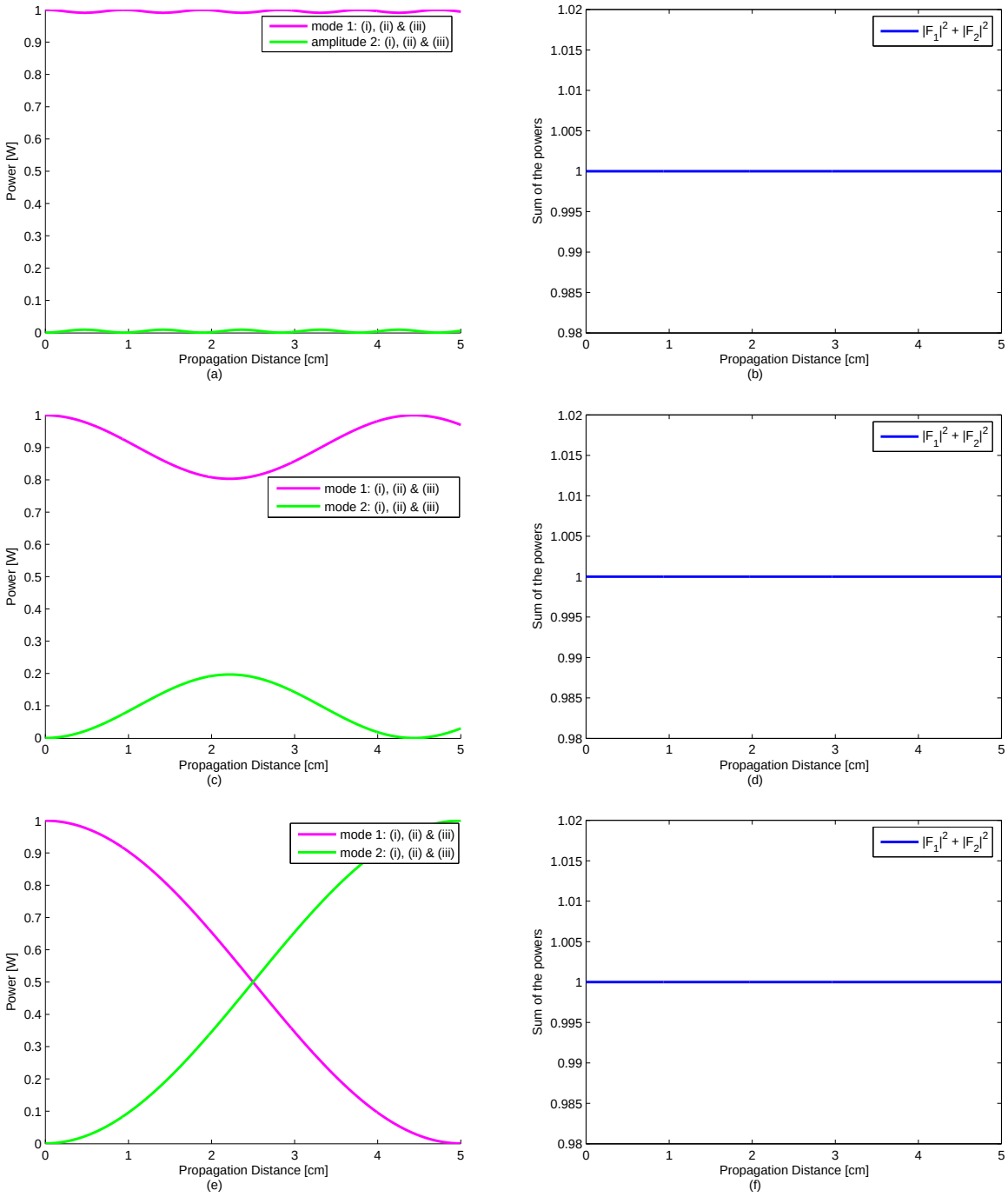

Figure 4.1: The evolution of the powers of the two forward propagating modes with propagation distance as calculated by (i) an analytical solution (ii) ODE45 and (iii) the propagator for two nonphase-matched conditions (a) $\lambda = 0.95\lambda_D$, (c) $\lambda = 0.99\lambda_D$ and phase-matched condition (e) $\lambda = \lambda_D$. (b) (d) and (f) show the sum of the powers of the two modes with propagation distance calculated using the propagator corresponding to (a), (c) and (e) respectively.

Parameters	Figure 4.1(a)	Figure 4.1(c)	Figure 4.1(e)	Figure 4.2(a)	Figure 4.2(b)
L	5 cm	5 cm	5 cm	8 cm	5 cm
λ_D	1550 nm	1550 nm	1550 nm	1550 nm	1550 nm
Λ	500 μm	500 μm	500 μm	500 μm	500 μm
λ	$0.95 \times \lambda_D$	$0.99 \times \lambda_D$	λ_D	λ_D	λ_D
Δn	0.0031	0.0031	0.0031	0.0031	0.0031
ϑL	$\frac{\pi}{2}$	$\frac{\pi}{2}$	$\frac{\pi}{2}$	$\frac{\pi}{2}$	π

Table 4.1: Parameters used in the modeling of the gratings corresponding to Figures 4.1(a), (c) and (e) and Figures 4.2(a) and (b).

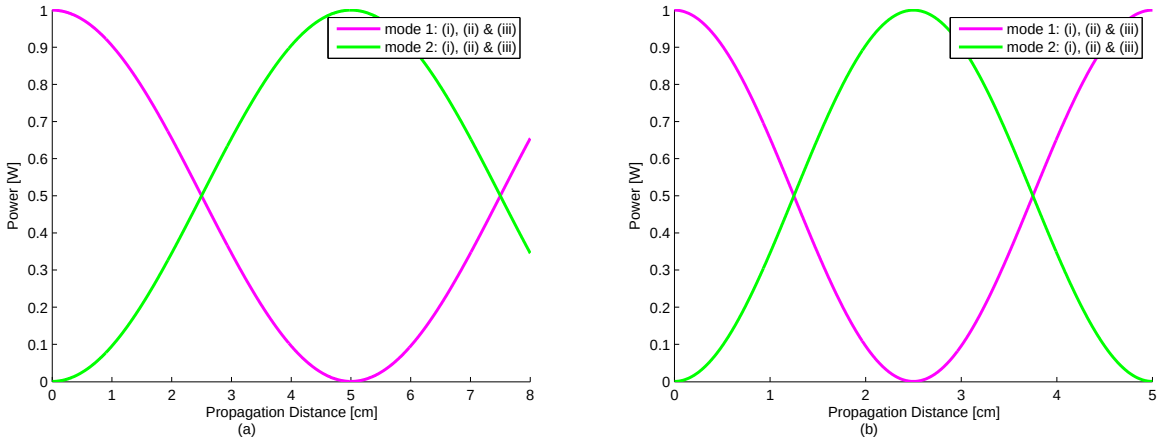

Figure 4.2: (a) The evolution of the power of the modes for an increased propagation distance of 8 cm with all the other parameters the same as for Figure 4.1(e). (b) The evolution of the power of the modes for a stronger cross-coupling coefficient of $\vartheta = 62.8319\,\mathrm{cm}^{-1}$ as opposed to $\vartheta = 31.415\,\mathrm{cm}^{-1}$ of Figure 4.1(e); all other parameters the same as for Figure 4.1(e).

of mode 1 at a minimum. Figure 4.2(a) illustrates the importance of this length. Extending the length of the grating corresponding to Figure 4.1(e) by another 3 cm, results in the recoupling of energy from mode 2 into mode 1, so that at the end of the grating neither mode attains a maximum power output.

When designing a grating, the magnitude of the cross-coupling coefficients must also be taken into account. The greater the magnitude of the cross-coupling coefficient the greater the coupling strength. Figure 4.2(b) illustrates the effect of increasing the coupling strength from $\vartheta = 31.415\,\mathrm{cm}^{-1}$ to $\vartheta = 62.8319\,\mathrm{cm}^{-1}$. Doubling the coupling strength halves the propagation distance over which a complete exchange of power occurs. The greater the strength of the cross coupling coefficients, the shorter the required length of the grating to obtain a complete exchange of energy between the modes.

The coupled-mode equations satisfy the conservation of energy which requires that

$$\frac{d}{dz}\left(|F_1|^2 + |F_2|^2\right) = 0, \tag{4.5}$$

regardless of phase-matching conditions. Figures 4.1(b), (d) and (f) show the corresponding energy curves for the respective operating wavelengths. For copropagation the sum of the power of the modes remains constant with propagation, hence Equation 4.5 holds for each operating wavelength. In satisfying Equation 4.5, the propagator produces results that are physically sensible.

In Table 4.2, the errors and time consumption of ODE45 and the propagator are compared. For the case where $\lambda = 0.95\lambda_D$, the propagator was an order of magnitude faster than ODE45. However, when

Simulation	Figure 4.1(a)	Figure 4.1(c)	Figure 4.1(e)
Wavelength	$0.95 \times \lambda_D$	$0.99 \times \lambda_D$	λ_D
ODE45 Error mode 1 [%]	1.8579×10^{-8}	4.0718×10^{-9}	2.5799×10^{-9}
ODE45 Error mode 2 [%]	1.8169×10^{-8}	4.3997×10^{-9}	2.6139×10^{-9}
ODE45 Time Consumption [s]	0.3280	0.2190	0.2030
Propagator Error mode 1 [%]	2.5165×10^{-14}	1.2578×10^{-14}	1.2787×10^{-14}
Propagator Error mode 2 [%]	1.0305×10^{-13}	3.8325×10^{-14}	0
Propagator Time Consumption [s]	0.0630	0	0

Table 4.2: The error and time consumption for the simulations associated with Figures 4.1(a), (c) and (e).

Parameters	Figure 4.3(a)	Figure 4.3(d)	Figure 4.5(a)
L	5 cm	5 cm	5 cm
λ_D	1550 nm	1550 nm	1545 nm
Λ	500 μm	500 μm	36.79 mm
Δn_{eff}	0.0031	0.0031	0.0042
ϑL	$\frac{\pi}{2}$	$\frac{5\pi}{2}$	0.39

Table 4.3: Parameters given and calculated from literature [3, 12] and used to generate Figures 4.3(a), 4.3(b) and 4.5(a).

$\lambda = 0.99\lambda_D$, still nonphase-matched, the time taken by the propagator was too small to be determined by Matlab. This was also the case under phase-matched conditions. The error that ODE45 produces is greater than that of the propagator. ODE45 produces errors ranging from 10^{-8}% to 10^{-9}% whereas the propagator produces errors of the order 10^{-13}% to 10^{-14}%. It should be stressed however, that the propagator produces an exact solution for this particular set of equations given the nature of the coupling coefficients, so it is to be expected that the error will be much smaller than that produced by ODE45.

The transmission spectra of the simulated LPGs were calculated using the propagator. The parameters, as given in Table 4.3, were chosen in such a way that the results can be compared to published results in addition to numerical and analytical solutions. Calculating the spectra is another important test to determine whether the propagator yields physically acceptable results.

For the LPG, two transmission spectra may be obtained, namely the cross transmission spectrum and the bar transmission spectrum. The cross transmission spectrum is the ratio of the output power of the mode gaining energy to the power of the input mode at the beginning of the waveguide. The cross transmission spectrum [3] is given by

$$T_{\times} = \frac{|F_2(z)|^2}{|F_1(0)|^2} \tag{4.6}$$

$$= \frac{1}{1+\frac{\varrho^{+2}}{\vartheta^2}} \sin^2\left(\sqrt{\vartheta^2+\varrho^{+2}}z\right). \tag{4.7}$$

The second transmission spectrum that can be measured or calculated, is the bar transmission spectrum which is the ratio of the output power to the input power of the input mode. It is expressed [3] as

$$T_{=} = \frac{|F_1(z)|^2}{|F_1(0)|^2} \tag{4.8}$$

$$= \cos^2\left(\sqrt{\vartheta^2+\varrho^{+2}}z\right) + \frac{1}{1+\frac{\vartheta^2}{\varrho^{+2}}} \sin^2\left(\sqrt{\vartheta^2+\varrho^{+2}}z\right). \tag{4.9}$$

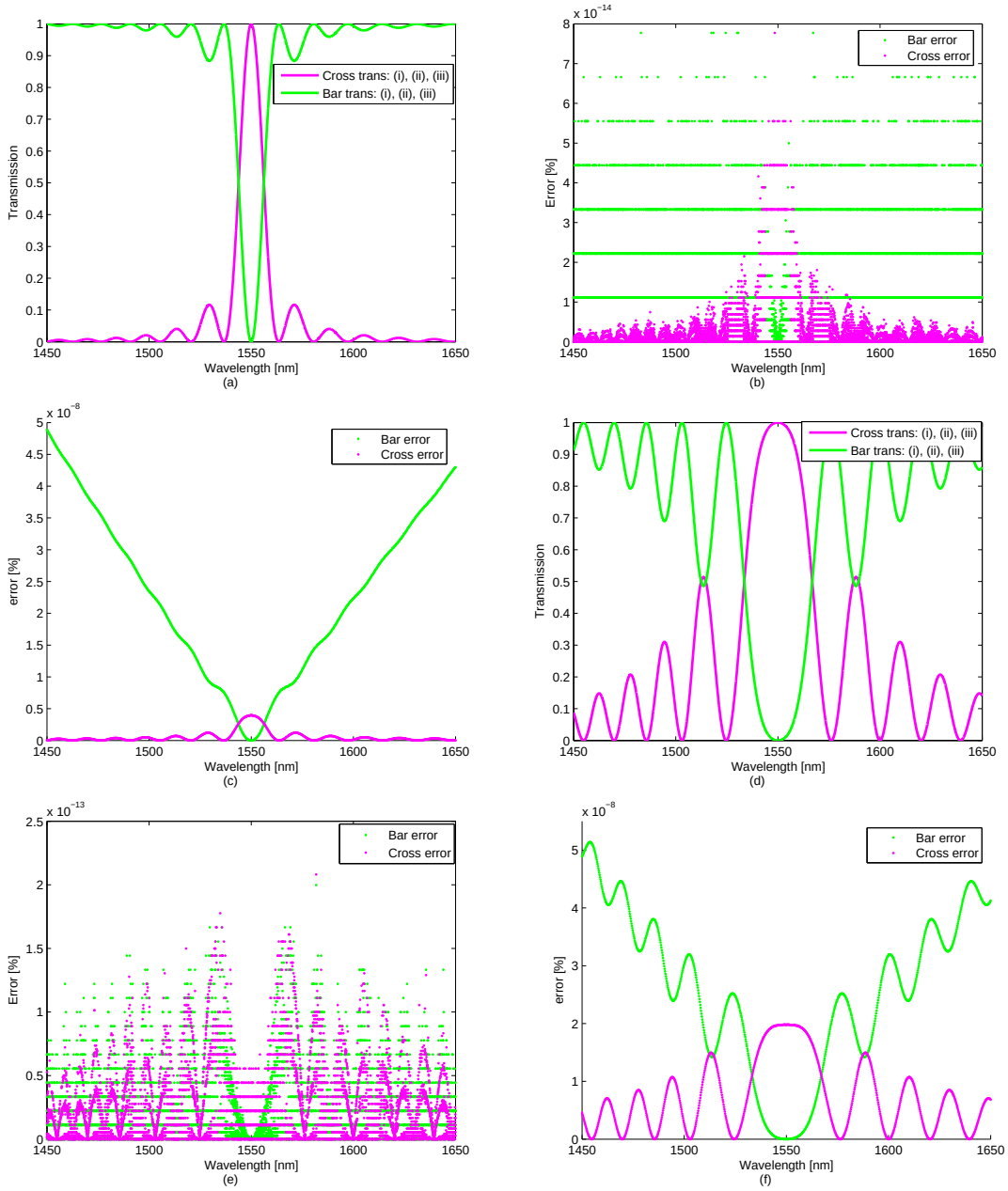

Figure 4.3: (a) The bar and cross transmission spectra in the weaker grating limit, $\vartheta L = \frac{\pi}{2}$, produced by (i) an analytical solution, (ii) ODE45 and (iii) the propagator. (b) The error in the propagators results as compared to the analytical solution for both the bar and cross transmission of (a). (c) The error in ODE45's results as compared to the analytical solution for both the bar and cross transmission of (a). (d) The bar and cross transmission spectra in the stronger grating limit, $\vartheta L = \frac{5\pi}{2}$, produced by (i) an analytical solution, (ii) ODE45 and (iii) the propagator. (e) The error in the propagators results as compared to the analytical solution for both the bar and cross transmission of (d). (f) The error in ODE45's results as compared to the analytical solution for both the bar and cross transmission of (d).

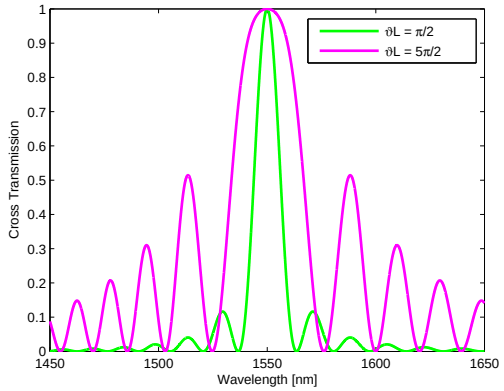

Figure 4.4: A comparison of the cross transmission spectra shown in Figures 4.3 (a) and (d) to facilitate a comparison with the results of Othonos et al. [12].

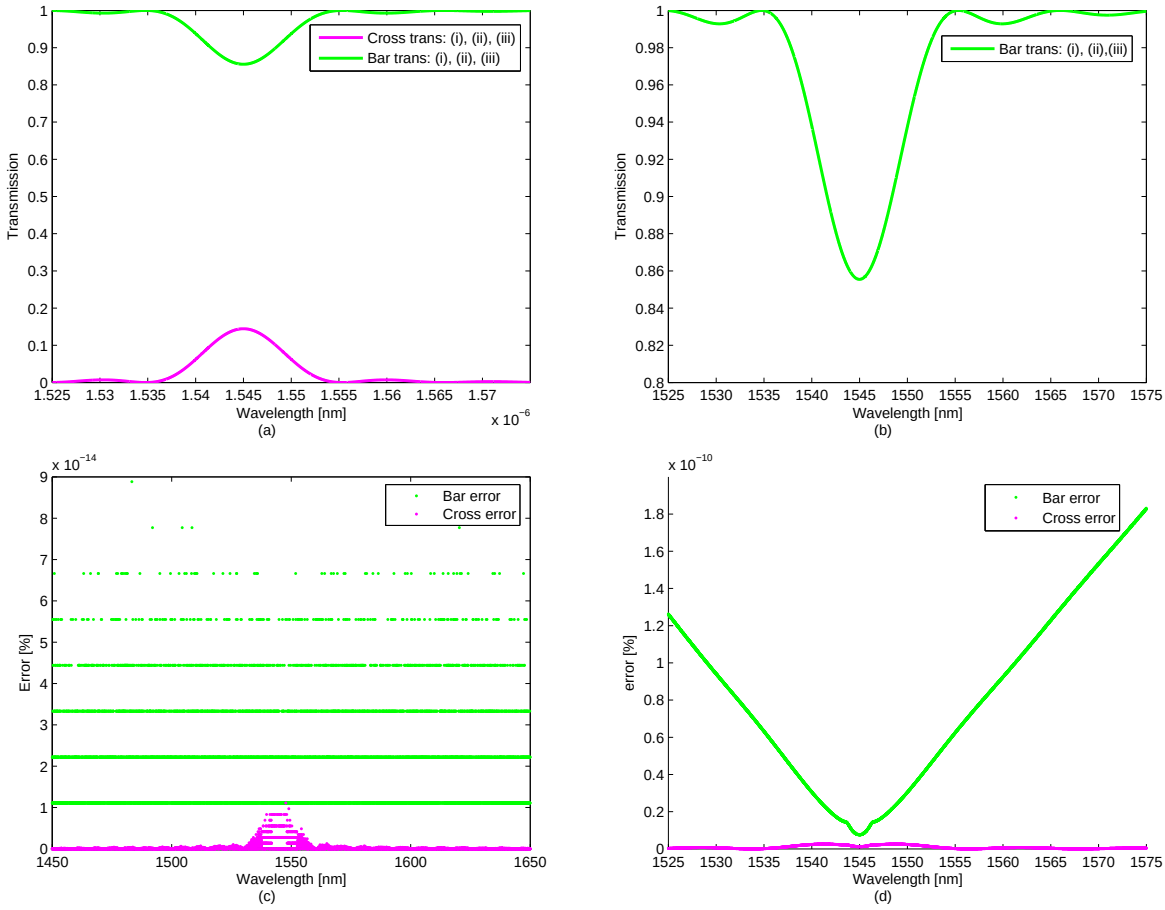

Figure 4.5: (a) The bar and cross transmission spectra in the weak grating limit, $\vartheta L = 0.39$, produced by (i) an analytical solution, (ii) ODE45 and (iii) the propagator. (b) A close up of the bar transmission spectrum shown in (a) facilitate a comparison with the results of Erdogan [3]. (c) The error in the propagators results as compared to the analytical solution for both the bar and cross transmission of (a). (c) The error in ODE45's results as compared to the analytical solution for both the bar and cross transmission of (a).

The cross transmission reveals those wavelengths for which mode 2 can gain energy and the bar transmission reveals those wavelengths for which mode 1 can give up its energy. Hence the two spectra are complementary.

Figures 4.3(a), 4.3(d) and 4.5(a) show the results of the LPG propagator compared to analytical solutions and numerical results. The parameters for these figures are provided in Table 4.3 and are chosen to correspond to parameters used in published results [3, 12]. All three LPGs have the same length. The gratings in Figure 4.3(a) and (d) differ only in their coupling-length product, ϑL. The greater the coupling-length product, the stronger the grating, the broader the bandwidth of the grating. Figure 4.4 shows a direct comparison between the bandwidth of the two spectra. This figure is a reproduction of a result by Othonos et al. [12]. The stronger grating has the broader bandwidth and also the most pronounced side lobes. These side lobes can be a disadvantage as they represent wavelengths other than the design wavelength for which coupling can occur. The strength of this undesirable coupling depends on the strength of the grating. For the weaker grating the transmission peak is around the design wavelength is sharper and the side lobes less prevalent. Figure 4.3(d) illustrates that coupling at these peripheral wavelengths can occur to the extent where the power output of mode 2 is equivalent to or greater than that of mode 1. This is seen at wavelengths for which the bar and cross transmission meet.

Figure 4.5(a) shows the bar and cross transmission spectrum for a much weaker grating than the previous two. Erdogan et al. [3] used these parameters to compare the theoretical results (Equation 4.9) with experimentally measured results. The agreement reported was excellent and here the propagator's result and the theoretical solution of Equations 4.7 and 4.9 are also in excellent agreement. Figure 4.5(b) is a reproduction of the result published [3].

Figures 4.3(a), 4.3(d) and 4.5(a) show the transmission spectra for gratings whereby the design wavelength of the grating coincides with the wavelength of maximum transmission. This need not always be the case. From Equations 4.7 and 4.9 it follows that the maximum transmission occurs when $\varrho^+ = 0$. The corresponding wavelength is given by

$$\lambda_{max} = \frac{1}{1-(\varrho_{11}-\varrho_{22})\frac{\Lambda}{2\pi}}\lambda_D.$$

However, in practice if the refractive index perturbation is only over the core of the optical fibre

$$\varrho_{11} = \frac{2\pi}{\lambda_D}\bar{\delta n}$$

and $\varrho_{11} \gg \varrho_{22}$ [3] so that λ_{max} can be approximated as

$$\lambda_{max} \approx \left(1+\frac{\bar{\delta n}}{\Delta n}\right)\lambda_D$$

where $\Delta n = n_1 - n_2$, the difference in the effective refractive indices seen by the modes. In the simulations corresponding to Figures 4.3 and 4.5 it was assumed that $\bar{\delta n} \ll \Delta n$, in accordance with the literature.

Figures 4.3(b) and (e) show the difference between the results produced by the propagator and the analytical solution, expressed as a percentage, for Figures 4.3(a) and (d) respectively. From the figures displaying the error, the propagator's results and the analytical solutions are in excellent agreement. The maximum error produced for the calculated spectra occurs for the grating corresponding to Figure 4.3(d) and is approximately $2 \times 10^{-13}\%$. The error in Figure 4.3(e) may be marginally higher than in the other two cases due to the occurrences of numerous and large side lobes to the central peak. This grating lies in the strong grating limit where side lobes in the spectrum become very prevalent in the case of a uniform

Transmission spectra	ODE45 time consumption [s]	Propagator time consumption [s]
Figure 4.3(a)	178.453	1.047
Figure 4.3(d)	237.094	1.203
Figure 4.5(a)	1956.9	1.234

Table 4.4: The time consumption for the three simulations both numerically and for the propagator.

grating. The spectrum itself is complex and substantial errors may occur in these strong gratings, in particular for wavelengths far removed from the wavelength of maximum transmission.

Figures 4.3(c) and (f) show the difference between the results produced by ODE45 and the analytical solution, expressed as a percentage, for Figures 4.3(a) and (d) respectively. According to the figures depicting the errors, the maximum error produced by ODE45 is approximately $5 \times 10^{-8}\%$, that is 5 orders of magnitude larger than that produced by the propagator. Comparing Figures 4.3(c) and (f) it appears that the stronger grating produces the highest error, however slight that difference may be.

Figures 4.5(c) and (d) show the propagator and ODE45 errors respectively as compared to the analytical solution for Figure 4.5(a). The maximum error for the propagator is approximately $9 \times 10^{-14}\%$ while that of ODE45 is approximately $1.9 \times 10^{-10}\%$. It must be noted that the spectra of Figure 4.5(a) correspond to a grating much weaker than those gratings corresponding to Figures 4.3(a) and (d) and that the errors are much smaller than the previous two cases.

Table 4.4 provides a comparison of the time consumption of ODE45 and the propagator for producing the transmission spectra of Figures 4.3 and 4.5. For Figure 4.3(a), the transmission spectra took approximately 170 times longer for ODE45 to calculate than it did for the propagator. For Figure 4.3(d), ODE45 took approximately 197 times longer than the propagator while for the transmission spectra of Figure 4.5(a) took approximately 1586 times longer for ODE45 to calculate than it did for the propagator. The strength of the propagator over numerical integration lies in the fact that, as an analytical solution one need only evaluate the amplitudes at the desired position. So to calculate the spectra one is only required to calculate the amplitudes at L and then use $F_1(L)$ and $F_2(L)$ to calculate the bar and cross transmission together with the given initial conditions. Numerical integration is iterative, so to calculate the fields at L, one has to calculate the amplitudes at each point along the waveguide. The number of points for which one must calculate the amplitudes also plays a role in the time consumption and accuracy. Generally, the more complex the solution the greater the number of points required for better accuracy but the greater the calculation's time consumption.

It can be concluded that in the case of a uniform grating, the LPG propagator is efficient and yields physically sensible results. The LPG propagator is more efficient than ODE45 as the time consumption in calculating the spectral properties of the gratings is smaller and a greater accuracy is achieved.

4.2 Bragg gratings

A Bragg grating is the most familiar form of a reflection grating, that is a grating responsible for coupling two counter propagating modes. The Bragg grating specifically couples identical counter propagating modes. The phase-matching condition for a Bragg grating in terms of the propagation constants of the

modes is given by Equation 4.3 where

$$\begin{aligned}\Delta\beta &= \beta_1 - \beta_2 \\ &= \beta_1 - (-\beta_1) \\ &= 2\beta_1.\end{aligned}$$

Hence the period, Λ, of a reflection grating being dependent on a large $\Delta\beta$ (large relative to that for a transmission grating) is shorter than that for a transmission grating.

4.2.1 Transforming the coupled-mode equations for a Bragg grating

As with the LPGs the coupled-mode equations (Equations 3.1 and 3.2) may be simplified by retaining only those terms that pertain to the particular modes of interest. In the case of a Bragg grating one retains the amplitude $F(z)$ of a forward propagating mode and amplitude $B(z)$ of an identical backward propagating mode. Synchronous transformations as described by Erdogan et al. [3] are used once again to avoid any explicit z-dependence in the coupling coefficients:

$$\begin{aligned}\tilde{F}(z) &= F(z)\exp\{i\delta\beta z\} \\ \tilde{B}(z) &= B(z)\exp\{-i\delta\beta z\}.\end{aligned}$$

Here $\delta\beta = \beta - \frac{\pi}{\Lambda}$ is the detuning parameter. It can then be shown [3, 12] that the coupled-mode equations reduce to

$$\begin{aligned}\frac{d\tilde{F}}{dz} &= i\varrho^{+}\tilde{F}(z) + i\vartheta\tilde{B}(z) \\ \frac{d\tilde{B}}{dz} &= -i\vartheta^{*}\tilde{F}(z) - i\varrho^{+}\tilde{B}(z).\end{aligned} \tag{4.10}$$

Here $\vartheta = \vartheta_{12} = \vartheta_{21}^{*}$ and $\varrho^{+} = \delta\beta + \varrho$. For the case of the Bragg grating there are simplifications that can be made regarding the coupling coefficients [3, 12], namely

$$\varrho = \frac{2\pi}{\lambda_D}\overline{\delta n} \tag{4.11}$$

$$\vartheta = \frac{\pi}{\lambda_D}v\overline{\delta n} \tag{4.12}$$

These coupling coefficients are constant over the length of the grating. Hence Equations 4.10 are reduced to two coupled ordinary differential equations with constant coefficients for which closed form solutions can be obtained.

4.2.2 The Bragg propagator

Due to the lack of any explicit z-dependence, the unperturbed propagator can be used to solve Equations 4.10 where off-diagonal components occur in the coupling matrix which account for the cross coupling of

the modes. The coupling matrix is given by

$$\begin{aligned} M_0 &= \begin{bmatrix} i\varrho^+ & i\vartheta \\ -i\vartheta & -i\varrho^+ \end{bmatrix} \\ &= \begin{bmatrix} i\left(\beta - \frac{\pi}{\Lambda} + \frac{2\pi}{\lambda_D}\overline{\delta n}\right) & i\frac{\pi}{\lambda_D}v\overline{\delta n} \\ -i\frac{\pi}{\lambda_D}v\overline{\delta n} & -i\left(\beta - \frac{\pi}{\Lambda} + \frac{2\pi}{\lambda_D}\overline{\delta n}\right) \end{bmatrix} \end{aligned}$$

Making use of co-factor expansion $(M_0 - ik)^{-1}$ and the poles of the propagator are calculated

$$\begin{aligned} (M_0 - ik)^{-1} &= \begin{bmatrix} i\varrho^+ - ik & i\vartheta \\ -i\vartheta & -i\varrho^+ - ik \end{bmatrix}^{-1} \\ &= \frac{1}{\det\left[M_0 - k\right]} \begin{bmatrix} -i\varrho^+ - ik & -i\vartheta \\ i\vartheta & i\varrho^+ - ik \end{bmatrix} \\ &= \frac{1}{i\left(k - e_1\right)\left(k - e_2\right)} \begin{bmatrix} -\varrho^+ - k & -\vartheta \\ \vartheta & \varrho^+ - k \end{bmatrix}. \end{aligned}$$

Hence the propagator expressed as an integral over real axis, given by

$$G\left(z, z'\right) = \frac{1}{2\pi i}\int_{-\infty}^{\infty} dk \frac{1}{\left(k - e_1\right)\left(k - e_2\right)} \begin{bmatrix} -\varrho^+ - k & -\vartheta \\ \vartheta & \varrho^+ - k \end{bmatrix} e^{ik\left(z - z'\right)}\left(\theta\left(z - z'\right) + \theta\left(z' - z\right)\right)$$

and as a contour integral by

$$G\left(z, z'\right) = \frac{1}{2\pi i}\oint_{\gamma} dk \frac{1}{\left(k - e_1\right)\left(k - e_2\right)} \begin{bmatrix} -\varrho^+ - k & -\vartheta \\ \vartheta & \varrho^+ - k \end{bmatrix} e^{ik\left(z - z'\right)}\left(\theta\left(z - z'\right) + \theta\left(z' - z\right)\right).$$

Solving the integral in the usual way we arrive at

$$\begin{aligned} G\left(z, z'\right) &= \left\{ \frac{1}{\left(e_1 - e_2\right)} \begin{bmatrix} -\varrho^+ - e_1 & -\vartheta \\ \vartheta & \varrho^+ - e_1 \end{bmatrix} \exp\left\{ie_1\left(z - z'\right)\right\} \right. \\ &+ \left. \frac{1}{\left(e_2 - e_1\right)} \begin{bmatrix} -\varrho^+ - e_2 & -\vartheta \\ \vartheta & \varrho^+ - e_2 \end{bmatrix} \exp\left\{ie_2\left(z - z'\right)\right\} \right\}. \end{aligned}$$

4.2.3 Results for the Bragg grating

As in Section 4.1.3, the associated power flow of the modes was investigated as well as the spectra of the simulated gratings. These results were then compared to numerical (ODE45), analytical and published results respectively.

To quantify the accuracy of ODE45 and the propagator, it was necessary to derive analytical solutions for each mode from Equations 4.10. These solutions are

$$\begin{aligned} \tilde{F}\left(z\right) &= \frac{\left(\varrho^+ - \alpha\right)e^{i2\alpha L}}{\left(\varrho^+ - \alpha\right)e^{i2\alpha L} - \varrho^+ - \alpha} e^{-i\alpha z} - \frac{\left(\varrho^+ + \alpha\right)}{\left(\varrho^+ - \alpha\right)e^{i2\alpha L} - \varrho^+ - \alpha} e^{i\alpha z} \\ \tilde{B}\left(z\right) &= -\frac{\vartheta e^{i2\alpha L}}{\left(\varrho^+ - \alpha\right)e^{i2\alpha L} - \varrho^+ - \alpha} e^{-i\alpha z} + \frac{\vartheta}{\left(\varrho^+ - \alpha\right)e^{i2\alpha L} - \varrho^+ - \alpha} e^{i\alpha z} \end{aligned}$$

where $\alpha = \sqrt{\varrho^{+2} - \vartheta^2}$. The derivation of these solutions can be found in Section 7.3 of the Appendix. The

Parameters	Figure 4.6(a)	Figure 4.6(c)	Figure 4.6(e)
L	1 mm	1 mm	1 mm
λ_D	1550 nm	1550 nm	1550 nm
λ	λ_D	$0.99 \times \lambda_D$	λ_D
Λ	53.45 μm	53.45 μm	53.45 μm
n	1.45	1.45	1.45
$v\delta n$	1×10^{-3}	1×10^{-3}	1×10^{-6}

Table 4.5: Parameters used in the modeling of the gratings corresponding to Figures 4.6(a), (c) and (e).

Simulation	Figure 4.6(a)	Figure 4.6(c)	Figure 4.6(e)
Wavelength	λ_D	$0.99 \times \lambda_D$	λ_D
$v\bar{\delta n}$	1×10^{-3}	1×10^{-3}	1×10^{-4}
ODE45 Error mode 1 [%]	1.1121×10^{-14}	2.6441×10^{-4}	1.1373×10^{-16}
ODE45 Error mode 2 [%]	1.2096×10^{-14}	0.4512	1.0184×10^{-14}
ODE45 Time Consumption [s]	0.3120	1.312	0.1880
Propagator Error mode 1 [%]	5.5235×10^{-16}	2.7845×10^{-4}	2.1121×10^{-16}
Propagator Error mode 2 [%]	4.394×10^{-16}	0.4450	1.3218×10^{-15}
Propagator Time Consumption [s]	0.047	4.0630	0.0160

Table 4.6: The error and time consumption for the simulations associated with the spectra of Figures 4.6.

results of the propagator and ODE45 are compared to the analytical solution to calculate the percentage difference, that is considered the error in ODE45 and the propagator results.

The parameters used to simulate the Bragg gratings corresponding to Figure 4.6 are given in Table 4.5. Figure 4.6(a) shows the behaviour of the Bragg grating under phase-matched conditions when $\lambda = \lambda_D$. It is important to note that the decrease in the amplitudes is not due to any attenuation but rather as the one mode propagates in the forward direction (amplitude 1 in the figure), energy is coupled into the backward propagating mode (amplitude 2). The conservation of energy must always be satisfied, just as in the case of the LPG. However this conservation of energy requires that the net power transfer between the two modes remains constant with propagation distance. This can be expressed as

$$\frac{d}{dz}\left(|F|^2 - |B|^2\right) = 0 \tag{4.13}$$

Figure 4.6(b) shows that the net power flow corresponding to Figure 4.6(a) is constant along the length of the grating. Hence Equation 4.13 is satisfied for the phase-matched case. Figure 4.6(c) shows the result for the case where $\lambda = 0.99\lambda_D$. Under these nonphase-matched conditions no observable transfer of energy takes place. However, the corresponding energy conservation curve, Figure 4.6(d), suggests that energy is transferred as the net power flow is less than 1 W. The curve of Figure 4.6(d) is constant with propagation distance so that Equation 4.13 is satisfied under the nonphase-matching conditions.

From Equation 4.12, it is seen that the cross-coupling coefficient is dependent on the factor $v\bar{\delta n}$ where v is the fringe visibility and $\bar{\delta n}$ is the dc index change. The gratings corresponding to Figures 4.6(a) and (c) have a $v\bar{\delta n} = 1\times10^{-3}$. Figure 4.6(e) corresponds to a weaker grating with $v\bar{\delta n} = 1\times10^{-4}$ under phase-matched conditions $\lambda = \lambda_D$. A comparison of Figures 4.6(a) and (e) illustrates the dependence of the coupling on $v\bar{\delta n}$ under phase-matched conditions. Figure 4.6(f) is the corresponding energy conservation curve which shows the small (as compared to Figure 4.6(b)) amount of power transfer. This curve also remains constant with propagation distance, satisfying Equation 4.13.

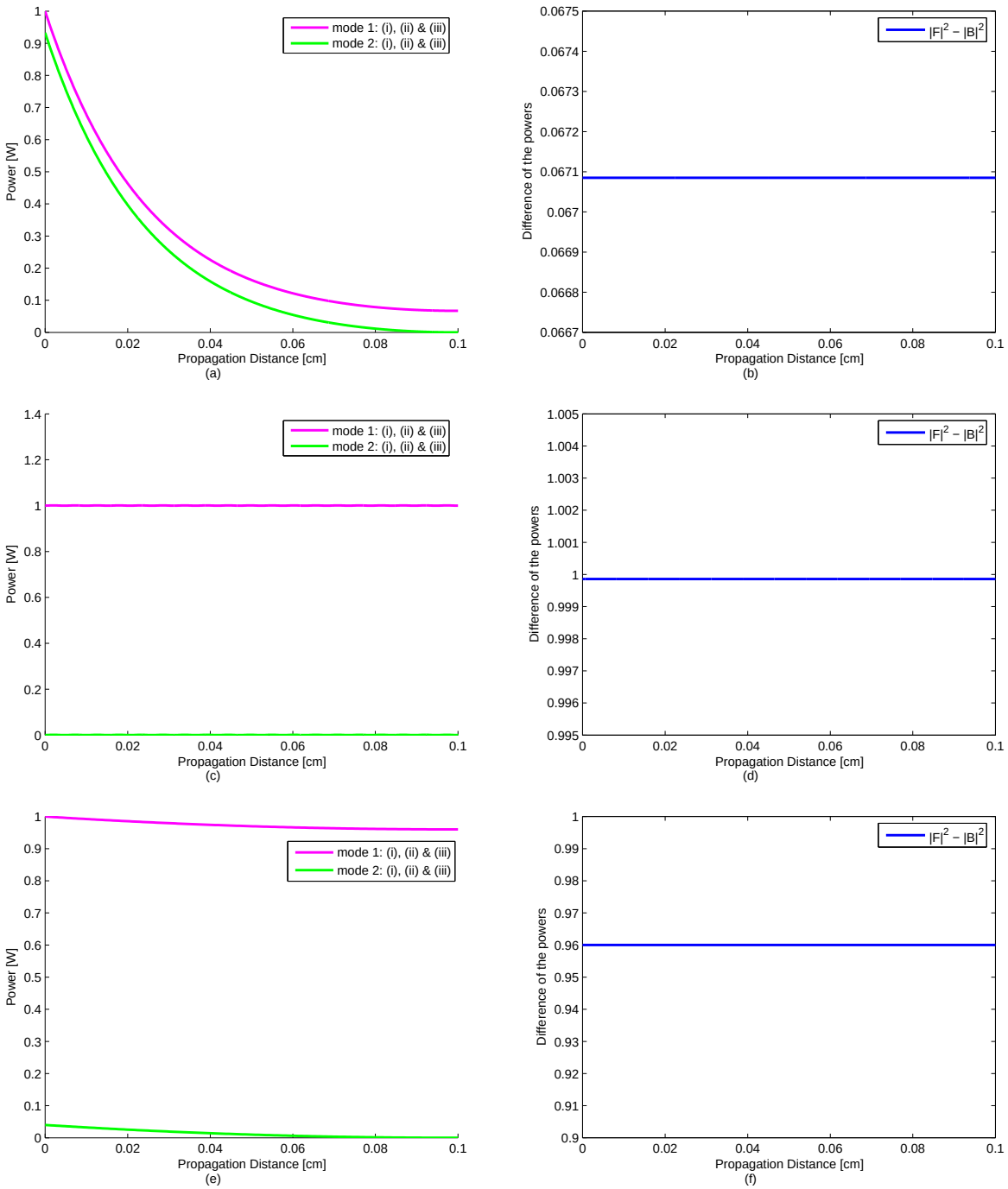

Figure 4.6: Results of the (i) analytical solution (ii) ODE45 and (iii) the propagator compared. (a) The evolution of the powers of the two counter propagating modes under phase-matched conditions, namely when $\lambda = \lambda_D$ with $v\bar{\delta n} = 1 \times 10^{-3}$. (b) The net power of the modes with propagation distance calculated using the propagator. (c) The evolution of the powers of the two counter propagating modes under nonphase-matched conditions, namely when $\lambda = 0.99\lambda_D$ with $v\bar{\delta n} = 1 \times 10^{-3}$. (d) The net power of the modes with propagation distance calculated using the propagator. (e) The evolution of the powers of the two counter propagating modes under phase-matched conditions with $v\bar{\delta n} = 1 \times 10^{-6}$. (f) The net power of the modes with propagation distance calculated using the propagator.

Parameters	Figure 4.7(a)	Figure 4.7(b)	Figure 4.8	Figure 4.9
L	1 cm	1 cm	1 mm	1 mm
λ_D	1550 nm	1550 nm	1545 nm	1550 nm
v	1	1	1	1×10^{18}
δn	1×10^{-4}	4×10^{-4}	8×10^{-4}	1×10^{-21}

Table 4.7: These are parameters given and calculated from literature [3, 12] used to generate the spectra of Figures 4.7, 4.8 and 4.9.

For the Bragg grating only one spectrum may be obtained, namely the reflection spectrum. The reflection spectrum is the ratio of the output power of the reflected mode at $z = 0$ to the power of the input mode at $z = 0$. Formulated after Erdogan et al. [3], the reflectivity is given by

$$\begin{aligned} R &= \frac{|B(z)|^2}{|F(z)|^2} \\ &= \frac{\sinh^2\left(\sqrt{\vartheta^2 - \varrho^{+2}}z\right)}{\cosh^2\left(\sqrt{\vartheta^2 - \varrho^{+2}}z\right) - \frac{\varrho^{+2}}{\vartheta^2}}. \end{aligned} \tag{4.14}$$

Figures 4.7(a), 4.7(d) and 4.8(a) show the results for the reflection spectrum of the Bragg propagator compared to those produced by ODE45 and the analytical solution for the reflectivity. The values for the parameters used to generate the spectra in Figures 4.7 and 4.8 are given in Table 4.7. Figures 4.7(a) and 4.7(d) show the effect that the the magnitude of the dc index change, $\bar{\delta n}$, has on the reflection spectrum. Both gratings, corresponding to Figures 4.7(a) and (d), have the same physical parameters with the exception of $\bar{\delta n}$. Figure 4.7(a) has a smaller $\bar{\delta n}$ than that of Figure 4.7(d). The effect of the dc index change on the cross-coupling coefficient, ϑ, is seen from Equation 4.12. The cross-coupling coefficient, is directly proportional to $\bar{\delta n}$. Hence the smaller $\bar{\delta n}$, the weaker the grating, the narrower the bandwidth and the less prevalent the side lobes.

Figure 4.8(a) shows the reflection spectrum for a much stronger grating than the previous two. Erdogan et al. [3] used these parameters to compare the theoretical results (Equation 4.14) with experimentally measured results. The agreement reported was excellent. In this study the Bragg propagator's result and the theoretical solution of Equation 4.14 are also in excellent agreement. Figures 4.7(a), 4.7(d) and 4.8(a) are reproductions of published results [3].

An interesting design feature of these Bragg reflection spectra is that the maximum reflectivity does not necessarily correspond to the design wavelength. From Equation 4.14 the reflectivity is at a maximum when $\varrho^{+2} = 0$. From $\varrho^{+} = \delta\beta + \varrho$ and Equation 4.11, the wavelength of maximum reflection occurs for

$$\lambda_{max} = \left(1 + \frac{\bar{\delta n}}{n}\right)\lambda_D. \tag{4.15}$$

Hence the larger $\bar{\delta n}$, the further λ_{max} shifts away from λ_D towards higher wavelengths. However, it is possible to design gratings whereby $\delta n \to 0$ but the fringe visibility, v, is very large. In this way ϑ, which is directly proportional to v (Equation 4.12), is still large enough for significant coupling between the modes but $\varrho \to 0$ since it is not dependent on v. In this way, a strong grating with $\lambda_{max} \approx \lambda_D$ may be realized. Figure 4.9 illustrates an example of a strong grating with a weak $\bar{\delta n}$ and large v. In this figure, $\bar{\delta n} = 1 \times 10^{-21}$ and $v = 1 \times 10^{18}$ so that $\vartheta \propto v\bar{\delta n} = 1 \times 10^{-3}$ which is technically in the strong grating limit while $\varrho \propto \bar{\delta n} = 1 \times 10^{-21}$.

Figures 4.7(b) and (e) and Figure 4.8(b) show the associated error between the analytical solutions

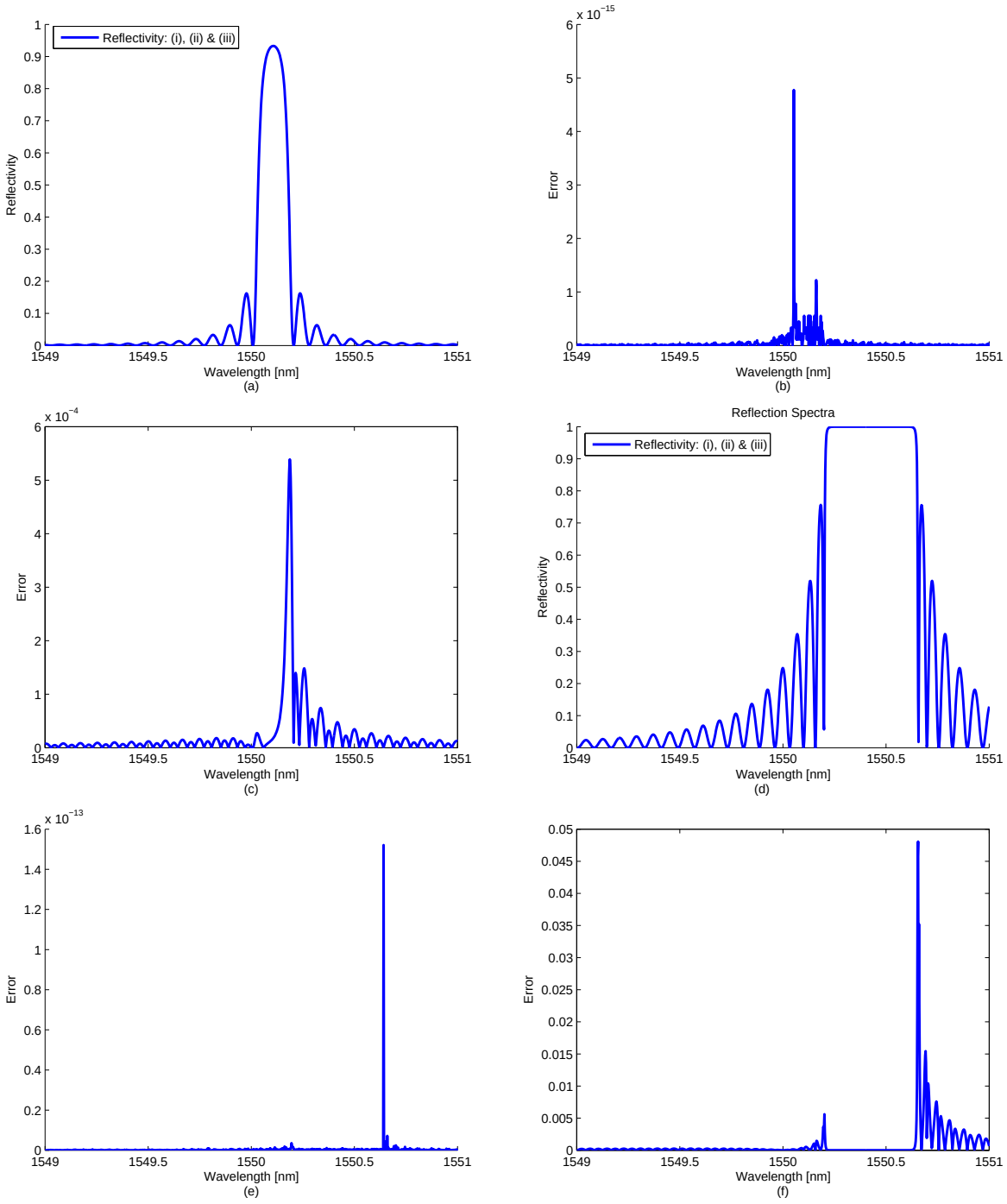

Figure 4.7: (a) The reflection spectrum in the weaker grating limit, $\delta n = 1 \times 10^{-4}$, produced by an (i) analytical solution (ii) ODE45 (iii) the propagator. (b) The error in the propagator's results as compared to the analytical solution for both the reflection (a). (c) The error in ODE45's results as compared to the analytical solution for the reflection of (a). (d) The reflection spectrum in the stronger grating limit, $\delta n = 4 \times 10^{-4}$, produced by (i) an analytical solution (ii) ODE45 (iii) the propagator. (e) The error in the propagator's results as compared to the analytical solution for the reflection of (d). (f) The error in ODE45's results as compared to the analytical solution for reflection of (d).

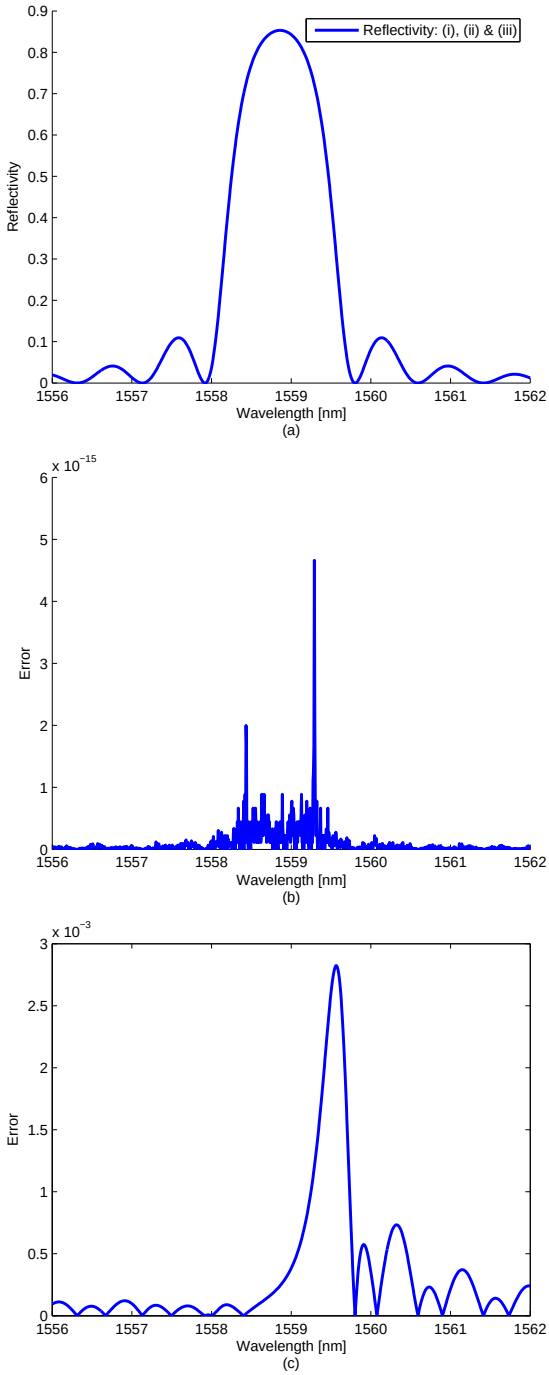

Figure 4.8: (a) The reflection spectrum in the strong grating limit, $\delta n = 8 \times 10^{-4}$, produced by (i) an analytical solution, (ii) ODE45 (iii) the propagator. (b) The error in the propagator's results as compared to the analytical solution for the reflection of (a). (c) The error in ODE45's results as compared to the analytical solution for the reflection of (a).

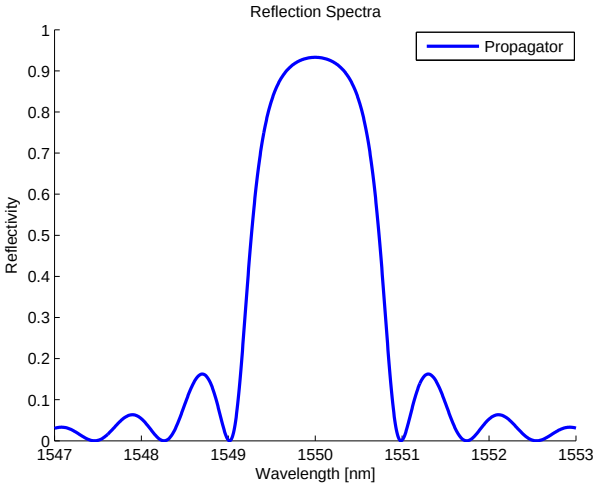

Figure 4.9: The reflection spectrum of a Bragg grating in the strong grating limit, $\vartheta \propto v\bar{\delta n} = 1 \times 10^{-3}$ where the maximum wavelength is equivalent to the design wavelength. In this case $\lambda_D = 1550\,\text{nm}$ and $L = 1\,\text{cm}$ just as the gratings corresponding to Figure 4.7.

Transmission spectra	ODE45 time consumption [s]	Propagator time consumption [s]
Figure 4.7(a)	325.781	0.062
Figure 4.7(d)	372.812	0.047
Figure 4.8(a)	523.047	0.078

Table 4.8: The time consumption for the three simulations both numerically and for the propagator.

and the propagator's results for each wavelength. The propagator's results and the analytical solutions are in excellent agreement with each other. The maximum error produced in all the simulations occurs for the grating simulated in Figure 4.7(d) and is approximately 1.6×10^{-13}, as seen in Figure 4.7(e). The fact that the error is higher for this grating than for the other two is most probably due to the combination of parameters that leads to the development of pronounced and closely spaced side lobes. In fact this error occurs at the wavelength where there is a sudden drop in the reflectivity. Should there be a substantial error it will most likely occur for wavelengths where there are sudden changes in the reflectivity, as where side lobes occur.

Figures 4.7(c) and (f) and Figure 4.8(c) show the error in the results produced by ODE45 as compared to the analytical solution. The error mirrors the spectra in the sense that the greatest error lies in the wavelength regions where the side lobes are most prevalent. As with the propagator the greatest error occurs for the grating corresponding to Figure 4.7(d) and is approximately 0.05, as seen in Figure 4.7(f).

Table 4.8 provides a comparison of the time consumption of ODE45 and the propagator for producing the reflection spectra of Figures 4.7 and 4.8. For Figure 4.7(a), the reflection spectra took approximately 5254 times longer for ODE45 to calculate than it did for the propagator. For Figure 4.3(d), ODE45 took approximately 7932 times longer than the propagator while the reflection spectra of Figure 4.8(a) took approximately 6705 times longer for ODE45 to calculate than it did for the propagator.

As discussed in Section 4.1.3, the strength of the propagator over numerical integration lies in the fact that the amplitudes need only be evaluated at the desired position whereas for numerical integration the amplitudes need to be evaluated at each position leading up to the position of interest. So to calculate the refection spectra using the propagator, it is only required to calculate the amplitudes at of the backward propagating mode at $z = 0$ and then use $F(0)$ (given) and $B(0)$ to calculate the reflectivity.

To calculate the amplitude of the backward propagating mode at $z = 0$, using ODE45, it is required that the amplitudes at each point along the waveguide from $z = L$ to $z = 0$ is calculated. The number of points for which one must calculate the amplitudes also plays a role in the time consumption and accuracy. Generally, the more complex the solution the greater the number of points required for better accuracy but the greater the calculation's time consumption.

It can be concluded from this section that in the case of a uniform grating, the Bragg propagator is efficient and yields physically sensible results. The Bragg propagator is more efficient than ODE45 as the time consumption in calculating the spectral properties of the Bragg gratings is smaller and a greater accuracy is achieved.

Chapter 5

Nonuniform Gratings: The Quest for the Perturbed Propagator

It was shown in Chapter 4 that increasing the magnitude of the dc index increases the bandwidth of the gratings, but the presence of increased side lobes is unfavourable in many practical applications. Modulating the uniform grating in a variety of ways can alter the optical properties of the grating, thereby suppressing many undesirable effects and inducing other desirable ones. To name a few: chirping the fibre grating to compensate for dispersion [3, 13], controlling and shaping short pulses in fibre lasers [3, 4] and increasing the stability of continuous-wave and tunable mode-locked external-cavity diode lasers [3, 10, 11]. Discrete phase shifts in a uniform grating can create a narrow transmission resonance in a reflection grating [3, 12]. Apodizing the coupling strength of a grating can produce a desired top-hat shape in the reflection spectrum [3, 12]. Gratings with a periodic superstructure where the grating period is varied periodically by a period much larger than the grating period, have been shown to work for a number of applications [3].

5.1 The Perturbed Propagator

The Green's function for the case of mode propagation in a perturbed waveguide was derived in Chapter 2 and is given by Equation 2.16

$$\begin{aligned} G(z,z') &= \int_{-\infty}^{\infty} \frac{dk}{2\pi} (M_0 - ik)^{-1} e^{ik(z-z')} \\ &\quad - \int_{-\infty}^{\infty} \frac{dk}{2\pi} \int_{-\infty}^{\infty} \frac{dq}{2\pi} \int_{-\infty}^{\infty} dx\, (M_0 - ik)^{-1} e^{ik(x-z')} \Delta M(x) (M_0 - iq)^{-1} e^{iq(z-x)} \end{aligned}$$

where M_0 is the coupling matrix for the unperturbed case. Rewriting this integral by grouping x-dependent terms yields:

$$\begin{aligned} G(z,z') &= \int_{-\infty}^{\infty} \frac{dk}{2\pi} (M_0 - ik)^{-1} e^{ik(z-z')} \\ &\quad - \int_{-\infty}^{\infty} \frac{dk}{2\pi} \int_{-\infty}^{\infty} \frac{dq}{2\pi} (M_0 - ik)^{-1} e^{-ikz'} \left\{ \int_{-\infty}^{\infty} dx \Delta M(x) e^{i(k-q)x} \right\} (M_0 - iq)^{-1} e^{iqz}. \quad (5.1) \end{aligned}$$

However, the integral of $\Delta M(x)$ is the Fourier transform of the perturbation. Hence

$$\begin{aligned} \int_{-\infty}^{\infty} dx \Delta M(x) e^{i(k-q)x} &= \mathcal{F}[\Delta M(x)] \\ &= \Delta M(k-q). \end{aligned}$$

Thus the x-dependence in the Green's function can be eliminated, yielding

$$\begin{aligned} G(z,z') &= \int_{-\infty}^{\infty} \frac{dk}{2\pi} (M_0 - ik)^{-1} e^{ik(z-z')} \\ &\quad - \int_{-\infty}^{\infty} \frac{dk}{2\pi} \int_{-\infty}^{\infty} \frac{dq}{2\pi} (M_0 - ik)^{-1} e^{-ikz'} \Delta M(k-q) (M_0 - iq)^{-1} e^{iqz}. \quad (5.2) \end{aligned}$$

5.2 The coupled-mode equations for a grating modulation

When modulating the uniform grating, a z-dependence is introduced to the coupling coefficients. The coupled-mode equations can no longer be treated as two coupled ordinary differential equations with constant coefficients and no closed form solutions can be found. For the case of two forward propagating modes the coupled-mode equations are given by

$$\begin{aligned} \frac{d\tilde{F}_1}{dz} &= i\varrho^+(z) \tilde{F}_1(z) + i\vartheta(z) \tilde{F}_2(z) \\ \frac{d\tilde{F}_2}{dz} &= i\vartheta(z)^* \tilde{F}_1(z) - i\varrho^+(z) \tilde{F}_2(z). \quad (5.3) \end{aligned}$$

Here $\varrho^+(z) = \delta\beta + \frac{(\varrho_{11}(z)+\varrho_{22}(z))}{2}$. $\varrho^+(z)$ is the same dc self-coupling coefficient introduced in Section 4.1.1 for the uniform grating, only now the z-dependence is introduced in the $\varrho_{11}(z)$ and $\varrho_{22}(z)$ self-coupling terms. They are given by

$$\begin{aligned} \varrho_{\mu\nu}(z) &= \frac{\omega}{2} n\bar{\delta n}(z) \int_{-\infty}^{\infty} \int_{-\infty}^{\infty} dxdy \bar{\xi}_\mu^*(x,y) \bar{\xi}_\nu(x,y) \\ &= \bar{\varrho}_{\mu\nu} \bar{\delta n}(z) \quad (5.4) \end{aligned}$$

The cross-coupling coefficient, $\vartheta(z)$, is given by

$$\begin{aligned}\vartheta_{\mu\nu}(z) &= \frac{\omega}{2} n\bar{\delta n}(z) \int_{-\infty}^{\infty}\int_{-\infty}^{\infty} dxdy\bar{\xi}_{\mu}^{*}(x,y)\,\bar{\xi}_{\nu}(x,y) \\ &= \bar{\vartheta}_{\mu\nu}\bar{\delta n}(z)\,. \end{aligned} \tag{5.5}$$

The z-dependence of both the self-coupling and cross-coupling coefficients is due to the z-dependent modulation to the refractive index, the dc index change, $\bar{\delta n} = \bar{\delta n}(z)$. In Equations 5.4 and 5.5 the terms $\bar{\varrho}_{\mu\nu}$ and $\bar{\vartheta}_{\mu\nu}$ are the z-independent factors of the coupling coefficients - largely due to the overlap of the respective modes - and are just real numbers.

The coupling coefficients (Equations 5.4 and 5.5) are also applicable to the case of two counter propagating modes. Their coupled-mode equations are given by

$$\begin{aligned}\frac{d\tilde{F}}{dz} &= i\varrho^{+}(z)\,\tilde{F}(z) + i\vartheta(z)\,\tilde{B}(z) \\ \frac{d\tilde{B}}{dz} &= -i\vartheta^{*}(z)\,\tilde{F}(z) - i\varrho^{+}(z)\,\tilde{B}(z)\,. \end{aligned} \tag{5.6}$$

In the case of a Bragg grating the coupling coefficients are reduced to

$$\begin{aligned}\varrho &= \frac{2\pi}{\lambda_D}\bar{\delta n}(z) \\ \vartheta &= \frac{\pi}{\lambda_D} v\bar{\delta n}(z)\,. \end{aligned}$$

The approach taken when using perturbation theory requires that the coupling coefficients be separated into z-independent and z-dependent parts. The z-independent part then represents the uniform or zeroth order part. The z-dependent part contains the information pertaining to the modulation.

5.3 Apodization of the LPG: The raised-cosine modulation

Apodization describes modulating the refractive index perturbation to suppress the side lobe structure associated with the uniform grating. The uniform fibre grating, where $\bar{\delta n}(z) = \bar{\delta n}$, begins and ends abruptly. The Fourier transform of such a rectangular function, $\bar{\delta n}$ is the sinc function having associated side lobes. This side lobe structure is seen in the reflection and transmission spectra of the uniform gratings modeled in Chapter 4. To illustrate the principle of apodization consider the Fourier transform of a Gaussian function which remains Gaussian with no side lobe structure. Modulating the periodic refractive index perturbation by a Gaussian or similar function yields a reflection spectrum with a suppressed side lobe structure. Changing the refractive index modulation amplitude also changes the design wavelength, as a distributed Fabry-Perot interferometer is formed. The result is side lobe structure on the blue side of the spectra [8]. To avoid this, the average refractive index must remain constant throughout the length of the grating while the refractive index modulation amplitude varies. As an initial example the raised-cosine modulation is used for its relative simplicity in applying perturbation theory. There are many examples available in the literature for which it is demonstrated that the raised-cosine and Gaussian apodizations yield virtually indistinguishable results [3, 12].

5.3.1 A perturbed propagator for a raised-cosine modulation

The raised-cosine modulation to the refractive index is expressed as

$$\begin{aligned} \bar{\delta n}(z) &= \bar{\delta n}\frac{1}{2}\left[1+\cos\left(\frac{\pi}{\sigma}z\right)\right] \\ &= \frac{1}{2}\bar{\delta n}+\frac{1}{2}\bar{\delta n}\cos\left(\frac{\pi}{\sigma}z\right) \end{aligned} \tag{5.7}$$

where σ is the full width at half maximum of the cosine function. Typically $\sigma = L$ for a raised-cosine modulation for a grating of a length L. This form of $\bar{\delta n}(z)$ is convenient to use directly for perturbation theory as it can be separated into z-dependent and z-independent parts.

The coupling matrix is given by

$$\begin{aligned} M(z) &= \begin{bmatrix} i\varrho^{+}(z) & i\vartheta(z) \\ i\vartheta(z) & -i\varrho^{+}(z) \end{bmatrix} \\ &= \begin{bmatrix} i\delta\beta+i\bar{\varrho}\bar{\delta n}(z) & i\bar{\vartheta}\bar{\delta n}(z) \\ i\bar{\vartheta}\bar{\delta n}(z) & -i\delta\beta-i\bar{\varrho}\bar{\delta n}(z) \end{bmatrix}. \end{aligned} \tag{5.8}$$

Applying a raised-cosine modulation to the LPG the uniform and perturbed parts of $M(z)$ are given by

$$M_0 = \begin{bmatrix} i\delta\beta+i\frac{1}{2}\bar{\varrho}\bar{\delta n} & i\frac{1}{2}\bar{\vartheta}\bar{\delta n} \\ i\frac{1}{2}\bar{\vartheta}\bar{\delta n} & -i\delta\beta-i\frac{1}{2}\bar{\varrho}\bar{\delta n} \end{bmatrix} \tag{5.9}$$

and

$$\Delta M(z) = \begin{bmatrix} i\frac{1}{2}\bar{\varrho}\bar{\delta n} & i\frac{1}{2}\bar{\vartheta}\bar{\delta n} \\ i\frac{1}{2}\bar{\vartheta}\bar{\delta n} & -i\frac{1}{2}\bar{\varrho}\bar{\delta n} \end{bmatrix}\cos\left(\frac{\pi}{\sigma}z\right) \tag{5.10}$$

respectively. To solve the Fourier transform

$$\begin{aligned} \int_{-\infty}^{\infty} dx\Delta M(x)\,e^{i(k-q)x} &= \mathcal{F}\left[\Delta M(x)\right] \\ &= \mathcal{F}\left[\begin{bmatrix} i\frac{1}{2}\bar{\varrho}\bar{\delta n} & i\frac{1}{2}\bar{\vartheta}\bar{\delta n} \\ i\frac{1}{2}\bar{\vartheta}\bar{\delta n} & -i\frac{1}{2}\bar{\varrho}\bar{\delta n} \end{bmatrix}\cos\left(\frac{\pi}{\sigma}x\right), x, (k-q)\right] \\ &= \begin{bmatrix} i\frac{1}{2}\bar{\varrho}\bar{\delta n} & i\frac{1}{2}\bar{\vartheta}\bar{\delta n} \\ i\frac{1}{2}\bar{\vartheta}\bar{\delta n} & -i\frac{1}{2}\bar{\varrho}\bar{\delta n} \end{bmatrix}\left\{\sqrt{\frac{\pi}{2}}\delta\left(k-q-\frac{\pi}{\sigma}\right)+\sqrt{\frac{\pi}{2}}\delta\left(k-q+\frac{\pi}{\sigma}\right)\right\}. \end{aligned}$$

Hence the perturbed part of the propagator, given by

$$G_1(z,z') = \int_{-\infty}^{\infty}\frac{dk}{2\pi}\int_{-\infty}^{\infty}\frac{dq}{2\pi}\left(M_0-ik\right)^{-1}e^{-ikz'}\Delta M(k-q)\left(M_0-iq\right)^{-1}e^{iqz}$$

is split up into two integrals corresponding to the two Dirac delta functions, namely

$$G_{11}(z,z') = \sqrt{\frac{\pi}{2}}\int_{-\infty}^{\infty}\frac{dk}{2\pi}\int_{-\infty}^{\infty}\frac{dq}{2\pi}\left(M_0-ik\right)^{-1}e^{-ikz'}\begin{bmatrix} i\frac{1}{2}\bar{\varrho}\bar{\delta n} & i\frac{1}{2}\bar{\vartheta}\bar{\delta n} \\ i\frac{1}{2}\bar{\vartheta}\bar{\delta n} & -i\frac{1}{2}\bar{\varrho}\bar{\delta n} \end{bmatrix}\delta\left(k-q-\frac{\pi}{\sigma}\right)\left(M_0-iq\right)^{-1}e^{iqz}$$

which, after carrying out the k integration, reduces to

$$G_{11}(z,z') = \frac{1}{2\sqrt{2\pi}} \int_{-\infty}^{\infty} \frac{dq}{2\pi} \left(M_0 - i\frac{\pi}{\sigma} - iq\right)^{-1} \begin{bmatrix} i\frac{1}{2}\bar{\varrho}\bar{\delta n} & i\frac{1}{2}\bar{\vartheta}\bar{\delta n} \\ i\frac{1}{2}\bar{\vartheta}\bar{\delta n} & -i\frac{1}{2}\bar{\varrho}\bar{\delta n} \end{bmatrix} (M_0 - iq)^{-1} \exp\left(-i\frac{\pi}{\sigma}z'\right) e^{iq(z-z')}$$

(5.11)

and

$$G_{12}(z,z') = \sqrt{\frac{\pi}{2}} \int_{-\infty}^{\infty} \frac{dk}{2\pi} \int_{-\infty}^{\infty} \frac{dq}{2\pi} (M_0 - ik)^{-1} e^{-ikz'} \begin{bmatrix} i\frac{1}{2}\bar{\varrho}\bar{\delta n} & i\frac{1}{2}\bar{\vartheta}\bar{\delta n} \\ i\frac{1}{2}\bar{\vartheta}\bar{\delta n} & -i\frac{1}{2}\bar{\varrho}\bar{\delta n} \end{bmatrix} \delta\left(k - q + \frac{\pi}{\sigma}\right) (M_0 - iq)^{-1} e^{iqz}$$

which is similarly reduced to

$$G_{12}(z,z') = \frac{1}{2\sqrt{2\pi}} \int_{-\infty}^{\infty} \frac{dq}{2\pi} \left(M_0 + i\frac{\pi}{\sigma} - iq\right)^{-1} \begin{bmatrix} i\frac{1}{2}\bar{\varrho}\bar{\delta n} & i\frac{1}{2}\bar{\vartheta}\bar{\delta n} \\ i\frac{1}{2}\bar{\vartheta}\bar{\delta n} & -i\frac{1}{2}\bar{\varrho}\bar{\delta n} \end{bmatrix} (M_0 - iq)^{-1} \exp\left(i\frac{\pi}{\sigma}z'\right) e^{iq(z-z')}.$$

(5.12)

The integrals of Equations 5.11 and 5.12 exhibit some interesting features. The break in the translation invariance of the propagating mode is clearly observable. For the homogeneous waveguide and the uniform grating, the propagator depends on the difference between the final and the initial position, $(z - z')$. However, adding a position dependent perturbation breaks that translation invariance, as can clearly be seen from the $\exp\left(-i\frac{\pi}{\sigma}z'\right)$ and $\exp\left(i\frac{\pi}{\sigma}z'\right)$terms.

To solve the integrals of Equations 5.11 and 5.12, as before in Chapters 3 and 4, the inverses of these matrices have to be calculated in the usual manner using cofactor expansion. Since there are two matrix inverses to calculate and two eigenvalues for each matrix corresponding to the number of modes, four poles occur instead of two. Should second order perturbative terms be included, the inverse of a third matrix would have to be accounted for and hence an integral with six poles would have to be solved. The mathematical method is well established and remains the same, but the problem becomes more involved and complicated the higher the order of the perturbative terms included.

The energy of the system should be conserved. Given that the coupled-mode equations can be expressed as (Equation 2.1)

$$\frac{d\overline{U}}{dz} = M(z)\overline{U}(z),$$

the conservation of energy requires that

$$\begin{aligned} \frac{d}{dz}\left(\overline{U}^{\dagger}\overline{U}\right) &= \overline{U}^{\dagger}\frac{d\overline{U}}{dz} + \frac{d\overline{U}^{\dagger}}{dz}\overline{U} \\ &= \overline{U}^{\dagger}(z) M(z) \overline{U}(z) + \overline{U}^{\dagger}(z) M^{\dagger}(z) \overline{U}(z) \\ &= 0. \end{aligned} \tag{5.13}$$

Parameters	Figure 5.1
L	10 cm
λ_D	1550 nm
Λ	15.5 μm
Δn	0.1
σ	10 cm
$\vartheta\sigma$	0.48π

Table 5.1: These are parameters calculated from literature [3] and used to model the LPG with a raised-cosine modulation.

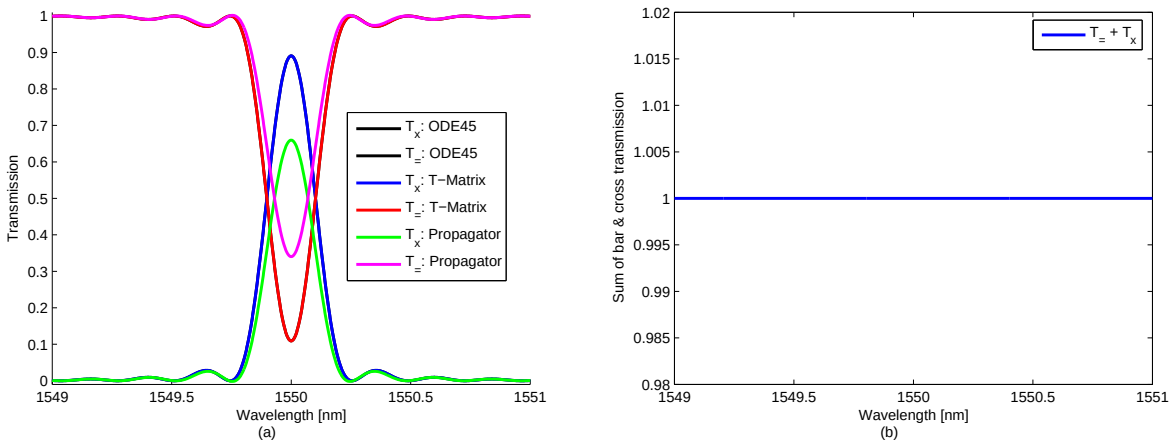

Figure 5.1: (a) Cross and bar transmission ($T_\times$ and $T_=$) for two copropagating modes in a grating modulated by a raised-cosine function as calculated using ODE45, transfer-matrix method and the perturbed propagator respectively. The curves produced by ODE45 coincide with those produced by the transfer-matrix (T-matrix) method. (b) The sum of the complementary cross and bar transmission calculated using the propagator.

Equation 5.13 is only satisfied if

$$M^\dagger(z) \quad = \quad -M(z)\,.$$

Thus the coupling matrix must be anti-Hermitian. From Equation 5.8, it can be seen that the coupling matrix meets this requirement

$$\begin{aligned} M^\dagger(z) &= \begin{bmatrix} -i\varrho^+(z) & -i\vartheta(z) \\ -i\vartheta(z) & i\varrho^+(z) \end{bmatrix} \\ &= -\begin{bmatrix} i\varrho^+(z) & i\vartheta(z) \\ i\vartheta(z) & -i\varrho^+(z) \end{bmatrix} \\ &= -M(z)\,. \end{aligned} \tag{5.14}$$

5.3.2 Results

The integrals of Equations 5.11 and 5.12 were solved and the resulting propagator was used to calculate the cross and bar transmission of the two copropagating modes in a grating modulated by a raised-cosine function. The propagator can be found in the Appendix, Section 7.4, it is rather lengthy. Table 5.1 provides the parameters of the grating modeled. In Figure 5.1(a) the results of the propagator are

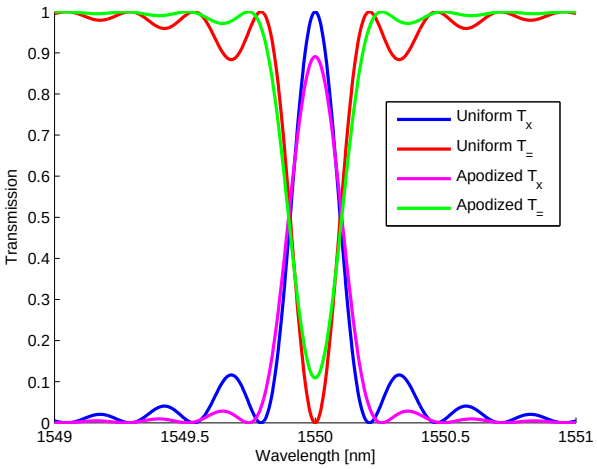

Figure 5.2: A comparison of the uniform grating with the apodized grating illustrating the effect of the apodization. The analytical solution was used to model the uniform grating while the transfer-matrix method was used to simulate the apodized grating.

Method	Time Consumption [s] for 1000 wavelength samples
ODE45	70.438
Transfer-matrix	8.687
Propagator	0.36

Table 5.2: Time consumption for the simulation the grating corresponding to Figure 5.1 and Table 5.1 for 1000 wavelength samples over the chosen wavelength range.

compared to those of ODE45 and the transfer-matrix method. In this case the propagator does not compare well with ODE45 nor the transfer-matrix method. Since perturbation theory is being used, the propagator cannot be expected to produce exactly the same result produced by the transfer-matrix method nor ODE45. However, the result produced by the propagator is qualitatively acceptable. The result is physically sensible in that the modulus squared of the complex amplitudes of the two coupled modes produced by the propagator does not exceed unity for any wavelength. The cross transmission of Figure 5.1(a) is the ratio of the output power of the second mode to the input power in the first mode (Equation 4.6), which should never exceed unity and does not here. The bar transmission is the ratio of the output power to the input power of the first mode (Equation 4.8) and is thus the complement of the cross transmission. Figure 5.1(b) is the sum of the bar and cross transmission corresponding to Figure 5.1(a) and serves to illustrate the fact that the total power in the system does not dip below nor, most importantly, exceed unity, but is conserved for all wavelengths. This agrees with the anti-Hermitian property of the coupling matrix (Equation 5.14).

At wavelengths far removed from the design wavelength ($\lambda_D = 1550\,\text{nm}$), the propagator's results compare well with the results of the transfer-matrix and numerical methods. At wavelengths approaching λ_D, near optimum phase-matching conditions, the propagator's results begin to diverge from that of the other two methods. The difference between the results is most significant around λ_D where the coupling is at a maximum. Hence the justification for using first order perturbation theory is weak as coupling is stronger for these wavelengths and higher order terms are required to accurately model this LPG.

Figure 5.2 depicts the effect of the apodization. The uniform grating exhibits the undesirable side lobe structure which is suppressed when the raised-cosine modulation is added. Table 5.2 provides the

time consumption for the respective methods. The propagator is an order of magnitude faster than the transfer-matrix method and two orders of magnitude faster than ODE45. However, although the propagator method, as applied here, yields qualitatively and physically sensible results, it cannot be used to predict the quantitative behaviour of an apodized grating close to the design wavelength of the grating.

Chapter 6

Summary & Conclusion

The aim of this study was to provide an alternative approach to solving the coupled-mode equations governing the propagation of electromagnetic modes in a waveguide such as an optical fibre. A method was sought that would not be subject to the numerical instability that is associated with the numerical integration of a large number of coupled differential equations and would not require the multiplication of hundreds of large matrices. The path integral formalism was applied to this problem because it is the analytical analogue of the transfer-matrix method, the numerical method of choice when investigating the spectral properties of fibre gratings.

In this study a path integral was derived which was then generalized to yield a generating functional. From the generating functional a Green's function or propagator describing mode propagation was extracted. The propagator is dependent on the coefficient matrix of the coupled-mode equations, the elements of which are the coupling coefficients between the interacting modes. In this way the propagator contains all the information pertaining to the interaction of the modes which in turn is heavily dependent on the nature of the medium through which they are propagating.

As a first case, the propagator was applied to mode propagation through a homogeneous medium. Specifically the cases of two forward propagating modes, two backward propagating modes and two counter propagating modes were investigated. The propagator produced physically sensible results. Both the real and imaginary components of the amplitudes obtained from the propagator were in exact agreement with the analytical solution. The square of the complex amplitudes had an error of the order 10^{-16} compared to the analytical solution. This error is of the same order of magnitude as Matlab's precision and is considered to be due to rounding errors. As far as time consumption is concerned, the propagator fared just as well as numerical integration using ODE45 function of Matlab.

Secondly the propagator method was applied to waveguides with a periodic variation of the index of refraction. A propagator was derived for a uniform long period grating, that couples two copropagating modes in a periodically perturbed waveguide. When modeling both the power of the modes with propagation and the associated bar and cross transmission spectra, physically sensible results were obtained. The propagator's results were in excellent agreement with analytical solutions with an maximum error of order $10^{-13}\%$. Regarding the time consumption, the propagator out performed ODE45. A propagator was derived for the uniform Bragg grating, that couples two identical counter propagating modes. It was shown that the propagator yields physically sensible results for both the evolution of modes' power and the reflection spectra of the gratings. When calculating the reflection spectra and the power evolution of the modes (under phase-matched conditions), the propagator's results are in excellent agreement with the analytical solutions with a maximum error of the order of $10^{-13}\%$. The propagator out performed ODE45

with regards to time consumption. Parameters used to model the gratings corresponding to Figures 4.3, 4.4, 4.5, 4.7 and 4.8 were obtained from the literature and all results were successfully reproduced.

Finally, a propagator was derived for a nonuniform long period grating, specifically an apodized grating with a raised-cosine modulation of the average index of refraction. For this case the propagator produced a physically sensible and qualitatively correct result. However, the quantitative agreement between the propagator's result and that produced by the transfer-matrix and ODE45 is poor for wavelengths approaching the design wavelength of the grating. The validity of first order perturbation theory for such wavelengths is questionable as the coupling. Higher order corrective terms are required to obtain a more accurate result. For what it is worth though, the propagator out performs the transfer-matrix method and ODE45 in terms of time consumption.

The application of perturbation theory to the problem should include higher order terms in future. The path integral formalism is convenient because all that is required is the diagonalization of the coupling matrix to find $(M_0 - ik)^{-1}$ and the poles of the propagator and then the application of Cauchy's Theorem. The benefits of using the propagator would become apparent when solving large systems of differential equations required to model the coupling of multiple optical modes in a waveguide. This work covered only the initial stages in the development of this approach and as such the problems encountered entailed solving a pair of coupled differential equations as opposed to a much larger set. Based on the result obtained in Section 5.3.2, it must be concluded that for a 2×2 system the transfer-matrix method is still the best approach to take until this problem of the propagator method is solved.

There is still much scope for research in this area. There are a variety of other cases to which the propagator method may be applied. These include different apodized as well as chirped gratings. It would be worth investigating other techniques such as the nonperturbative $\frac{1}{N}$-expansion for solving the coupled-mode equations for the cases where there are hundreds of modes or more. Further, this study has also only considered the linear effects produced by gratings however, there is an entire smorgasbord of intensity dependent nonlinear effects that, given the appropriate conditions, need to be taken into account and the $\frac{1}{N}$-expansion could be particularly convenient approach to take as it is in many areas of field theory. In such intensity regimes one is required to solve a set of nonlinear coupled-mode equations which for certain intensity regimes reduces to the nonlinear Schrodinger equation.

Chapter 7

Appendix

7.1 Calculating $\left(\overline{a}^{\dagger} \otimes \overline{a}\right) \overline{b}$

$$
\begin{aligned}
\left(\overline{a}^{\dagger} \otimes \overline{a}\right) \overline{b} &= \left[a_1^* \begin{bmatrix} a_1 \\ \vdots \\ a_N \end{bmatrix} \cdots a_N^* \begin{bmatrix} a_1 \\ \vdots \\ a_N \end{bmatrix} \right] \begin{bmatrix} b_1 \\ \vdots \\ b_N \end{bmatrix} \\
&= \begin{bmatrix} a_1^* a_1 & a_2^* a_1 & \cdots & a_N^* a_1 \\ a_1^* a_2 & a_2^* a_2 & \cdots & a_N^* a_2 \\ \vdots & \vdots & \ddots & \vdots \\ a_1^* a_N & a_2^* a_N & \cdots & a_N^* a_N \end{bmatrix} \begin{bmatrix} b_1 \\ \vdots \\ b_N \end{bmatrix} \\
&= \begin{bmatrix} \left(a_1^* a_1\right) b_1 + \left(a_2^* a_1\right) b_2 + \ldots + \left(a_N^* a_1\right) b_N \\ \left(a_1^* a_2\right) b_1 + \left(a_2^* a_2\right) b_2 + \ldots + \left(a_N^* a_2\right) b_N \\ \vdots \\ \left(a_1^* a_N\right) b_1 + \left(a_2^* a_N\right) b_2 + \ldots + \left(a_N^* a_N\right) b_N \end{bmatrix} \\
&= \begin{bmatrix} \sum_{j=1}^{N} \left(a_j^* a_1\right) b_j \\ \sum_{j=1}^{N} \left(a_j^* a_2\right) b_j \\ \vdots \\ \sum_{j=1}^{N} \left(a_j^* a_N\right) b_j \end{bmatrix} \\
&= \begin{bmatrix} \sum_{j=1}^{N} \left(a_j^* b_j\right) a_1 \\ \sum_{j=1}^{N} \left(a_j^* b_j\right) a_2 \\ \vdots \\ \sum_{j=1}^{N} \left(a_j^* b_j\right) a_N \end{bmatrix} \\
&= \left[\sum_{j=1}^{N} \left(a_j^* b_j\right) a_i \right]_i \\
&= \left(\overline{a}^{\dagger} \overline{b}\right) \overline{a}.
\end{aligned}
$$

In the text $\overline{b}_1$ corresponds to $\overline{a}$ in the appendix and $\overline{b}_2$ in the text corresponds to $\overline{b}$ in the appendix.

7.2 Analytical solution for 2×2 copropagation

The coupled-mode equations for copropagation in a uniform grating after the synchronous approximation has been made, are given by [3]

$$\frac{d\tilde{F}_1}{dz} = i\varrho^+ \tilde{F}_1(z) + i\vartheta \tilde{F}_2(z) \tag{7.1}$$

$$\frac{d\tilde{F}_2}{dz} = i\vartheta^* \tilde{F}_1(z) - i\varrho^+ \tilde{F}_2(z). \tag{7.2}$$

Rearranging Equation 7.2, to obtain $\tilde{F}_1(z)$ in terms of $\tilde{F}_2(z)$ yields

$$\begin{aligned} \tilde{F}_1(z) &= \frac{1}{i\vartheta}\left(\frac{d\tilde{F}_2}{dz} + i\varrho^+ \tilde{F}_2(z)\right) \\ &= \frac{1}{i\vartheta}\frac{d\tilde{F}_2}{dz} + \frac{i\varrho^+}{i\vartheta}\tilde{F}_2(z). \end{aligned} \tag{7.3}$$

Substitution of Equation 7.3 into Equation 7.1 yields

$$\begin{aligned} \frac{d}{dz}\left(\frac{1}{i\vartheta}\frac{d\tilde{F}_2}{dz} + \frac{i\varrho^+}{i\vartheta}\tilde{F}_2(z)\right) &= i\varrho^+\left(\frac{1}{i\vartheta}\frac{d\tilde{F}_2}{dz} + \frac{i\varrho^+}{i\vartheta}\tilde{F}_2(z)\right) + i\vartheta\tilde{F}_2(z) \\ \frac{1}{i\vartheta}\frac{d^2\tilde{F}_2}{dz^2} + \frac{i\varrho^+}{i\vartheta}\frac{d\tilde{F}_2}{dz} &= \frac{i\varrho^+}{i\vartheta}\frac{d\tilde{F}_2}{dz} + \frac{i^2\varrho^{+2}}{i\vartheta}\tilde{F}_2(z) + i\vartheta\tilde{F}_2(z) \\ \frac{1}{i\vartheta}\frac{d^2\tilde{F}_2}{dz^2} &= \frac{i\varrho^{+2}}{\vartheta}\tilde{F}_2(z) + i\vartheta\tilde{F}_2(z) \\ \frac{d^2\tilde{F}_2}{dz^2} &= i^2\varrho^{+2}\tilde{F}_2(z) + i^2\vartheta^2\tilde{F}_2(z) \\ \frac{d^2\tilde{F}_2}{dz^2} &= -\left(\varrho^{+2} + \vartheta^2\right)\tilde{F}_2(z). \end{aligned}$$

Let $\alpha = \sqrt{\varrho^{+2} + \vartheta^2}$. Then

$$\frac{d^2\tilde{F}_2}{dz^2} = -\alpha^2\tilde{F}_2(z)$$

which has the following general solution

$$\tilde{F}_2(z) = a_1 e^{i\alpha z} + a_2 e^{-i\alpha z}.$$

The task is now to find constants a_1 and a_2, for which the initial conditions are used

$$\tilde{F}_1(0) = 1 \tag{7.4}$$

$$\tilde{F}_2(0) = 0 \tag{7.5}$$

From Equation 7.5,

$$\begin{aligned} a_1 + a_2 &= 0 \\ a_1 &= -a_2 \end{aligned}$$

from which it follows that

$$\begin{aligned}\tilde{F}_2(z) &= -a_2 e^{i\alpha z} + a_2 e^{-i\alpha z} \\ &= i2a_2 \sin(\alpha z). \end{aligned} \tag{7.6}$$

Now, if $\tilde{F}_2(z) = i2a_2 \sin(\alpha z)$ then

$$\frac{d\tilde{F}_2}{dz} = i2a_2\alpha \cos(\alpha z)$$

so that from Equation 7.3

$$\begin{aligned}\tilde{F}_1(z) &= \frac{1}{i\vartheta}(i2a_2\alpha\cos(\alpha z)) + \frac{i\varrho^+}{i\vartheta}(i2a_2\sin(\alpha z)) \\ &= a_2\frac{2\alpha}{\vartheta}\cos(\alpha z) + a_2\frac{i2\varrho^+}{\vartheta}\sin(\alpha z). \end{aligned} \tag{7.7}$$

From Equation 7.4

$$\begin{aligned}\tilde{F}_1(0) &= a_2\frac{2\alpha}{\vartheta} \\ &= 1\end{aligned}$$

such that

$$a_2 = \frac{\vartheta}{2\alpha}.$$

Hence from Equation 7.6,

$$\tilde{F}_2(z) = i\frac{\vartheta}{\alpha}\sin(\alpha z)$$

and from Equation 7.7,

$$\begin{aligned}\tilde{F}_1(z) &= \frac{\vartheta}{2\alpha}\frac{2\alpha}{\vartheta}\cos(\alpha z) + \frac{\vartheta}{2\alpha}\frac{i2\varrho^+}{\vartheta}\sin(\alpha z) \\ &= \cos(\alpha z) + i\frac{\varrho^+}{\alpha}\sin(\alpha z).\end{aligned}$$

7.3 Analytical solution for 2×2 counter propagation

The coupled-mode equations for counter propagation in a uniform grating after the synchronous approximation has been made, are given by

$$\frac{d\tilde{F}}{dz} = i\varrho^+\tilde{F}(z) + i\vartheta\tilde{B}(z) \tag{7.8}$$

$$\frac{d\tilde{B}}{dz} = -i\vartheta^*\tilde{F}(z) - i\varrho^+\tilde{B}(z). \tag{7.9}$$

Rearranging Equation 7.9, to obtain $\tilde{F}(z)$ in terms of $\tilde{B}(z)$ yields

$$\begin{aligned}\tilde{F}(z) &= -\frac{1}{i\vartheta}\left(\frac{d\tilde{B}}{dz} + i\varrho^{+}\tilde{B}(z)\right) \\ &= -\frac{1}{i\vartheta}\frac{d\tilde{B}}{dz} - \frac{i\varrho^{+}}{i\vartheta}\tilde{B}(z). \end{aligned} \tag{7.10}$$

Substitution of Equation 7.10 into Equation 7.8 yields

$$\begin{aligned}\frac{d}{dz}\left(-\frac{1}{i\vartheta}\frac{d\tilde{B}}{dz} - \frac{i\varrho^{+}}{i\vartheta}\tilde{B}(z)\right) &= i\varrho^{+}\left(-\frac{1}{i\vartheta}\frac{d\tilde{B}}{dz} - \frac{i\varrho^{+}}{i\vartheta}\tilde{B}(z)\right) + i\vartheta\tilde{B}(z) \\ -\frac{1}{i\vartheta}\frac{d^2\tilde{B}}{dz^2} - \frac{i\varrho^{+}}{i\vartheta}\frac{d\tilde{B}}{dz} &= -\frac{i\varrho^{+}}{i\vartheta}\frac{d\tilde{B}}{dz} - \frac{i^2\varrho^{+2}}{i\vartheta}\tilde{B}(z) + i\vartheta\tilde{B}(z) \\ -\frac{1}{i\vartheta}\frac{d^2\tilde{B}}{dz^2} &= -\frac{i\varrho^{+2}}{\vartheta}\tilde{B}(z) + i\vartheta\tilde{B}(z) \\ -\frac{d^2\tilde{B}}{dz^2} &= -i^2\varrho^{+2}\tilde{B}(z) + i^2\vartheta^2\tilde{B}(z) \\ \frac{d^2\tilde{B}}{dz^2} &= i^2\varrho^{+2}\tilde{B}(z) - i^2\vartheta^2\tilde{B}(z) \\ \frac{d^2\tilde{B}}{dz^2} &= -\left(\varrho^{+2} - \vartheta^2\right)\tilde{B}(z). \end{aligned}$$

Let $\alpha = \sqrt{\varrho^{+2} - \vartheta^2}$. Then

$$\frac{d^2\tilde{B}}{dz^2} = -\alpha^2\tilde{B}(z)$$

which has the following general solution

$$\tilde{B}(z) = a_1 e^{-i\alpha z} + a_2 e^{i\alpha z}.$$

The task is now to find constants a_1 and a_2, for which the boundary conditions are used

$$\tilde{F}(0) = 1 \tag{7.11}$$

$$\tilde{B}(L) = 0 \tag{7.12}$$

From Equation 7.12,

$$\begin{aligned}a_1 e^{-i\alpha L} + a_2 e^{i\alpha L} &= 0 \\ a_1 e^{-i\alpha L} &= -a_2 e^{i\alpha L} \\ a_1 &= -a_2 e^{i2\alpha L}\end{aligned}$$

from which it follows that

$$\tilde{B}(z) = -a_2 e^{i2\alpha L} e^{-i\alpha z} + a_2 e^{i\alpha z} \tag{7.13}$$

Now, if $\tilde{B}(z) = -a_2 e^{i2\alpha L} e^{-i\alpha z} + a_2 e^{i\alpha z}$ then

$$\frac{d\tilde{B}}{dz} = ia_2\alpha e^{i2\alpha L} e^{-i\alpha z} + ia_2\alpha e^{i\alpha z}$$

so that from Equation 7.10

$$\begin{aligned}
\tilde{F}(z) &= -\frac{1}{i\vartheta}\left(ia_2\alpha e^{i2\alpha L}e^{-i\alpha z} + ia_2\alpha e^{i\alpha z}\right) - \frac{i\varrho^+}{i\vartheta}\left(-a_2e^{i2\alpha L}e^{-i\alpha z} + a_2e^{i\alpha z}\right) \\
&= -\left(\frac{a_2\alpha e^{i2\alpha L}}{\vartheta}\right)e^{-i\alpha z} - \frac{a_2\alpha}{\vartheta}e^{i\alpha z} + \left(\frac{a_2\varrho^+e^{i2\alpha L}}{\vartheta}\right)e^{-i\alpha z} - \frac{a_2\varrho^+}{\vartheta}e^{i\alpha z} \\
&= \left(\frac{a_2\varrho^+e^{i2\alpha L}}{\vartheta} - \frac{a_2\alpha e^{i2\alpha L}}{\vartheta}\right)e^{-i\alpha z} - \left(\frac{a_2\varrho^+}{\vartheta} + \frac{a_2\alpha}{\vartheta}\right)e^{i\alpha z} \\
&= a_2\frac{e^{i2\alpha L}}{\vartheta}\left(\varrho^+ - \alpha\right)e^{-i\alpha z} - a_2\frac{1}{\vartheta}\left(\varrho^+ + \alpha\right)e^{i\alpha z} \qquad (7.14)
\end{aligned}$$

From Equation 7.11

$$\begin{aligned}
\tilde{F}(0) &= a_2\frac{e^{i2\alpha L}}{\vartheta}\left(\varrho^+ - \alpha\right) - a_2\frac{1}{\vartheta}\left(\varrho^+ + \alpha\right) \\
&= a_2\left(\frac{\left(\varrho^+ - \alpha\right)e^{i2\alpha L} - \varrho^+ - \alpha}{\vartheta}\right) \\
&= 1
\end{aligned}$$

such that

$$a_2 = \frac{\vartheta}{\left(\varrho^+ - \alpha\right)e^{i2\alpha L} - \varrho^+ - \alpha}.$$

Hence from Equation 7.13,

$$\tilde{B}(z) = -\frac{\vartheta e^{i2\alpha L}}{\left(\varrho^+ - \alpha\right)e^{i2\alpha L} - \varrho^+ - \alpha}e^{-i\alpha z} + \frac{\vartheta}{\left(\varrho^+ - \alpha\right)e^{i2\alpha L} - \varrho^+ - \alpha}e^{i\alpha z}$$

and from Equation 7.14,

$$\begin{aligned}
\tilde{F}(z) &= \frac{\vartheta}{\left(\varrho^+ - \alpha\right)e^{i2\alpha L} - \varrho^+ - \alpha}\frac{e^{i2\alpha L}}{\vartheta}\left(\varrho^+ - \alpha\right)e^{-i\alpha z} - \frac{\vartheta}{\left(\varrho^+ - \alpha\right)e^{i2\alpha L} - \varrho^+ - \alpha}\frac{1}{\vartheta}\left(\varrho^+ + \alpha\right)e^{i\alpha z} \\
&= \frac{\left(\varrho^+ - \alpha\right)e^{i2\alpha L}}{\left(\varrho^+ - \alpha\right)e^{i2\alpha L} - \varrho^+ - \alpha}e^{-i\alpha z} - \frac{\left(\varrho^+ + \alpha\right)}{\left(\varrho^+ - \alpha\right)e^{i2\alpha L} - \varrho^+ - \alpha}e^{i\alpha z}.
\end{aligned}$$

7.4 The perturbed propagator for a raised-cosine modulation

The solution to Equation 5.2 with a modulation given by Equation 5.7 is expressed as

$$
\begin{aligned}
G(z,z') &= \left\{ \frac{1}{(e_1-e_2)} \begin{bmatrix} -\delta\beta - \frac{1}{2}\bar{\varrho}\bar{\delta n} - e_1 & -\frac{1}{2}\bar{\vartheta}\bar{\delta n} \\ -\frac{1}{2}\bar{\vartheta}\bar{\delta n} & \delta\beta + \frac{1}{2}\bar{\varrho}\bar{\delta n} - e_1 \end{bmatrix} \exp\{ie_1(z-z')\} \right. \\
&+ \left. \frac{1}{(e_2-e_1)} \begin{bmatrix} -\delta\beta - \frac{1}{2}\bar{\varrho}\bar{\delta n} - e_2 & -\frac{1}{2}\bar{\vartheta}\bar{\delta n} \\ -\frac{1}{2}\bar{\vartheta}\bar{\delta n} & \delta\beta + \frac{1}{2}\bar{\varrho}\bar{\delta n} - e_2 \end{bmatrix} \exp\{ie_2(z-z')\} \right\} \\
&+ \frac{1}{2\sqrt{2\pi}} \left\{ \frac{1}{(e_1-e_2)(e_1-e_3)(e_1-e_4)} \begin{bmatrix} -\delta\beta - \frac{1}{2}\bar{\varrho}\bar{\delta n} - e_1 & -\frac{1}{2}\bar{\vartheta}\bar{\delta n} \\ -\frac{1}{2}\bar{\vartheta}\bar{\delta n} & \delta\beta + \frac{1}{2}\bar{\varrho}\bar{\delta n} - e_1 \end{bmatrix} [dM] \right. \\
&\quad \times \left. \begin{bmatrix} -\delta\beta - \frac{1}{2}\bar{\varrho}\bar{\delta n} - e_1 & -\frac{1}{2}\bar{\vartheta}\bar{\delta n} \\ -\frac{1}{2}\bar{\vartheta}\bar{\delta n} & \delta\beta + \frac{1}{2}\bar{\varrho}\bar{\delta n} - e_1 \end{bmatrix} \exp\{ie_1(z-z')\} \right. \\
&+ \frac{1}{(e_2-e_1)(e_2-e_3)(e_2-e_4)} \begin{bmatrix} -\delta\beta - \frac{1}{2}\bar{\varrho}\bar{\delta n} - \frac{\pi}{\sigma} - e_2 & -\frac{1}{2}\bar{\vartheta}\bar{\delta n} \\ -\frac{1}{2}\bar{\vartheta}\bar{\delta n} & \delta\beta + \frac{1}{2}\bar{\varrho}\bar{\delta n} - \frac{\pi}{\sigma} - e_2 \end{bmatrix} [dM] \\
&\quad \times \begin{bmatrix} -\delta\beta - \frac{1}{2}\bar{\varrho}\bar{\delta n} - e_2 & -\frac{1}{2}\bar{\vartheta}\bar{\delta n} \\ -\frac{1}{2}\bar{\vartheta}\bar{\delta n} & \delta\beta + \frac{1}{2}\bar{\varrho}\bar{\delta n} - e_2 \end{bmatrix} \exp\{ie_2(z-z')\} \\
&+ \frac{1}{(e_3-e_1)(e_3-e_2)(e_3-e_4)} \begin{bmatrix} -\delta\beta - \frac{1}{2}\bar{\varrho}\bar{\delta n} - \frac{\pi}{\sigma} - e_3 & -\frac{1}{2}\bar{\vartheta}\bar{\delta n} \\ -\frac{1}{2}\bar{\vartheta}\bar{\delta n} & \delta\beta + \frac{1}{2}\bar{\varrho}\bar{\delta n} - \frac{\pi}{\sigma} - e_3 \end{bmatrix} [dM] \\
&\quad \times \begin{bmatrix} -\delta\beta - \frac{1}{2}\bar{\varrho}\bar{\delta n} - e_3 & -\frac{1}{2}\bar{\vartheta}\bar{\delta n} \\ -\frac{1}{2}\bar{\vartheta}\bar{\delta n} & \delta\beta + \frac{1}{2}\bar{\varrho}\bar{\delta n} - e_3 \end{bmatrix} \exp\{ie_3(z-z')\} \\
&+ \frac{1}{(e_4-e_1)(e_4-e_2)(e_4-e_3)} \begin{bmatrix} -\delta\beta - \frac{1}{2}\bar{\varrho}\bar{\delta n} - \frac{\pi}{\sigma} - e_4 & -\frac{1}{2}\bar{\vartheta}\bar{\delta n} \\ -\frac{1}{2}\bar{\vartheta}\bar{\delta n} & \delta\beta + \frac{1}{2}\bar{\varrho}\bar{\delta n} - \frac{\pi}{\sigma} - e_4 \end{bmatrix} [dM] \\
&\quad \times \left. \begin{bmatrix} -\delta\beta - \frac{1}{2}\bar{\varrho}\bar{\delta n} - e_4 & -\frac{1}{2}\bar{\vartheta}\bar{\delta n} \\ -\frac{1}{2}\bar{\vartheta}\bar{\delta n} & \delta\beta + \frac{1}{2}\bar{\varrho}\bar{\delta n} - e_4 \end{bmatrix} \exp\{ie_4(z-z')\} \right\} \exp\left(-\frac{\pi}{\sigma}z'\right) \\
&+ \frac{1}{2\sqrt{2\pi}} \left\{ \frac{1}{(e_1-e_2)(e_1-e_5)(e_1-e_6)} \begin{bmatrix} -\delta\beta - \frac{1}{2}\bar{\varrho}\bar{\delta n} + \frac{\pi}{\sigma} - e_1 & -\frac{1}{2}\bar{\vartheta}\bar{\delta n} \\ -\frac{1}{2}\bar{\vartheta}\bar{\delta n} & \delta\beta + \frac{1}{2}\bar{\varrho}\bar{\delta n} + \frac{\pi}{\sigma} - e_1 \end{bmatrix} [dM] \right. \\
&\quad \times \left. \begin{bmatrix} -\delta\beta - \frac{1}{2}\bar{\varrho}\bar{\delta n} - e_1 & -\frac{1}{2}\bar{\vartheta}\bar{\delta n} \\ -\frac{1}{2}\bar{\vartheta}\bar{\delta n} & \delta\beta + \frac{1}{2}\bar{\varrho}\bar{\delta n} - e_1 \end{bmatrix} \exp\{ie_1(z-z')\} \right. \\
&+ \frac{1}{(e_2-e_1)(e_2-e_5)(e_2-e_6)} \begin{bmatrix} -\delta\beta - \frac{1}{2}\bar{\varrho}\bar{\delta n} + \frac{\pi}{\sigma} - e_2 & -\frac{1}{2}\bar{\vartheta}\bar{\delta n} \\ -\frac{1}{2}\bar{\vartheta}\bar{\delta n} & \delta\beta + \frac{1}{2}\bar{\varrho}\bar{\delta n} + \frac{\pi}{\sigma} - e_2 \end{bmatrix} [dM] \\
&\quad \times \begin{bmatrix} -\delta\beta - \frac{1}{2}\bar{\varrho}\bar{\delta n} - e_2 & -\frac{1}{2}\bar{\vartheta}\bar{\delta n} \\ -\frac{1}{2}\bar{\vartheta}\bar{\delta n} & \delta\beta + \frac{1}{2}\bar{\varrho}\bar{\delta n} - e_2 \end{bmatrix} \exp\{ie_2(z-z')\} \\
&+ \frac{1}{(e_5-e_1)(e_5-e_2)(e_5-e_6)} \begin{bmatrix} -\delta\beta - \frac{1}{2}\bar{\varrho}\bar{\delta n} + \frac{\pi}{\sigma} - e_5 & -\frac{1}{2}\bar{\vartheta}\bar{\delta n} \\ -\frac{1}{2}\bar{\vartheta}\bar{\delta n} & \delta\beta + \frac{1}{2}\bar{\varrho}\bar{\delta n} + \frac{\pi}{\sigma} - e_5 \end{bmatrix} [dM] \\
&\quad \times \begin{bmatrix} -\delta\beta - \frac{1}{2}\bar{\varrho}\bar{\delta n} - e_5 & -\frac{1}{2}\bar{\vartheta}\bar{\delta n} \\ -\frac{1}{2}\bar{\vartheta}\bar{\delta n} & \delta\beta + \frac{1}{2}\bar{\varrho}\bar{\delta n} - e_5 \end{bmatrix} \exp\{ie_5(z-z')\} \\
&+ \frac{1}{(e_6-e_1)(e_6-e_2)(e_6-e_5)} \begin{bmatrix} -\delta\beta - \frac{1}{2}\bar{\varrho}\bar{\delta n} + \frac{\pi}{\sigma} - e_6 & -\frac{1}{2}\bar{\vartheta}\bar{\delta n} \\ -\frac{1}{2}\bar{\vartheta}\bar{\delta n} & \delta\beta + \frac{1}{2}\bar{\varrho}\bar{\delta n} + \frac{\pi}{\sigma} - e_6 \end{bmatrix} [dM] \\
&\quad \times \left. \begin{bmatrix} -\delta\beta - \frac{1}{2}\bar{\varrho}\bar{\delta n} - e_6 & -\frac{1}{2}\bar{\vartheta}\bar{\delta n} \\ -\frac{1}{2}\bar{\vartheta}\bar{\delta n} & \delta\beta + \frac{1}{2}\bar{\varrho}\bar{\delta n} - e_6 \end{bmatrix} \exp\{ie_6(z-z')\} \right\} \exp\left(\frac{\pi}{\sigma}z'\right)
\end{aligned}
$$

where

$$[dM] \quad = \quad \begin{bmatrix} \frac{1}{2}\bar{\varrho}\bar{\delta n} & \frac{1}{2}\bar{\vartheta}\bar{\delta n} \\ \frac{1}{2}\bar{\vartheta}\bar{\delta n} & -\frac{1}{2}\bar{\varrho}\bar{\delta n} \end{bmatrix}$$

and e_3 and $e_4$are the poles associated with the integral of Equation 5.11 and e_5 and e_6 are the poles associated with the integral of Equation 5.12. Poles e_1 and e_2 correspond to the leading order term and are common to the integrals 5.11 and 5.12 too.

Bibliography

[1] Walter Appel. *Mathematics for Physics & Physicists*. Princeton University Press, 2007.

[2] Turan Erdogan. Cladding-mode resonances in short- and long-period fiber grating filters. *Journal of the Optical Society of America A*, 14(8):1760–1773, 1997.

[3] Turan Erdogan. Fiber grating spectra. *Journal of Lightwave Technology*, 15(8):1277–1294, 1997.

[4] M. E. Fermann, K. Sugden, and I. Bennion. High-power soliton fiber laser based on pulse width control with chirped fiber bragg gratings. *Optics Letters*, 20:172–174, 1995.

[5] J. L. Frolik and A. E. Yagle. An asymmetric discrete-time approach for the design and analysis of periodic waveguide gratings. *IEEE Journal of Lightwave Technology*, 13:175–185, 1995.

[6] Raymond J. Hawkins. Propagation properties of single-mode dielectric waveguide structures: a path integral approach. *Applied Optics*, 26:1183–1188, 1987.

[7] T. Hirono and Y. Yoshikuni. A hamiltonian formulation for coupled wave equations. *IEEE Journal of Quantum Electronics*, QE-8:1751–1755, 1974.

[8] Raman Kashyap. *Fiber Bragg Gratings*. Optics and Photonics. Academic Press, 1999.

[9] Alexandre V. Morozov. Two-frequency mutual coherence function of electromagnetic waves in random media: a path-integral variational solution. *Journal of the Optical Society of America A*, 19:2074–2084, 2002.

[10] P. A. Morton, V. Mizrahi, P. A. Andrekson, T. Tanbun-Ek, R. A. Logan, P. Lemaire, D. L. Coblentz, A. M. Sergent, K. W. Wecht, and Jr P. F. Sciortino. Mode-locked hybrid soliton pulse source with extremely wide operating frequency range. *IEEE Photon. Technology Letters*, 5:28–31, 1993.

[11] P. A. Morton, V. Mizrahi, T. Tanbun-Ek, R. A. Logan, P. J. Lemaire, H. M. Presby, T. Erdagon, S. L. Woodward, J. E. Sipe, M. R. Phillips, A. M. Sergent, and K. W. Wecht. Stable single mode hybrid laser with high power and narrow linewidth. *Applied Physics Letters*, 64:2634–2636, 1994.

[12] Andreas Othonos and Kyriacos Kalli. *Fiber Bragg Gratings*. Artech House, 1999.

[13] F. Ouellette. Disperion cancellation using linearly chirped bragg grating filters in optical waveguides. *Optics Letters*, 12:847–849, 1987.

[14] L. Poladian. Variational technique for nonuniform gratings and distributed feedback lasers. *Journal of the Optical Society of America A*, 11(6):1846–1853, 1994.

[15] William H. Press, Brian P. Flannery, Saul A. Teukolsky, and William T. Vetterling. *Numerical Recipes in C: The Art of Scientific Computing*. Cambridge University Press, 1992.

[16] J. E. Sipe, L. Poladian, and C. Martijn de Sterke. Propagation through nonuniform grating structures. *Journal of the Optical Society of America A*, 11(4):1307–1320, 1994.

[17] Shiv R. Vatsya. Path-integral formulation of optical beam propagation. *Journal of the Optical Society of America B*, 22:2512–2518, 2005.

[18] L. A. Weller-Brophy and D. G. Hall. Analysis of waveguide gratings: Application of rouard's method. *Journal of the Optical Society of America A*, 2:864–871, 1985.

[19] K.A. Winick. Effective-index method and coupled-mode for almost periodic waveguide gratings: A comparison. *Applied Optics*, 31:757–764, 1992.

[20] M. Yamada and K. Sakuda. Analysis of almost-periodic distributed feedback slab waveguide via a fundamental matrix approach. *Applied Optics*, 26:3474–3478, 1987.

[21] Amnon Yariv. Coupled-mode theory for guided-wave optics. *IEEE Journal of Lightwave Technology*, QE-9(9):919–933, 1973.

[22] Amnon Yariv and Pochi Yeh. *Optical Waves in Crystals: Propagation and Control of Laser Radiation*. John Wiley & Sons,Inc, 2003.